Chapter 1

Introduction

The phenomenon of the exchange coupling basically originates from the magnetic interaction between electron spins. When two magnetic layers are in contact on an atomic scale, the electron spins of magnetic atoms at the interface are coupled to each other through exchange interaction, resulting in the different magnetic properties in the layers. Because of its fundamental interest and important technical applications, the exchange-coupling interaction at the interface of two magnetic layers has been widely explored over the past fifty years [1-3]. The typical phenomenon of exchange coupling in the bilayer systems is the exchange bias (EB), discovered by Meiklejohn and Bean in the Co-CoO system in 1956 [4]. In their experiments, the ferromagnetic (FM) Co particles covered by its native antiferromagnetic (AFM) oxide CoO exhibited shifted magnetic hysteresis loops, the characteristic of EB. This phenomenon was not only observed in the particles and thin-film systems of the FM-AFM bilayers, but also in those of the ferrimagnetic (FIM)-AFM [5], FIM-FM [6], and FIM/FIM [7].

The focus of this dissertation is on studying the exchange-coupling interaction of the magnetic bilayer system consisting of ferrimagnetic films of rare-earth-transition-metal (RE-TM) alloys with perpendicular anisotropy. In this chapter, the motivation and the scope of the dissertation are described.

1.1 Motivation

Because of the applications for spin-valve read head [7], and magnetic random access memories (MRAM) [8], the investigations of exchange coupling in the bilayer systems are concentrated in the FM-AFM films with longitudinal anisotropy. Several models, which will be specifically described in the following chapter, have been proposed to clarify the physical mechanism of the EB in the FM-AFM bilayer. But each model has the weak points regarding to the correspondence with experimental observations. It is generally believed that the interfacial uncompensated spins and the domain formation in AFM layers significantly affected the strength of the EB in FM-AFM bilayers [9]. But the concepts are difficult to be concretely evidenced by experiments.

In addition to FM/AFM systems, the EB phenomenon was also observed in the bilayers with FIM materials such as amorphous RE-TM alloys of TbFeCo [10], GdCo [11], or TbCo [6]. Because of perpendicular anisotropy, amorphous structure, high Kerr effect, and adjustable magnetic properties, the amorphous RE-TM materials have been practically utilized in the magneto-optical (MO) recording, and considered as a candidate of recording media for ultra-high-density storage. The exchange-coupled RE-TM multilayers with perpendicular anisotropy were also investigated for the applications of new super resolution methods for high density MO recording, like magnetically induced super resolution (MSR) [12-13], and magnetic amplifying MO system (MAMMOS) [14]. With the strong exchange interaction [15]

between the RE-TM films, the magnetic domains can be reliably written at high temperature and stably preserved even after thousands times of reading processes. A micromagnetic analysis, conducting the concept of a Block wall existing at the interface between magnetic layers, has been performed to interpret the strong exchange interaction [16]. Kobayashi *et al.* further theoretically calculated the magnetization-switching curves for the exchange-coupling bilayers with perpendicular anisotropy. At the first of the study, we explored the difference of exchange-coupling strength among FI/FI, FM/ FM, and FM/ AFM bilayers, based on the view of spin-spin coupling at interface. By exploring the EB dependence on interface roughness, and spin-spin coupling states, a highly-uncompensated-spin interface model is proposed to explain the ultra high interfacial coupling between perpendicular TbFeCo layers. By utilized the characteristics of adjustable magnetic anisotropy in RE-TM films, we further demonstrated that the dependence of the EB strength on the magnetic anisotropy of the pinning layer, which was hardly clarified in the experiments of the FM-AFM systems due to the difficulty in measuring the AFM Ku.

Furthermore, we proposed the exchange-coupled double-layer TbFeCo with high magnetization and coercivity as the recording media of hybrid recording, which will be discussed in details in chapter 3. The advance recording technology requires high-magnetization media yielding high flux density for GMR sensing. To ensure adequate stability of small-size domains, the media should possess large coercivity. Commonly used single-layer MO film can not meet these requirements since, intrinsically, high magnetization MO film possess low coercivity.

In the thesis work, we attempted to enhance the coercivity of the TbFeCo films with high magnetization through the strong exchange coupling between the RE-TM films. To make the TbFeCo bilayers practicable for the applications in heat-assisted-magnetic-recording (HAMR), the media noises of TbFeCo media fabricated at different processing parameters were examined by a GMR sensor in a dynamic hard-disk tester.

Interestingly, the planar exchange anisotropy was found in the bilayers composed of the ferromagnetic layer with in-plane anisotropy and the ferrimagnetic rare-earth-transition-metal (RE-TM) films with perpendicular anisotropy [17]. Since RE-TM films are amorphous with strong exchange anisotropy coupled to FM, these bilayers can potentially replace the FM-AFM for applications [18-19]. Cain et al. proposed that the strong exchange coupling between RE-TM and FM resulted from the existence of a homogeneous and continuous interface in the bilayers. However, the biasing mechanism was only described by theoretical calculations and indirect results [20-21]. Over the last few years, X-ray magnetic circular dichroism (XMCD) technique has evolved into an important magnetometry tool [22-24]. It possesses the high sensitivity to element-specifically determine spin and orbital magnetic moments and their anisotropy in ferromagnets or ferrimagnets. In the experiments, by XMCD measurements, we attempted to understand the orientation of specific magnetic spins near the interface between the TbFe and Co films respectively with perpendicular and longitudinal anisotropy. From the results, the source of exchange bias in the TbFe/Co bilayers was concretely explored and discussed.

The GMR effect, originating from the spin-dependent scattering of the conduction electrons in the magnetic layers or at their interface, was extensively explored in the magnetic multilayers containing the FM/spacer/FM structure [25]. But no GMR effect was shown in the multilayers consisting of rare earth metals and transition metals [26]. In additional, the GMR effect mostly was observed in the multilayers with the magnetization in the plane. It is a very interesting topic to investigate the GMR effect in the multilayers with RE-TM-alloy films with perpendicular anisotropy. Therefore, we fabricated a structure of spin valves composed of RE-TM/spacer/RE-TM layers to explore their magnetoresistance behavior. The interface between the spacer and ferrimagnetic layer was further manipulated by inserting thin Co layers with the out-of-plane magnetization induced by RE-TM films.

1.2 Outline of the Dissertation

This chapter briefly introduces the reported researches about the exchange coupling in the magnetic films, and describes the motivation of the studies in the dissertation. In the following two chapters, I will further present the backgrounds relevant to the discussions in this dissertation. For the comparison with the results in the bilayers composed of ferrimagnetic RE-TM films, I summarize the previous models established for the exchange bias in FM/AFM layers in the chapter 2. The application of the FM/AFM bilayers is included in the section. Chapter 3 will focus on the introduction of RE-TM thin films, magnetization-switching mechanism of the double layers, and new MO-recording technologies by utilized the RE-TM multilayers. Then, the fabrication of the RE-TM films and some important measurements will be described in the chapter 4. Chapter 5 is a discussion of the exchange coupling in the TbFeCo bilayers with perpendicular anisotropy. The studies of the exchange-coupled TbFeCo media with high magnetization and coercivity will be discussed in the chapter 6. Then, the exchange coupling between two magnetic layers respectively with perpendicular and longitudinal anisotropy will be described in the chapter 7. Chapter 8 will discuss the GMR effect in the spin valves consisting of RE-TM films. The dissertation is summarized in Chapter 9.

Chapter 2

Background I --

Exchange coupling in the FM/AFM bilayers

This chapter introduces the background associated with exchange-coupling phenomenon in FM/AFM systems. Section 2.1 first explains the terms of exchange anisotropy and exchange bias (EB). Several models explaining the origin of the exchange anisotropy in FM/AFM systems are described in Section 2.2. Section 2.3 presents the experiments about positive and negative EB. The applications of the EB in the FM/AFM are described in Section 2.4.

2.1 Exchange Anisotropy

Exchange anisotropy, the typical exchange-coupling phenomenon in the magnetic multilayers, was first discovered in partially oxidized Co particles by Meiklejohn and Bean in 1957 [1-2]. Their discovery was initiated by the observation that the hysteresis loop below room temperature of nominal Co nano-particles was shifted along the field axis after cooling in an applied field. It was subsequently established that the particles had been partially oxidized to CoO, which is an antiferromagnet. Thus, the particles could be considered to consist of a core of single-domain Co with a shell of antiferromagnetic CoO. A compact of

these particles was then cooled in a magnetic field to 77K, and its hysteresis loop was measured at that temperature. The hysteresis loop, as shown in Fig. 2.1(a), is not symmetrical about the origin but is shifted to one side. The shift of the center of the hysteresis loop from the origin is defined as the magnitude of the exchange field H_e.

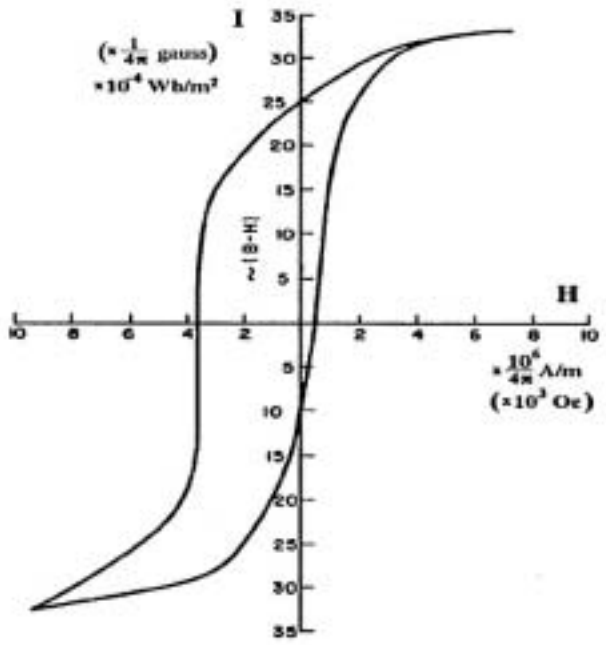

Fig.2.1: Hysteresis loop for the Co-CoO sample cooled in the field and measured at 77K [1].

Since the first experiments of Meiklejohn and Bean, many FM/AFM systems have been explored to increase the scientific understanding of them. Exchange anisotropy was not of interest to industry until Hempstead et al. [3] proposed that unidirectional exchange anisotropy between NiFe and FeMn could be useful for biasing small magnetoresistive sensors and also for suppressing Barkhausen noise. Comparing to standard GMR multilayer systems [4], the saturation field for obtaining GMR can be significant reduced by using the FM/AFM

bilayers in the structure of the magnetic sensors, which triggered a renewed interest in these phenomena [5-6]. In the Section 2.4, the application of the exchange coupling in FM/AFM will be further described.

2.2 Models for Exchange Anisotropy

In this section, we discuss several important models for the exchange anisotropy in FM/AFM films.

2.2.a Ideal Interface Model

The first simple model for exchange anisotropy was built by Meiklejohn and Bean [1-2]. They examined the exchange coupling across an ideal interface as shown in Fig. 2.2. The FM and AFM layers are both single crystalline and epitaxial across an atomically smooth interface. The spins of the first monolayer in the AFM adjacent to the FM layers are aligned toward the same direction, thus calling the interface as the uncompensated one. In this model, the switching field of the FM coupled to the AFM is determined by balancing the Zeeman, magnetocrystalline anisotropy, and exchange anisotropy energies. By assuming that the external field is not large enough to affect the sublattice magnetization of AFM, and the dominant anisotropy energy in FM and AFM is uniaxial magnetocrystalline anisotropy and their easy axes are aligned with each other, the general formula of total energy per unit area E (erg/cm^2) in this system can be expressed as:

$$E = -H M_s t_F \cos(\theta-\theta_F) + K_F t_F \sin^2\theta_F - K_e \cos\theta_F \qquad (2.1)$$

where the $M_s, t_F, K_F, K_e, \theta$, and θ_F represent the saturation magnetization

of the FM, the thickness of the FM, the uniaxial anisotropy constant of the FM, the interfacial coupling constant, the angle between applied field and easy axis, and the angle between magnetization of FM and easy axis, respectively.

The energy consists of the following three energies: (1) the Zeeman energy, $H\ M_s\ t_F\ \cos\ (\theta\text{-}\theta_f)$, (2) the magnetocrystalline anisotropy of the FM, $K_F\ t_F \sin^2\theta_F$, and (3) the exchange anisotropy energy, $-K_e \cos\ \theta_F$. Now, considering the switching field of FM, if the applied field H is changed from θ = 0° to θ = 180°, the required field to switch the ferromagnet can be calculated by taking the first derivative of Equation (2.1). The switching field can be expressed as:

$$H_{\text{switching}} = (2K_F\ /M_s) + [K_e/(M_s\ t_F)] \tag{2.2}$$

In Equation (2.2), the first term corresponds to the switching field for the intrinsic FM by a coherent rotational process, and the second term corresponds to the exchange field for the FM coupled to the AFM. Therefore, the exchange field (the shift of the loop center) is

$$H_e = K_e/(M_s t_F.) \tag{2.3}$$

To estimate the magnitude of K_e, taking the exchange energy per atom at the interface as J_i and the number of atoms at the interface as N results in a coupling energy of NJ_i. The number of interfacial atoms N is approximately equal to A/a^2, where A is the area of the interface and "a"

is the atomic spacing. This leads to an energy per unit area of interface of $\sigma_w = J_i/a^2$. K_e can be approximated by this interfacial exchange energy σ_w. Combining σ_w with $H_e = K_e/(M_s t_F)$ gives

$$H_e = J_i/(M_s t_F a^2) \tag{2.3}$$

The exchange field H_e is directly proportional to σ_w, but inversely proportional to both the magnetization and thickness of FM. The $1/t_F$ dependence of H_e is characteristic of a surface effect.

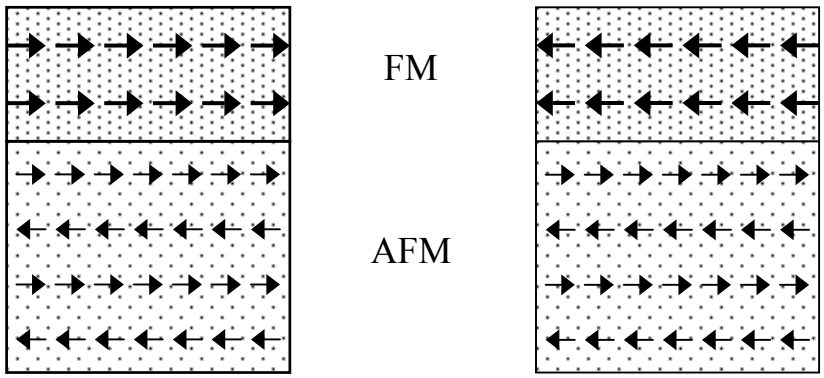

(a) $\theta = 0°$ (b) $\theta = 180°$

Fig. 2.2: Schematic diagrams of spin configurations of the ideal FM/AFM interface.

This model for exchange anisotropy is straightforward and describes the observed shifted hysteresis loop and $\sin\theta$ torque curve. However, the exchange field estimated by the model is two-to-three orders larger than the experimental value of the exchange field in the NiFe/FeMn system [7-8]. It is interesting to point out that, if one adopts this ideal

model as a guide for an intuitive picture, one is to expect: (1) the uncompensated interfaces should exhibit the largest magnitudes of H_e; and (2) the roughness of a compensated interface should increase the magnitudes of H_e. However, the experimental results [9] show that none of these expectations is fulfilled.

2.2.b Random Field Model

The assumption of the exchange coupling through an atomically perfect uncompensated boundary is refused by Malozemoff. He proposed a random-field model [10] to take the consideration of an interfacial AFM moment imbalance which originates from features such as roughness or structural defects. Consider a rough interface, starting with a single monatomic bump in the compensated simple cubic interface, as shown in Fig. 2.3. In these two configurations, the orientation of the spins in AFM is the same, but in FM the spins oppose each other. The local bump introduces more antiparallel pairs, marked as crosses, in configuration (a) than in configuration (b). Consequently, the local roughness leads to a difference of local interfacial exchange energy

$$\sigma_w = zJ/a^2, \tag{2.4}$$

where z is the number of order unity, i.e., the correlation number related to the number of antifarallel pairs, J is the interfacial exchange-coupling

constant, and "a" is the atomic spacing. This model argues that a net average non-zero interfacial energy will exist, particularly when the average is taken over a small number of sites. Statistically, the average σ_w in an area of L^2 will decrease as $\sigma_w \approx (\sigma_l/\sqrt{N})$ where $N = (L^2/a^2)$ is the number of sites projected onto the interface plane. Given the random field and assuming a single domain FM film, the AFM film will divide into domain-like regions normal to the interface to minimize the net random unidirectional anisotropy.

Although expansion of the domain size L would lower the random field energy, in-plane uniaxial anisotropy energy K_{AF} in the AFM layer will limit the domain size. Anisotropy energy confines the domain wall width to $\pi\sqrt{A_{AF}/K_{AF}}$, and creates an additional surface energy term of the domain wall $4\sqrt{A_{AF}K_{AF}}$ (surface tension in bubble domain), where the $A_{AF} \approx J/a$ is the exchange stiffness in AFM and K_{AF} is the anisotropy constant of the AFM. The balance between exchange and anisotropy energy is attained when $L \approx \pi\sqrt{A_{AF}/K_{AF}}$. Therefore, the average interfacial exchange energy density becomes

$$\sigma_w = \frac{4zJ}{\pi aL} \tag{2.4}$$

Accordingly, the exchange field due to the interfacial random-field energy density is

$$H_e = \frac{\sigma_w}{2 M_F t_F} = \frac{2z\sqrt{A_{AF}K_{AF}}}{\pi^2 M_F t_F} \qquad (2.5)$$

The factor of $\sqrt{A_{AF}K_{AF}}$ reduces the predicted exchange field to the levels observed in experiments of the NiFe/FeMn system. However, the most debatable point in this model is the estimation of the AFM domain size. If the size of the AFM domains is on the same order as that of the domain walls, this implies that most of the interface area actually consists of domain walls. It is not clear from this model how the exchange field is affected by the AFM domain walls at the interface.

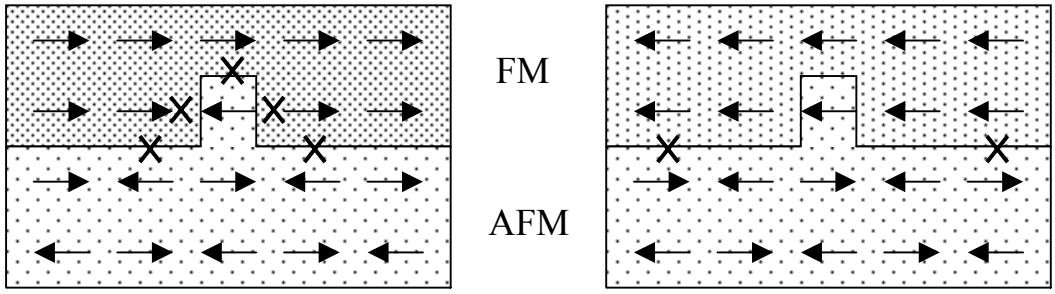

(a) (b)

Fig. 2.3: Schematic diagrams of possible spin configurations in the random field model.

2.2.c AFM Domain Wall Model

Shortly after Malozemoff's proposal, Mauri et al. proposed an alternative model to explain the discrepancy between the exchange field

value predicted by Equation (2.3) and experimental observations, [11]. The model proposed the formation of a planar domain wall at the interface with the reversal of the FM orientation. Assuming that the thickness of FM, t_F, is much smaller than the FM domain wall width, the domain wall will develop inside the AFM, as shown in Fig.2.4.

The energy required per unit area of this domain wall is $2\sqrt{A_{AF}K_{AF}}$. The FM reverses when the Zeeman energy of the ferromagnet is greater than the energy required to form a domain wall in the AFM. This leads to the more realistic equation $H_e M_s t_F = 2\sqrt{A_{AF}K_{AF}}$. Therefore, the model predicts that the exchange field is given by

$$H_e = \frac{2\sqrt{A_{AF}K_{AF}}}{M_F t_F} \tag{2.6}$$

In this model, the exchange energy is not concentrated across a single atomic interface but spreads out over a domain wall of width $\sqrt{A_{AF}K_{AF}}$. This leads to a reduction of H_e by a factor of $\sqrt{A_{AF}K_{AF}}$, the same reduction arrived at as with the random field model. However, the AFM domain wall model fails to explain the persistence of exchange anisotropy without diminution of H_e in the bilayers with AFM thickness of 25 Å, an order of magnitude lower than the characteristic domain wall width. In addition, it does not provide the clues to understand how compensated interface can yield values of H_e as large as, or even larger than, uncompensated ones [1].

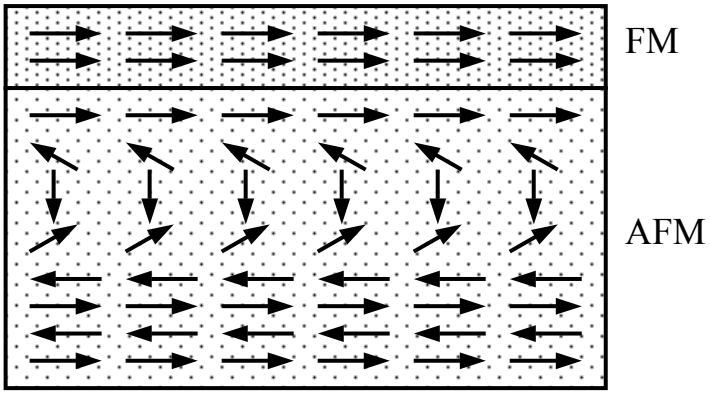

Fig. 2.4: Schematic diagram of spin configurations in the AFM domain wall model.

2.2.d "Spin-Flop" Orthogonal Interfacial Coupling

In 1997, Koon [12] dealt with the problem of exchange anisotropy in compensated FM/AFM interfaces by using micromagnetic calculations based on a Heisenberg model. His calculations indicate that the stable interfacial exchange coupling between the FM and AFM spin axes is in a perpendicular orientation. He refers to the perpendicular interfacial coupling as "spin-flop" coupling. In Koon's model, a single-crystal body centered tetragonal (bct) AFM structure was considered, as shown in Fig. 2.5 (a). The bct structure can be oriented to have a fully uncompensated interfacial spin plane (100) or a fully compensated interfacial spin plane (110). He included uniaxial anisotropy in the AFM crystal along the (001) direction, and assumed no intrinsic anisotropy in the FM layer. Two different cases of the AFM interfacial spin plane were applied in the model: (1) a fully compensated interface and (2) a fully

uncompensated interface. For both cases, he calculated the interfacial energy density as a function of the angle between the FM spins and the Néel axis of the AFM spins. The fully uncompensated interface gives the expected results of collinear coupling, a minimum at $\theta = 0°$. However, the fully compensated interface gives the surprising result of an energy minimum at $\theta \sim 90°$, indicating that the interfacial coupling between the FM and AFM spins prefers to the perpendicular coupling. In fact, Koon also showed that the spins in the AFM interface exhibit canting. The minimum energy is achieved with the AFM spins adopting a relatively small canting angle (<10°) relative to the Néel axis, as shown in Fig. 2.5 (b).

The Koon's model is an important and interesting milestone in the development of a satisfactory understanding, and thus of a comprehensive theory of exchange anisotropy. It pointed out the importance of relative orthogonal directions of the FM and AFM spins. While the model does not yield exchange anisotropy, it strongly influenced later works. In 1998, Schulthess and Butler [13-14] claimed that the spin-flop at the FM/AFM interfaces was insufficient to cause an exchange bias, but only induced a uniaxial anisotropy perpendicular to the AFM spins. Uncompensated spins at interface between FM and AFM are essential to produce exchange bias.

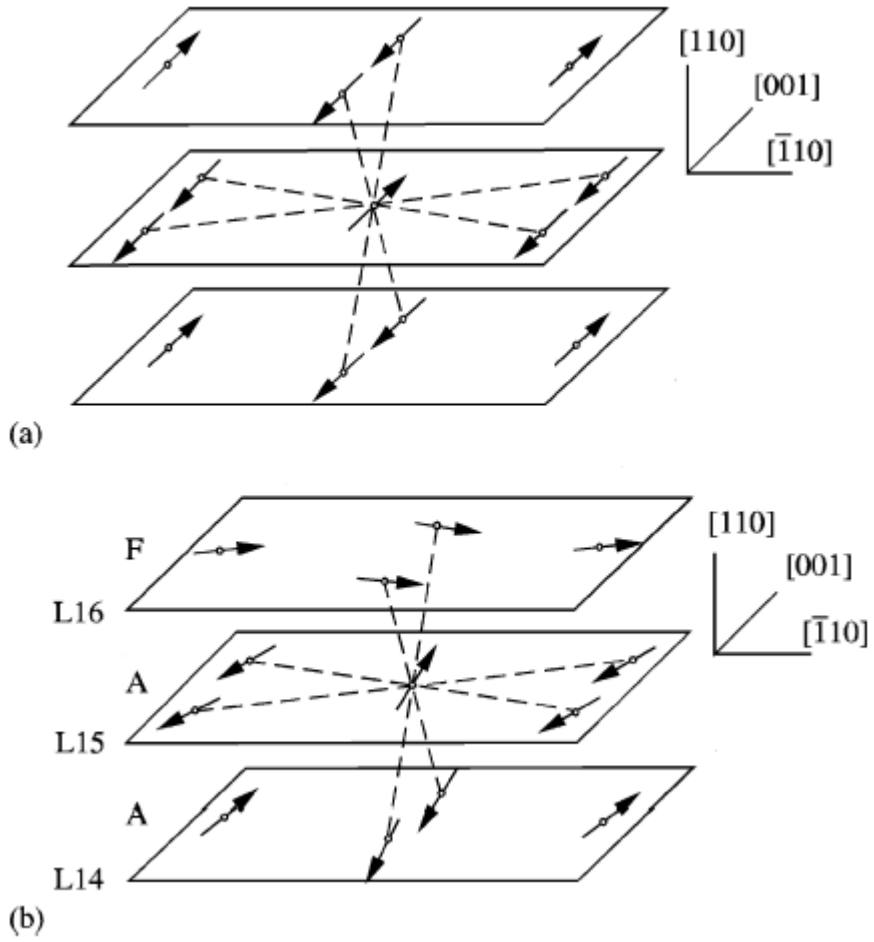

Fig: 2.5. (a) Magnetic structure of a body centered tetragonal (bct) AFM. (b) Lowest energy spin configuration near the interface plane. The interfacial AFM plane (L15) is fully compensated, and the interfacial FM plane (L16) is oriented perpendicular. The dashed lines represent the exchange bonds [13].

2.2.e Uncompensated Interface for Exchange Anisotropy

In addition to the above models, Takano *et al.* studied the CoO/MgO multilayers and NiFe/CoO bilayers to clarify the importance of uncompensated spins of AFM layer at the interface in exchange

anisotropy [l5]. CoO/MgO multilayers were used to determine the magnetic properties of uncoupled CoO films since MgO is nonmagnetic. The multilayers were cooled from 350 to 10 K in zero field (ZFC) and in +10 kOe (FC) and their thermoremanent moments (TMR) were measured. Fig. 2.6(a) shows the FC and ZFC measurements for the [CoO (103 Å)/MgO (30 Å)]$_{15}$ multilayers. The interfacial TMR density exhibits two feature (i) an intermediate temperature region (200≧T ≧50 K), where the magnetization is independent of temperature and (ii) a low temperature increase (T≦50K). The magnitudes of these two features scale closely with the number of CoO layers and have no dependence on the net CoO thickness in the multilayers. Therefore, the uncompensated moment of both features is an interface effect but not a bulk effect. From the neutron data, the measured interfacial uncompensated moment represents ~1% of the spins in a CoO monolayer. The permalloy/CoO bilayers were cooled from 350 to 10 K in a +10 kOe. Figure 2.6(b) shows H_e(T) of the bilayers with various CoO thicknesses. H_e(T) of the permalloy/CoO films exhibit the plateau and low temperature increase features in identical temperature regions, similar with the TMR of the Co. If the TRM of the CoO (103 Å)/MgO (30 Å) multilayers and H_e(T) of the permalloy/CoO (100 Å) bilayer are normalized at 70 K, the curves overlap at all temperatures. This correlation strongly suggests that the interfacial uncompensated spins which are responsible for the TRM play an important role in the exchange field mechanism. The ~1% of the interfacial uncompensated AFM spins is consistent with measured permalloy/CoO exchange field of ~1% derived from ideal interface model

[15]. In addition, the H_e dependence with the CoO thickness suggests a structural origin for the density of uncompensated spins. The exchange bias in the systems exhibits inverse proportional to the CoO crystallite diameter resulting from the different growth thickness. From the theoretical calculations, Takano et al. proposed that the surface morphology including roughness and grain size strongly affect the amounts of uncompensated spins at the interface and, thus, exchange bias in the FM/AFM bilayers.

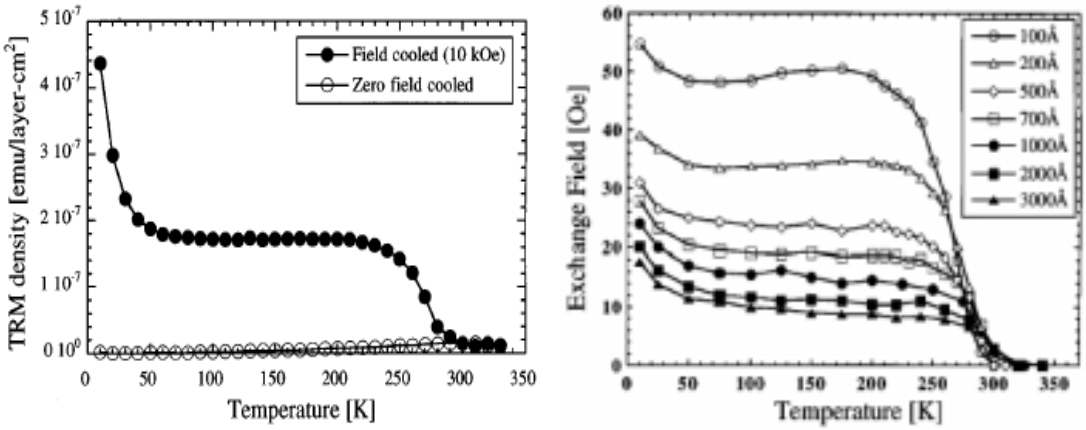

Fig. 2.6: (a) FC and ZFC moment density vs. temperature of the [CoO (103 Å)/MgO (30 Å)]$_{15}$ multilayer; (b) temperature dependence of H_e for permalloy (300 Å)/CoO bilayers with CoO thicknesses of 100 to 3000 Å [l5].

In additional to the above mentioned model, there are still some models to explain the exchange-coupling phenomenon in different FM/AFM systems. Although many studies have been done in the exchange-coupling phenomenon of FM/AFM, no one can successfully explain all the experimental findings.

2.3 Positive and Negative Exchange Bias

The main feature of normal EB is the displacement of the hysteresis loop to the direction opposite to the applied cooling field H_a. This shift of the hysteresis loop in the negative direction of H_a was invariable observed in weak field-cooled samples, thus called negative EB. However, in 1996, Nogués et al. discovered positive EB in FeF_2/Fe and MnF_2/Fe systems, a shift of hysteresis loop to the direction parallel to H_a [16]. In experiments, they sequentially deposited the antiferromagnetic FeF_2 with the Neel temperature T_N of 78.4K and ferromagnetic Fe on MgO (100) substrate by E-beam evaporator. The FeF_2 grows in the (110) orientation with compensated spins in the plane. As the FeF_2/Fe bilayer was cooled from 100 to 10 K under a weak positive magnetic field of + 2 kOe, the negative EB was observed at the temperature lower than T_N of FeF_2, as shown in Fig. 2.7(a). But if a strong applied field of + 70 kOe was adopted during the cooling process, the hysteresis loop of Fe was shifted toward to the direction of applied field and the exchange bias became positive, as shown in Fig. 2.7(b). Based on the assumption of the existence of an antiferromagnetic exchange interaction between the FM and AFM spins at the interface, a possible mechanism of the positive exchange bias is a competition between the FM-AFM exchange interaction and the magnetic static coupling between the external field and uncompensated spins of AFM at the FM-AFM interface. If the positive cooling field is large enough to align the uncompensated AFM spins in the positive direction as the AFM is cooled through T_N, the

FM-AFM system is in a state of high interface magnetic energy after cooling process because both of FM and interfacial uncompensated AFM spins are in the positive direction After the cooling field moves away at lower temperature than T_N, the interfacial uncompensated AFM spins remains toward the positive direction, leading to the positive exchange bias in FM layer because of antiferromagnetic exchange interaction between the FM and AFM spins at the interface. In the case of low cooling field, the static coupling between the cooling field and interfacial uncompensated AFM spins cannot overcome the antiferromagnetic exchange coupling between FM and interfacial AFM spins. The antiferromagnetic exchange coupling becomes dominated during the cooling process. Therefore, the FM spins are always in the positive direction of applied field during cooling while the uncompensated interfacial AFM spins aligned in the negative direction. After field-cooling, the FM spins and interfacial AFM spins are antiparallel and in a low-interfacial-energy state, leading to the normal negative exchange bias in the FeF_2/Fe bilayers.

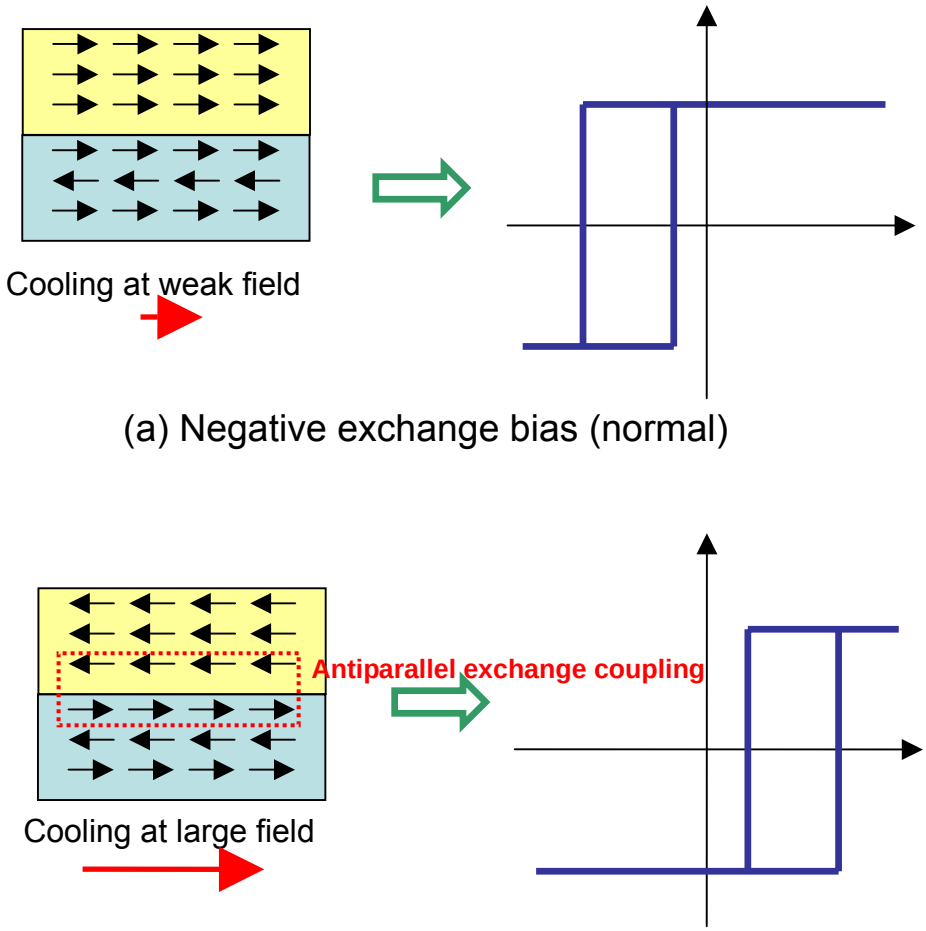

Fig. 2.7: (a) Negative and (b) positive exchange bias in FeF_2/Fe bilayers.

2.4 Application of FM/AFM Bilayers in Spin Valves

The exchange-coupling effect in magnetic thin-film systems has been extensively explored and even applied in the commercial products. The first proposed application of EB in the bilayers was as magnetic media [17-18]. By exchange coupling between FM-AFM the coercivity of recording layer was enhanced for the stability of recorded domains. In the writing process, small areas of an FM-AFM bilayer were heated up to $T_N < T < T_c$ of in the presence of a field opposite to the exchange bias field. At the moments, the coercivity of recording media was reduced and the magnetic moments were aligned toward the direction of applied field. However, the most important application of exchange-coupled FM-AFM systems is in the recording head with GMR sensors [19]. In the following content, the GMR effect and the spin-valve with FM/AFM bilayers will be introduced in detail.

2.4.a Giant Magnetoresistance (GMR) Effect

The first announcement of the GMR effect was reported in 1988 by Baibich et al in Fe (001)/Cr (001) superlattices prepared by molecular-beam-epitaxy (MBE) [20]. They discovered that the resistance of the sandwich-type superlattices with magnetizations aligned initially antiparallel at zero field decreased more than 50% after applying an external magnetic field of several Tesla, as shown in Fig 2.8. Because this decrease of resistance was very large, they called this effect as giant

magnetoresistance (GMR). The magnetoresistance in Fig 2.8 was measured at 4.2 K for different thicknesses of the Cr spacer. In the superlattices with specific thickness of thin Cr, the magnetization of adjacent Fe layers prefers the antiparallel alignment at a zero field because of Ruderman-Kittel-Kasuya-Yosida (RKKY) effect [21-22]. The resistance gradually drops when the magnetic external field overcomes the antiferromagnetic coupling and the alignment of magnetizations becomes a parallel arrangement, as shown in Fig. 2.9. Since the discovery, many studies have been devoted to clarify the physical origin of this phenomenon. Early theories using the free electron or single-band tight-binding model predict the existence of the GMR effect in the magnetic transition metal/ nonmagnetic metal mutilayer systems by assuming that the transport is carried out by the *s*-electrons [23]. In general, it is believed that the GMR effect can be explained by spin-dependent scattering, which results in different resistivities for the parallel and antiparallel configurations of the magnetization in adjacent magnetic layers through a non-magnetic layer. This spin dependence results from two main sources. One is the change in the electronic band structure due to alternation of the magnetization from antiferromagnetic to ferromagnetic alignment [24-25], which causes a change in the effective mass of conduction electrons or a change in the number of channels contributing to transport. For example, the majority electrons of Fe are much stronger scattered at Cr impurities than are the minority electrons [26]. This leads to different resistivities for the parallel and antiparallel alignment of the magnetization directions of the magnetic layers. The other one is spin-dependent random potentials [27-28]. Random potentials seem to be more relevant to GMR than the change in the electronic structure because GMR is also observed in granular magnetic alloys where no translational invariance exists.

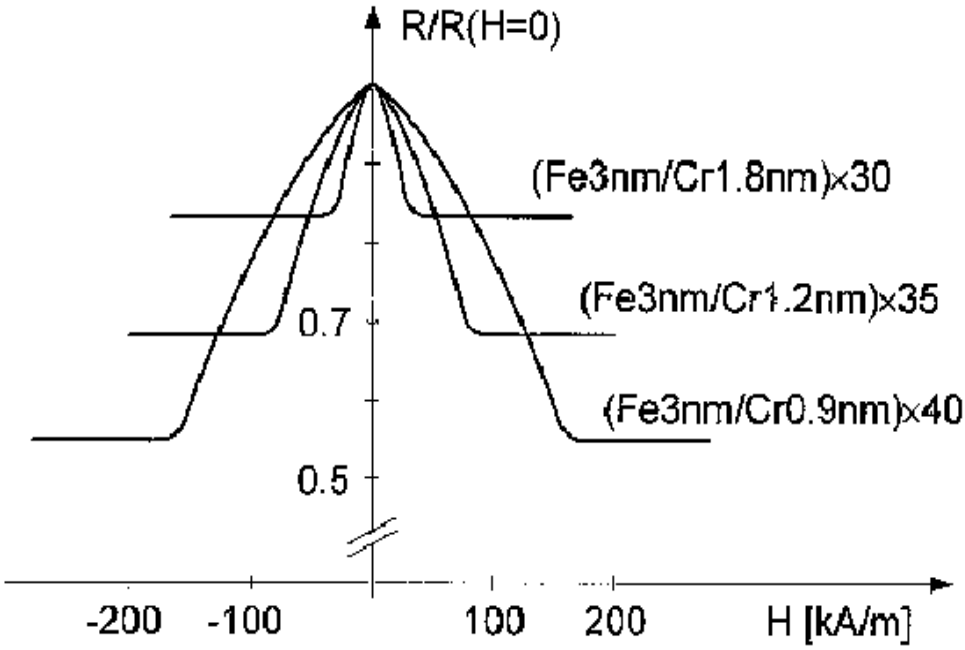

Fig. 2.8: First announcement of GMR effects [20].

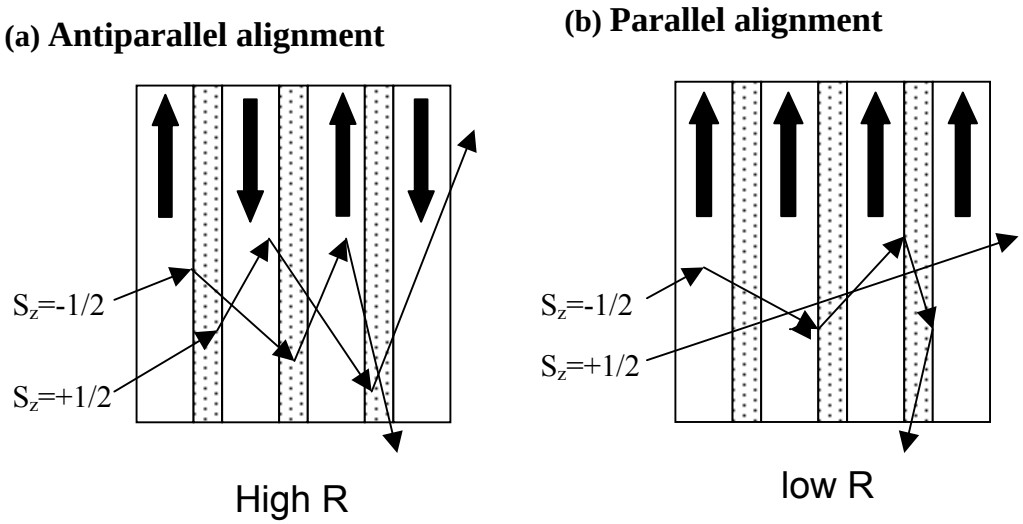

Fig. 2.9: Dependence of resistivity on magnetization alignment.

Many experiments later described evidence of GMR effects in the exchange-coupled multilayer structures. The best result was reported by Parkin, which obtained more than 60% of magnetoresistance in Co/Cu/Co multilayers at room temperature [29]. In addition, Parkin also proved that it was not necessary to produce epitaxial films to obtain the GMR effect. He obtained large magnetoresistance in polycrystalline samples manufactured using the faster sputtering method [30].

2.4.b Spin-valve Sensor with FM-AFM Bilayers

The main disadvantage of exchange-coupled GMR sensors composed of Fe/Cr or Co/Cu superlattices, compared to AMR sensors, is that a larger magnetic field is necessary to obtain the change of resistance. In the original experiment of Fe/Cr superlattices, the magnetic field of 2 kOe is necessary to obtain the saturated GMR. Therefore, the sensitivity of these sensors is smaller than AMR sensors despite their large magnetoresistance variation. An effective method of improving of the sensitivity of GMR sensors was introduced in 1991 by Dieny et al. [5]. They proposed a new type of GMR sandwich structure termed a spin-valve (SV) sensor. The SV films consist of two uncoupled ferromagnetic layers with in-plane anisotropy separated by a nonmagnetic metal. One of the FM layers is grown on or covered by an AFM layer, as shown in Fig. 2.10. The FM layer (called pinned layers) in contact with AFM layer has a shifted loop, but the other FM layer (called free

layer) has a conventional hysteresis loop like a single FM, as indicated in Fig. 2.11. Thus, there is a field range where the FM layers have antiparallel magnetization [5]. Because of the spin dependence scattering, the resistance is low when the magnetizations in the layers are parallel, but becomes high when the magnetizations are antiparallel [31]. In addition to the larger magnetoresistive effect than the usual anisotropic magnetoresistance (AMR), what makes these spin-valve devices attractive for applications is that the variation of the resistance occurs at rather low fields. In addition, an AFM layer was proposed to be deposited on the edges of the FM layer to avoid closure domains, and thus reduce the Barkhausen noise of the spin-valve devices [32-33]. Since the discovery of GMR in the form of spin valves composed of FM-AFM bilayers, a variety of devices have been built and proposed, such as read heads in hard disk, magnetic sensor, and so on [9]. As early as 1997, GMR was incorporated into the read-heads of magnetic hard disc recording systems, where it has been one of the main factors enabling the tremendous increase in storage density over the past decade.

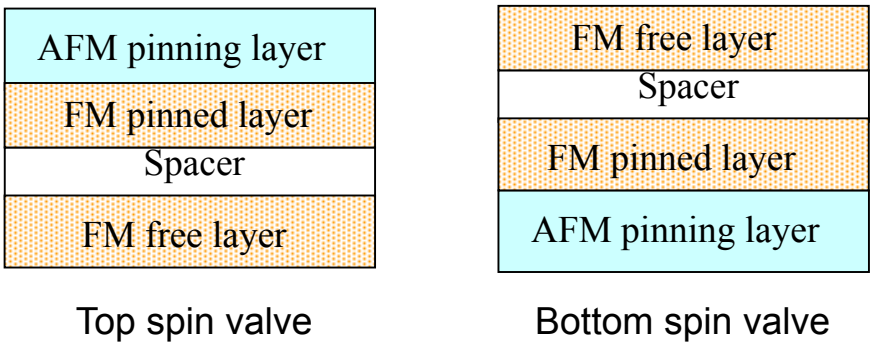

Fig. 2.10: Structure of spin valve.

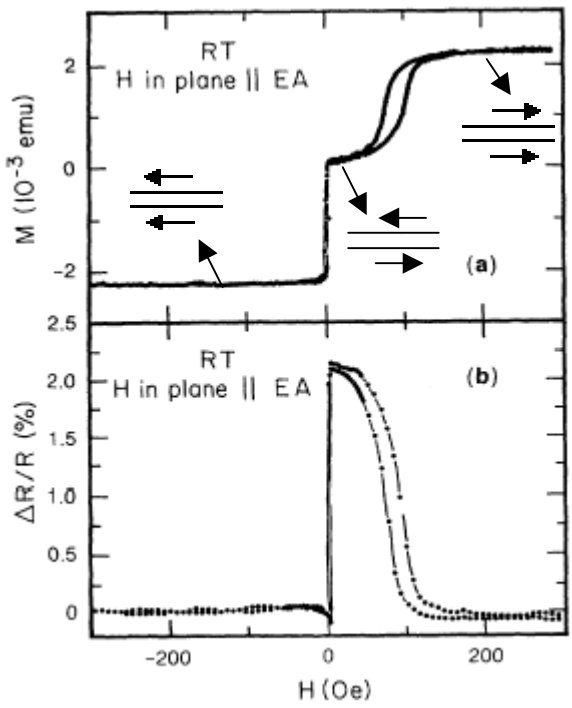

Fig. 2.11: Magnetic curve (a) and relative change in resistance (b) for Si/ NiFe 150Å/ Cu 26Å/ NiFe 150Å/ FeMn 100Å/ Ag 20Å. The field is applied parallel to the exchange anisotropy field created by FeMn [5].

Another important breakthrough was the demonstration in 1995 of large tunnel magnetoresistance (TMR) in tunnel junctions in which two ferromagnetic electrodes are separated by an ultrathin insulator [34]. Similar with that in spin valve, the FM-AFM bilayers was utilized in the TMR structure to manipulate the magnetization switching field of FM layers through the exchange-coupled mechanism. Key features [35] are the large spin dependence of the tunneling process, even at room temperature, and the reproducible fabrication of reliable tunnel barriers typically using 1–2 nm of Al_2O_3. These features facilitated the development of a high performance magnetic random access memory (MRAM). It is non-volatile, has low power consumption and fast

switching speed, and has the potential of becoming a universal memory. The first introduction of tunneling based MRAM into the market is imminent.

2.4.c GMR Effect in the Thin Films Containing Rare-earth Layers

Large GMR effect has been extensively reported in the transition metal multilayer and spin valve structures over the past decade. They have been interpreted as the consequence of either (1) spin-dependent potential that scatter itinerant magnetic charge carries at the interface between magnetic and specific non-magnetic layers or (2) the spin-dependent density of states at the Fermi level [36-37]. A variety of mechanisms are indeed possible in the transition metals because the same carriers are responsible for both magnetism and charge transport. This is not the case for the rare-earth metal, where the magnetism derives mainly from 4f states while charge transport is associated with 6s and 5d conduction orbitals. Therefore, multilayers consisting of rare earth metals and transition metals show no GMR [31]. However, an anomalous phenomenon of "positive" GMR was observed in the films of $(Co/Dy/Co/Cu/Co/Cu)_n$ multilayers and $Co_{65}Fe_{35}/Ag/(Co_{65}Fe_{35})_{50}Gd_{50}$ [38-39]. Most of the researches in GMR effect indicated the resistance was low as the magnetizations of adjacent magnetic layers preferred parallel alignment under large applied fields, and the resistance became high if the magnetizations preferred antiparallel alignment, as represented in Fig. 2.12 (a). The normal observed results are called as negative

GMR. The opposite is called positive GMR, shown in Fig. 2.12(b). In the experiments of Stanley *et al*. [38], a positive GMR of close to 4 % has been found at 4.2 K in the hybrid 3d/4f magnetic multilayer of the form Si/ Ta(45)/ {Co (8)/ Dy(18)/ Co(8)/ Cu(9)/ Co(26)/ Cu(9)}×*N*/ Ta(45) (numbers are nominal thickness in angstroms), as shown in the Fig. 2.13(b). In each repeat unit of this multilayer there are two main magnetic regions; the Co/Dy/Co part and the single Co layer, referred to as the composite layer and the free layer, respectively. In the part of Co/Dy/Co, the Dy and Co preferred antiferromagnetic coupling, and Dy moments are dominated because of its larger moments than Co, leading to the total moment of the composite layer is parallel to the Dy. Figs. 12.13(a) and 12.13(b) indicate the M-H and R-H loops of the 3d/4f magnetic multilayer. The switching fields determined by both methods are the same, which confirms that the magnetoresistance is associated with the magnetic alignment of the layers. The arrows in the magnetoresistance loop indicate the direction of the moments of the magnetic layers at the applied field. The small Co layers are represented by the small black arrows surrounding the larger chequered Dy arrow in the composite layer. The moments of these layers are always anti-parallel to the Dy moments. The large magneto- crystalline anisotropy of Dy leads to the higher coercivity of the composite layer than that of the free layer Co. While the net magnetizations of the composite and free layers are toward the positive direction at a positive saturation field, the Co magnetizations across the Cu spacer layer are anti-parallel, results in a high magnetoresistance state. As the field was reduced to zero, the moments of soft free layer Co reversed but the moments in the composite

layer remained in the original direction. As a result, the multilayer was in the low magnetoresistance state at low field because Co magnetizations across the Cu spacer layer are parallel.

In addition, as discussed in the above content, the GMR effect was only observed in the film with in-plane anisotropy. In the thesis, the positive GMR effect in the rare-earth-transition-metal (RE-TM)/ Cu/ RE-TM with perpendicular anisotropy will be shown and discussed in the chapter 8.

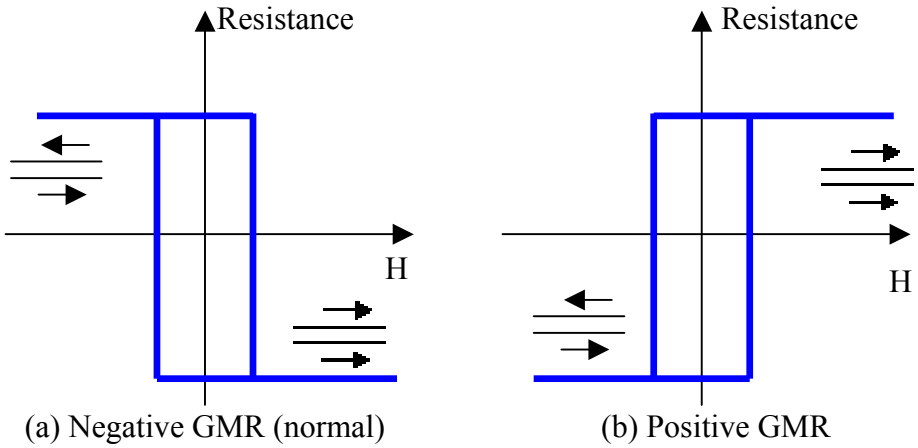

Fig. 2.12 R-H loops of (a) negative and (b) positive GMR structures.

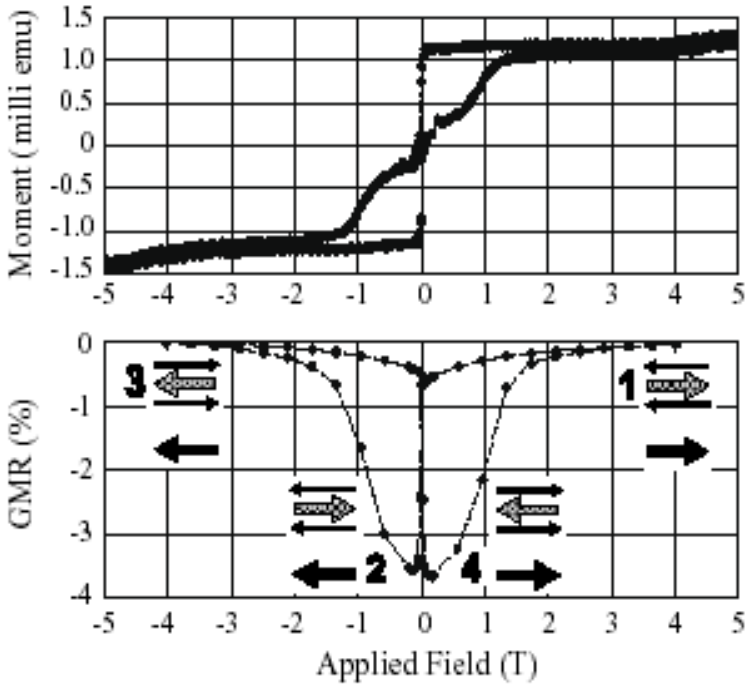

Fig. 2.13: Magnetization and magnetoresistance loops for an inverse GMR sample of the form Si/Ta(45)/{Co(8)/Dy(18)/Co(8)/Cu(9)/Co(26)/Cu(9)} ×10/Ta(45) at 4.2 K. The directions of the moments of the magnetic layers in one repeat unit of the structure are shown schematically on the magnetoresistance loop. The black arrows represent the Co layers and the chequered arrows represent the Dy layers [38].

Chapter 3

Background II--

Amorphous Rare-earth-transition-metal-alloy Films

The materials composing of heavy rare-earth (RE), like Gd and Tb, and transition metal (TM) are ferrimagnetism [1], which is composed of two kinds of magnetic sublattices preferring antiparallel exchange-coupling. Because of the characteristics of perpendicular anisotropy, amorphous structure, suitable thermomagnetic properties, and high Kerr effect, the RE-TM-alloy films have been widely explored and commercially used in magneto-optical (MO) recording since the end of 1990s. This chapter focuses on the introduction of RE-TM materials with perpendicular anisotropy, especially those used in MO disks, like TbFeCo, TbFe, DyCo, and GdFeCo. At the first, I will introduce the magnetic properties of single-layer RE-TM. Then, domain-wall model and the magnetization-switching mechanism of exchange-coupled double-layer (ECDL) films will be discussed. Finally, I will describe the applications of the material in MO recording and an advanced storage technique of heat-assisted magnetic recording.

3.1 Magnetic Properties of RE-TM Films

3.1.a Ferrimagnetic RE-TM Materials

The development of the RE-TM materials can be traced to early work on RE-TM intermetallic compounds [2]. The alloys like $GdCo_5$ were studied in the early 1960s for the application of permanent magnets. The heavy REs like Gd and Tb have high magnetic moments but low Curie temperatures. It was supposed that the Curie temperature of RE could be significantly increased by exchange coupling between RE and TM spins to take the advantage of high moments of RE in the alloy at room temperature. However, it was found that the heavy REs (Gd to Lu) always couple antiferromagnetically to TM moments [1]. On the other hand, the light REs prefer ferromagnetically coupled to the TM so they are used in permanent magnets. A typical example is $SmCo_5$, which possesses very high magnetic energy product.

The difference of exchange-coupling behavior between the light and heavy RE is considered as the consequence of the nature of the RE-TM exchange interaction combining with Hund's rule based on the quantum mechanics [3].

1. Hund's first rule:

   In the ground state, the spin angular momentum quantum ***S*** of an atomic subshell will have the largest possible value consistent with the exclusion principle.

2. Hund's second rule:

The orbital angular momentum quantum number $\boldsymbol{L}$ of an atomic subshell has the largest value consistent with the first rule and with the exclusion principle.

3. Hund's third rule:

If the subshell is less than half-filled, the spin and orbital angular momenta couple in an antiparallel fashion (in the low-lying energy states). Under these circumstance the total angular momentum quantum number $\boldsymbol{J}$ is given by $\boldsymbol{J} = |\boldsymbol{L} - \boldsymbol{S}|$. On the other hand, if the subshell is more than half-filled, the spin and orbital momenta couple parallel to each other, and the net angular momentum quantum number will be $\boldsymbol{J} = |\boldsymbol{L} + \boldsymbol{S}|$.

According to the statements, the light REs have a less than half filled 4f shell so that $\boldsymbol{J} = |\boldsymbol{L} - \boldsymbol{S}|$, meaning that $\boldsymbol{J}$ and $\boldsymbol{S}$ have the opposite direction. The heavy REs follow $\boldsymbol{J} = |\boldsymbol{L} + \boldsymbol{S}|$ and their $\boldsymbol{J}$ and $\boldsymbol{S}$ have the same direction. In addition, the exchange between the RE spin and TM moment is always negative [1]. Therefore, the net moment of RE is always antiparallel to the TM in the heavy RE-TM materials because of the same direction of $\boldsymbol{J}$ and $\boldsymbol{S}$, as shown in Fig. 3.1(a). In the light RE, $\boldsymbol{L}$ is typical greater than $\boldsymbol{S}$ and thus $\boldsymbol{J}$ is antiparallel to $\boldsymbol{S}$. However, the $\boldsymbol{S}$ of the RE is antiparallel to TM moment; consequently, the net moments of the light RE and TM are parallel as shown in Fig 3.1(b). As for the negative exchange between the RE spin and TM moment, it mainly due to the exchange of RE is directly associated with the outside 6s and 5d electrons which have much greater radical extent than the 4f. The

exchange between the RE 5d and TM 5d spins prefer ferromagnetic interaction but the 5d-4f intra-atomic exchange in the RE is strongly antiferromagnetic [4], resulting in the observation of the negative exchange between the RE spin and TM moment. In the following content, the description of the materials composed of heavy RE and TM elements will be concentrated.

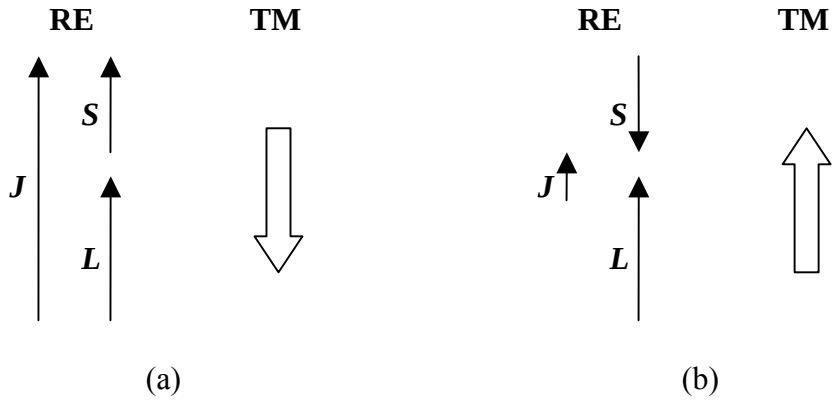

Fig. 3.1: Diagram of exchange coupling of (a) heavy RE- and (b) light RE-TM.

3.1.b Magnetization and Coercivity Dependence on Composition

Because of the applications in MO recording, the amorphous heavy RE-TM alloy films, like TbFeCo, DyCo, GdCo and so on, have been extensively studied [5]. The magnetic properties of the RE-TM film are strongly dependent on the composition because they are ferrimagnetism. As described in the above, the net magnetization reflects the difference of the RE and TM magnetic moments rather than the sum. That is

$$M_{net} = \mid M_{RE} - M_{TM} \mid , \qquad (3.1)$$

where M_{net} is the net magnetization, and M_{RE} and M_{TM} respectively represent the RE- and TM-subnetwork magnetic moments. Fig 3.2 typically shows the dependence of magnetization and coercivity of the RE-TM films on the composition. The zero magnetization occurs as the M_{RE} and M_{TM} are completely offset by each other at some composition, called compensation composition. The coercivity of RE-TM alloy is extremely large at the content. With varying the composition far away from the compensation, the net magnetization and coercivity respectively become high and small. If the RE content is larger that the composition, the RE becomes dominated in the alloy and determine the direction of net magnetization, thus called the alloy is RE-rich. The opposite is TM-rich.

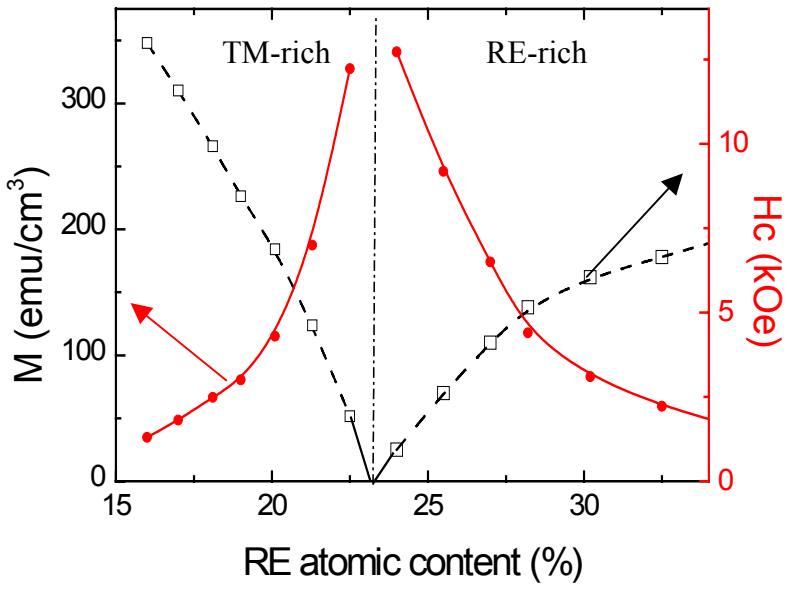

Fig. 3.2: Dependence of net magnetization and coercivity of heavy RE-TM films on the composition.

3.1.c Thermomagnetic Properties of RE-TM Films

Another important characteristic of the RE-TM films is their thermomagnetic properties. As indicated in Fig. 3.3, the M_{RE} decrease rapidly with increasing temperature while the M_{TM} slightly reduces until the drop near Curie temperature Tc. The net magnetization becomes zero because of the offset between M_{RE} and M_{TM} at the compensation temperature (T_{com}) where the coercivity of RE-TM film is close to infinite. With increasing temperature to Tc, the coercivity gradually decreases to zero. At the temperature lower than T_{com}, the RE-TM films are RE-rich. However, the films become TM-rich as the temperature is more than T_{com}. Because of the temperature dependence of magnetic properties, the RE-TM films are practically utilized in the commercial MO disks. It will be discussed in details later.

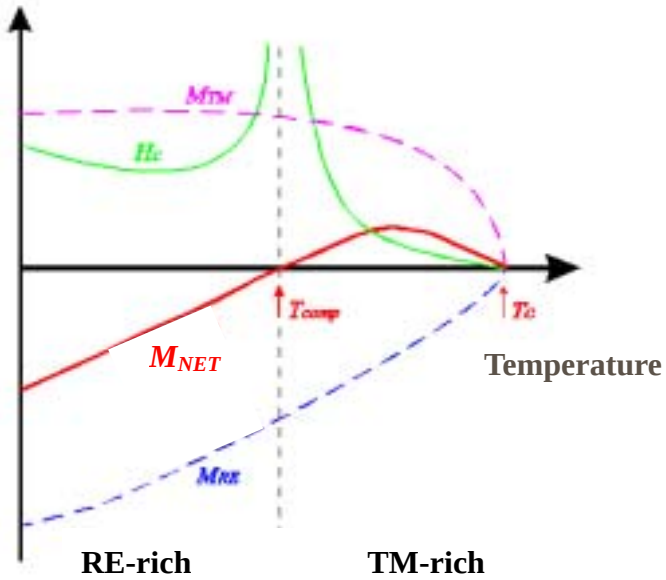

Fig. 3.3: Relationship between temperature and magnetic properties in RE-TM alloys.

3.1.d Perpendicular Anisotropy of RE-TM Films

The RE-TM films also exhibited high perpendicular anisotropy. The origins of the perpendicular anisotropy have more than one mechanism. Some believable mechanisms are showed at the below.

1. Single-ion anisotropy :

Spin-orbital coupling is often the dominated mechanism of anisotropy in the alloys and compounds of the non-S-state RE elements. These elements, like Tb and Dy, have non-spherical 4f electron density distributions, meaning that orbital moments exist. The orbital moment is coupled to the spin magnetic moment. At the same time, the charge distribution interacts electrostatically with the charge distribution of the site in the solids where the rare-earth elements are located, further induced a preferred orientation of moments. This is referred to as the crystal field or the local field in the amorphous solids. The orientation of a given crystal field depends on the shape of the rare-earth 4f charge density distribution which can usually be described as a prolate or oblate ellipsoid [6-7].

2. Stress-induced anisotropy:

The magnetic anisotropy can be induced by the stress in the films or from the substrate in the magnetic systems [8]. The mechanism is through the inverse magnetostriction effect [9]. The stress-induced anisotropy can be given by

$$K_{\sigma} = -(3/2)(\delta l/l)\,\sigma \qquad (3.2),$$

where $\delta l/l$ and σ are the linear magnetostriction and planar stress. Because of the non-spherical 4f-electron charge density distribution, the heavy REs have large magnetostriction. The sign of the magneto-striction also depend on whether the 4f charge distribution is prolate or oblate.

3. Shape anisotropy:

Because of diploe-diploe interaction, the demagnetizing field H_d, a internal field, is produced in the magnetic films and induced an magnetic anisotropy [11]. H_d can be given by

$$H_d = - N_d M \qquad (3.3),$$

where N_d is the demagnetizing factor which depends on the shape of the sample. In the c.g.s. system of units, the sum of the demagnetizing factors is equal to 4π or in rectilinear coordinates:

$$N_x + N_y + N_z = 4\pi \qquad (3.4),$$

Thus, for a sphere, $N_x = N_y = N_z = 4\pi/3$ because of the symmetric shape. In the prolate ellipsoid with a large ratio of major and minor axis, the shape anisotropy K_s can be shown by:

$$K_s = (1/2)\,(N_x - N_z)\,M^2 \qquad (3.5).$$

In discussing shape anisotropy in the amorphous RE-TM film, the microstructure should be taken into the consideration. The growth mechanism of columnar structure has been found in some RE-TM films, especially in those with rich Co [12]. The structure leads to a perpendicular anisotropy in the films. Other microstructural feature such as elongated, oriented voids can also cause shape anisotropy.

4. Pair-ordering anisotropy:

The anisotropy originates from the difference in the number of neighbors in-plane and out-of-plane due to relaxed growth-induced local stress [13]. It usually is observed in the crystalline alloys. Néel et al. has shown that when NiFe is annealed in a magnetic field under neutron irradiation, it develops a uniaxial anisotropy because of ordering of Fe-Fe pairs [14]. After field-annealing, more Fe-Fe pairs are oriented with the pair axis perpendicular to the applied field direction. The pair ordering was detected by neutron diffraction. The easy axis is along the direction that the field was applied during annealing. The pair ordering is certainly possible to exist in an amorphous alloy by short-range ordering [13].

5. Bond-orientational anisotropy:

The anisotropy is associated with anisotropic bonding at the film surface which originated from the classical dipole-dipole interactions [15].

Fig. 3.4 shows two bonding states of RE and TM atoms related with the spin orientation. The spins of antiparallel RE and TM are perpendicular to the bonding plane in the Fig 3.4(a), and lie in the plane in the Fig. 3.4(b). Considering the dipole-dipole interactions and exchange coupling of adjacent RE and TM spins, two atoms whose moments are antiferromagnetically coupled by exchange force will have the lowest value of dipole-dipole energy (U) when their dipole moments are perpendicular to the bond ($U_{\perp} = - m_{RE}m_{TM}/(r_{RE}+r_{TM})^3$). On the other hand, the dipole-dipole energy will be maximized when the antiparallel moments are aligned with the bond ($U_{/\!/} = +2m_{RE}m_{TM}/(r_{RE}+r_{TM})^3$). In addition, the bonding plane of the atoms near the surface generally is parallel to the film surface. Based on the two arguments, the antiferromagnetic-coupling spin pairs of RE-TM near the surface contributed a perpendicular anisotropy to the film.

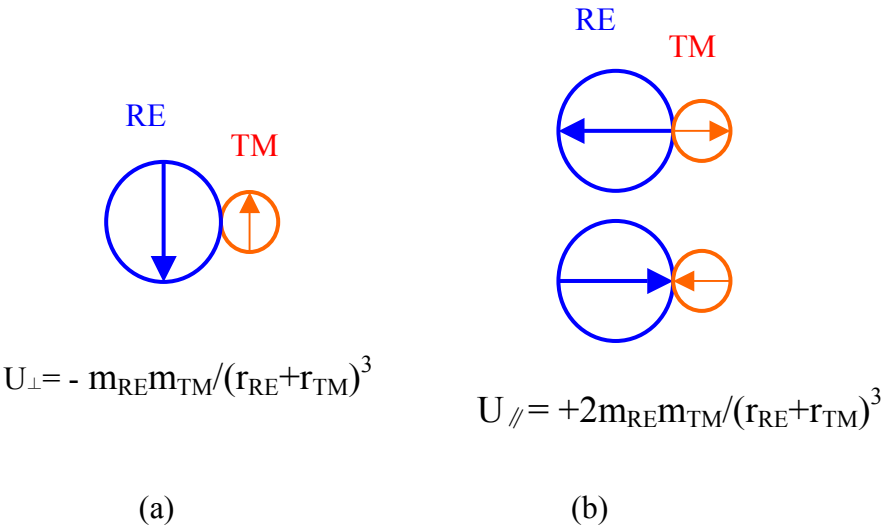

Fig. 3.4: Two bonding states of RE and TM atoms related with the spin orientation. The spins of antiparallel RE and TM are (a) perpendicular and (b) parallel to the plane.

3.1.e Strong Kerr Effect

When linearly polarized light is incident upon the surface of a magnetic material, the reflected light in most cases is elliptically polarized with the major axis of the ellipse rotated through some angle, called Kerr angle, from the vibration direction of the incident linearly polarized beam. The portion of the ellipticity and rotation is known as the Kerr magneto-optical effect [3]. Generally, the amount of the rotation is small, much less than one degree, and depends on the direction and the magnitude of 3d moments in TMs. The 4f spins in the REs are less contributed to the Kerr effect. The effect is classified as polar, longitudinal, or transverse depending on the direction of the magnetization relative to the surface and the plane of incidence. As shown in the Fig 3.5(a), the polar Kerr effect is usually measured in the magnetic films with perpendicular anisotropy where the beam illuminates perpendicularly to the film surface. The Fig 3.5(b) indicates the measurement of longitudinal Kerr effect in which the magnetization is in both the plane of the surface and the plane of incidence. The transverse effect, shown in Fig 3.5(c), is where magnetization lies in the plane of the film and perpendicular to the plane of incidence.

Heavy RE-TM films with perpendicular anisotropy exhibits strong Kerr effect with the rotation more than 0.5 degree [4]. Thus, the signal recorded in the MO disks composed of RE-TM films can be read by Kerr-angle detection. We will introduce the reading mechanism in MO recording in details later.

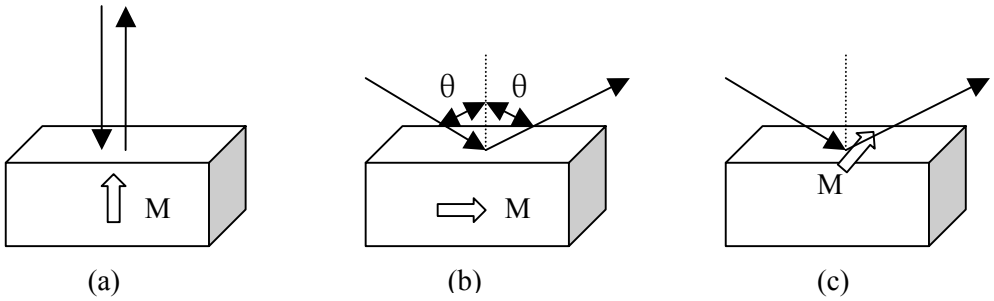

Fig. 3.5: Kerr effect --- (a) polar, (b) longitudinal, and (c) transverse.

3.2 Magnetic Behaviors in ECDL RE-TM Films

To improve the recording performance in MO recording, the RE-TM multilayers were theoretically and experimentally studied since 1990s [5]. The magnetic properties, such as coercivity, switching field, and Curie temperature, were manipulated through exchange coupling between the RE-TM layers. In the following, the magnetic behaviors in ECDL RE-TM films will be described.

3.2.a Interfacial Wall in ECDL RE-TM Films

As discussed in the beginning of this chapter, the heavy RE and TM moments are antiferromagnetically exchange-coupled. When a double-layer RE-TM film composed of TM-rich and RE-rich layers are under a sufficiently strong magnetic field, a net magnetization of both layers aligns themselves parallel to the field to minimize Zeeman energy. Since the magnetic spins of TM (RE) are oppositely directed in the two layers, a region appears between the layers where the spin gradually changes in its direction, as illustrated in Fig. 3.6. A domain wall similar to a Block wall [5] appears at the interface between two layers, so called an interfacial wall. Similar to Block wall, exchange and anisotropy energies are stored in this region and the classical equation of the Block-wall energy $\Delta\sigma$ can be given by [16]

$$\Delta\sigma = 4\sqrt{AK_u} \qquad (3.6).$$

Here, “A” indicates the exchange stiffness coefficient of magnetic spins in the film. A micromagnetic analysis of interfacial walls has been performed by Kaneko et al. [17]. Their results indicate that the interfacial exchange energy in ECDL films depends on the wall position. The lowest energy is obtained where the wall position is shifted from the center of the interface toward the layer side with the lower anisotropy energy.

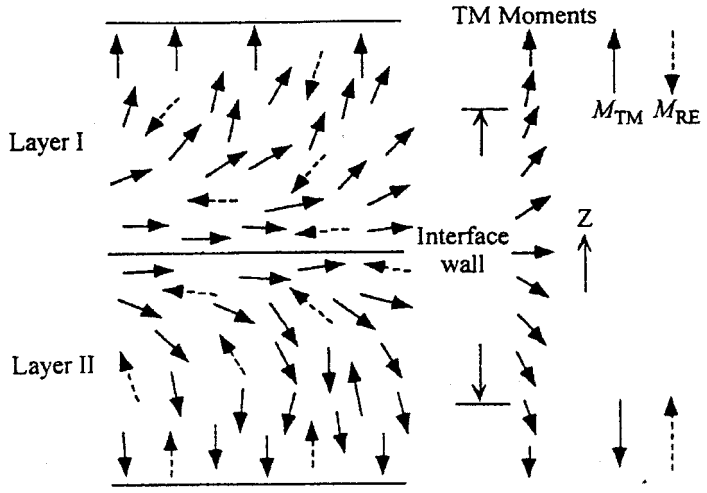

Fig. 3.6: Schematic illustration of the interfacial wall in a ECDL RE-TM film [5].

3.2.b Magnetization-switching Mechanism in ECDL RE-TM Films

In principle, the magnetization-switching mechanism of ECDL films should be treated on the basis of micromagnetic model. A model proposed by Kobayashi et al. [18] has been widely employed in the

analysis of magnetization processes of exchanged-coupled rare earth-transition metal films. The model deals with exchange-coupled dual-layer films consisting of ferromagnetic materials with the following assumptions: (1) the magnetization within each layer is directed along the film normal, leading to the hysteresis loop of each layer completely square; (2) the coercivity exists unique to each other, which opposes the magnetization to reverse; (3) the magnetic walls are created and annihilated only at the interface between two layers; (4) the interfacial wall energy $\Delta\sigma$ remains constant during the magnetization switching process; and (5) the thickness of each layer is large compared to the domain wall width.

The ECDL film consisting of two layers respectively with TM-rich and RE-rich composition is called the antiparallel (A-) type. As both the two layers are TM-rich (or RE-rich), the film is parallel (P-) type. Fig. 3.7 illustrates the four magnetization states and switching mechanisms of the A-type ECDL film. Because the TM (or RE) spins of two layers is ferromagnetically exchange-coupled to each other and the exchange between RE and TM spins are antiferromagnetic, the magnetizations of TM-rich and RE-rich layers prefer to align antiparallel at zero field, as shown in the states 2 and 3. As a positive or negative saturation field is applied to the film, the magnetizations of two layers are parallel while the interfacial walls are formed between two layers, as indicated in the states 1 and 4. As the field is reduced from positive to negative saturation, the magnetization state change from the state 1 toward the 2 through various paths. The actual magnetization process is determined by comparing the magnitude of the switching field H_{ij} at which the change of magnetization

state from i to j occurs.

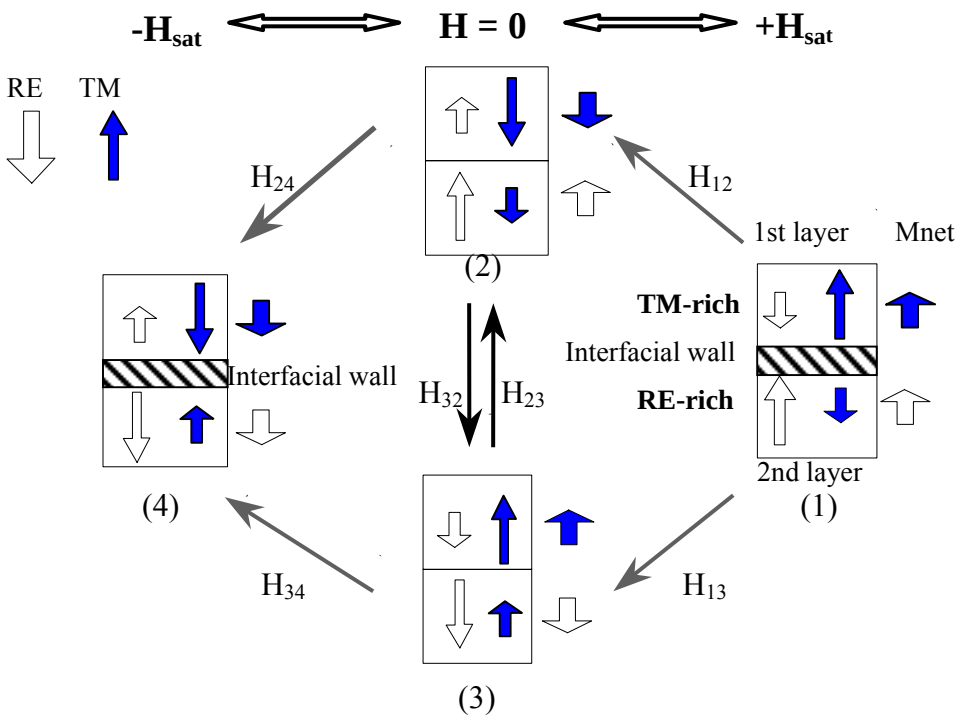

Figure 3.7 Paths and switching fields of A-type ECDL film.

To obtain the switching field H_{ij}, we consider the free energy of magnetization state, which only takes the Zeeman energy and exchange interaction energy into account for simplification. In A-type ECDL field, the switching field H_{12} is obtained as follows. The total free energies E_1 and E_2 of the magnetization states 1 and 2 under some applied field H are given as

$$E_1 = -M_1 t_1 H - M_2 t_2 H + \Delta\sigma \tag{3.7}$$

and

$$E_2 = +M_1 t_1 H - M_2 t_2 H \quad . \tag{3.8}$$

Here, M, t, and subscripts 1 and 2 respectively denote magnetization, thickness, and the first and second layers. Because the anisotropy energy of Ku does not vary with magnetization switching, after the subtraction E2 from E1, the term will be canceled. Consequently, we do not need to take Ku into account. In this transition, the magnetization reversal takes place only in the first layer so that the difference of E_1 and E_2 should be the coercivity energy of the first layer as

$$E_1 - E_2 = -2M_1 t_1 H_{c1} \tag{3.9}.$$

Combining Eq. (3.7), (3.8), and (3.9), the switching field H_{12} can be obtained as

$$H_{12} = \frac{\Delta\sigma}{2M_1 t_1} - H_{c1} \tag{3.10}.$$

By the same manner, the other switching field H_{ij} can be derived in the following.

$$H_{13} = \frac{\Delta\sigma}{2M_2 t_2} - H_{c2} \tag{3.11}$$

$$H_{14} = -\frac{M_2 t_2 H_{c2} + M_1 t_1 H_{c1}}{M_2 t_2 + M_1 t_1} \tag{3.12}$$

$$H_{23} = -\frac{M_2 t_2 H_{c2} + M_1 t_1 H_{c1}}{M_2 t_2 - M_1 t_1} \tag{3.13}$$

$$H_{24} = -\frac{\Delta\sigma}{2M_2 t_2} - H_{c2} \tag{3.14}$$

$$H_{34} = -\frac{\Delta\sigma}{2M_1 t_1} - H_{c1} \tag{3.15}$$

The conditions to realize a certain specified process are determined by comparing the magnitude of switching fields given by Eqs. (3.10) - (3.15). It is assumed that the magnetic moments of the second layer is larger than the first, meaning $M_2\ t_2 > M_1\ t_1$.

For the A-type film under an applied field decreasing from the positive to negative saturation, the first transition beginning from state 1 is either 1→2, 1→3, or 1→4. As the magnetic field varies from the positive saturation to the negative, the reversal at larger switching field first happens, therefore, the condition for 1→2 is that $H_{12} > H_{13}$ and $H_{12} > H_{14}$, rewritten as

$$\frac{\Delta\sigma}{2M_1 t_1} - \frac{\Delta\sigma}{2M_2 t_2} > H_{c1} - H_{c2} \tag{3.16}$$

The next transition starting from state 2 is either 2→3 or 2→4, which can be realized because H_{23} and H_{24} are smaller than H_{12} as mentioned above. The condition for the transition 2→3 is

$$\frac{\Delta\sigma}{2M_1t_1} - \frac{\Delta\sigma}{2M_2t_2} > H_{c1} + H_{c2} \tag{3.17}$$

In this case, the final transition is 3→4. Combining the Eqs. (3.16) and (3.17), the condition for the process 1→2→3→4 is given by Eq. (3.17). If $H_{24} > H_{23}$, the transition 2→4 is realized. Thus, the condition for the process 1→2→4 is obtained as

$$H_{c1} + H_{c2} > \frac{\Delta\sigma}{2M_1t_1} - \frac{\Delta\sigma}{2M_2t_2} > H_{c1} - H_{c2} \tag{3.18}$$

Fig. 3.8 shows the typical M-H loop of the A-type ECDL film following the magnetization-switching mechanism 1→2→4. The dash line is the initial curve indicating the transition from state 2 to 1. The switching field H_{21} can be given by

$$H_{21} = \frac{\Delta\sigma}{2M_1t_1} + H_{c1} \tag{3.19}$$

From the combination of Eqs. (3.10) and (3.19), we can experimentally obtain the interfacial exchange energy and biasing field of the first layer H_{b1} produced through exchange interaction with the second layer by the equations

$$\Delta\sigma = M_1t_1(H_{12} + H_{21}) = M_1t_1H_{b1} \tag{3.20}$$

and

$$H_{b1} = \frac{(H_{12} + H_{21})}{2} \tag{3.21}$$

The conditions for magnetization-switching mechanisms in P-type ECDL films can also be derived by the same manner. Fig. 3.9 exhibits the magnetization states and switching paths in P-type films. The process 1→4 is realized for

$$\frac{\Delta\sigma}{2M_1t_1} + \frac{\Delta\sigma}{2M_2t_2} > \left|H_{c1} - H_{c2}\right| \tag{3.22}$$

The process 1→2→4 is for

$$H_{c2} - H_{c1} > \frac{\Delta\sigma}{2M_1t_1} + \frac{\Delta\sigma}{2M_2t_2} \tag{3.23}$$

It should be noted here that the theory for P-type is applicable to ferromagnetic double-layer films.

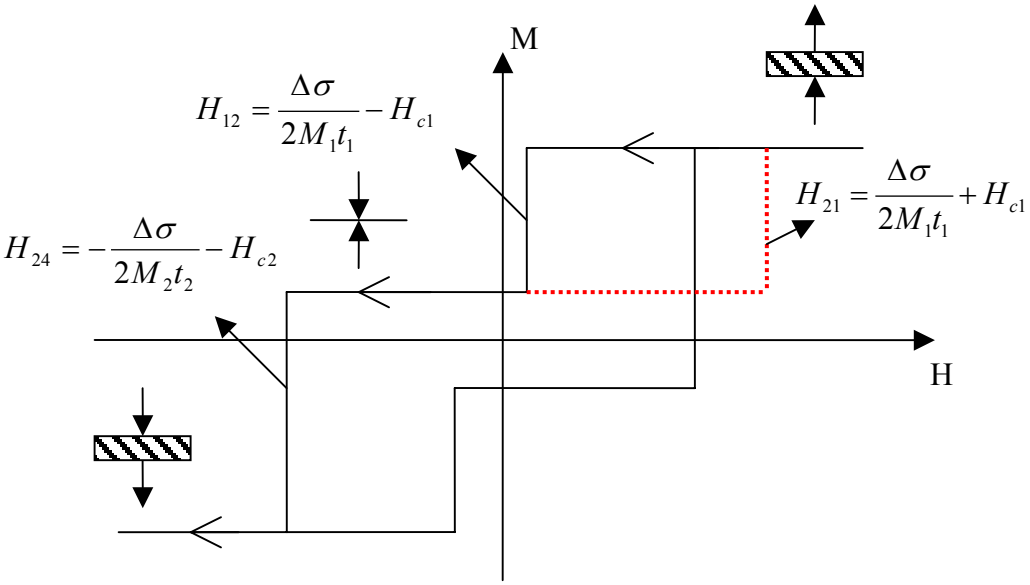

Figure 3.8: M-H loop of A-type ECDL film following the magnetization-switching process 1→2→4.

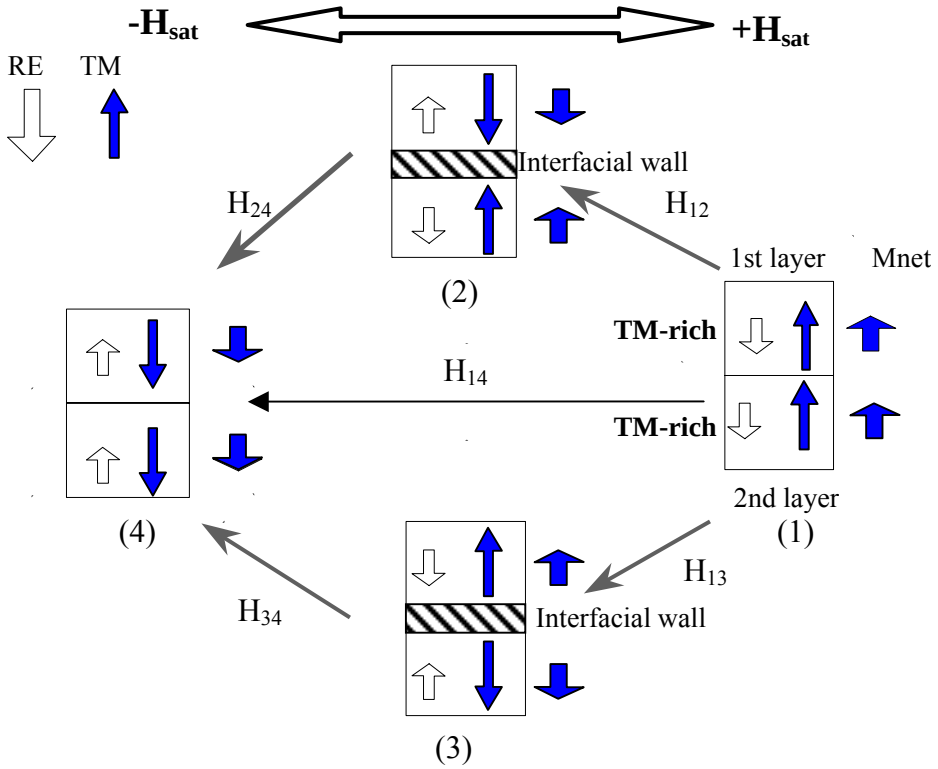

Figure 3.9: Paths and switching fields of P-type ECDL film.

3.3 Applications of RE-TM Films

3.3.a Magneto-optical Recording

Since the discovery in the late 1960s, amorphous RE-TM materials are considered as the promising media for MO storage [19-23]. After the development on the optimization of fabrication and composition, the RE (Gd,Tb,Dy)- TM (Fe,Co) films have become the recording materials of rewritable MO disk. In the following, the reading and writing in MO recording will be introduced.

3.3.a.1 Writing Mechanism

In MO recording, the signal writing and erasing are both achieved by the thermomagnetic process [20-21], so the temperature characteristics of the magnetic properties play dominant roles. Because of consideration of stability of recorded domain, the recording media have to possess the coercivity of several thousand Oe at the ambient temperature by properly choosing the composition. On the other hand, the coercivity should be less than a few hundred Oe at high temperature to reliably write the signal in the media by low external field. Fig. 3.10 shows the temperature dependence of the coercivity for an MO film whose T_{comp} is near room temperature so that its coercivity is extremely large here. With

temperature increase to Tc, the coercivity rapidly decreases to zero. In the writing process, a laser beam is focused on the disk to heat a small area to the vicinity of its Curie point, as indicated in Fig. 3.11. Simultaneously, a small external field was applied to decide the direction of magnetization of the heated spot. After the laser moves away from the area, the material cools down soon and the written domain recovers to high-coercivity state. Since the direction of magnetic moments is determined by the extra magnetic field, we may define the magnetic domains with upward magnetizations as mark "1" and those with downward magnetizations as mark "0".

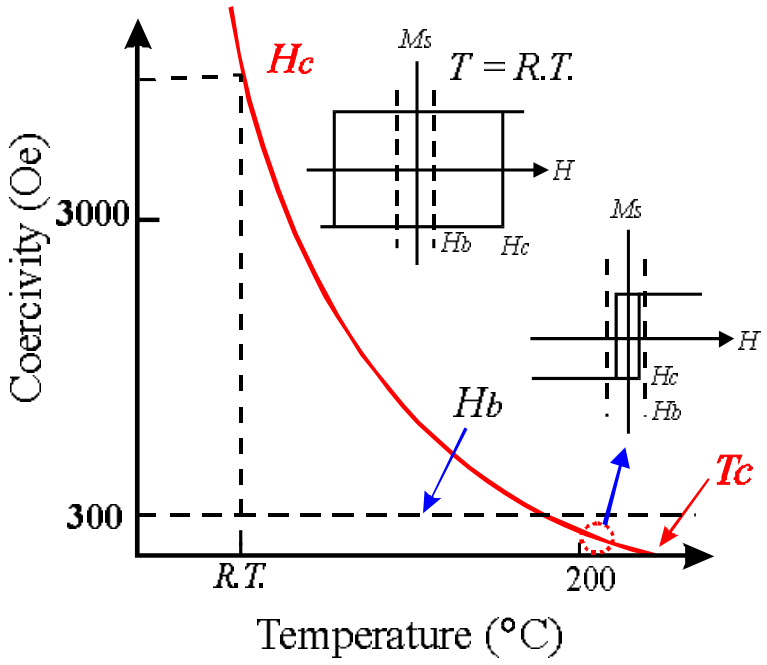

Fig. 3.10: Temperature dependence of the coercivity for an MO film whose T_{comp} is near room temperature [21].

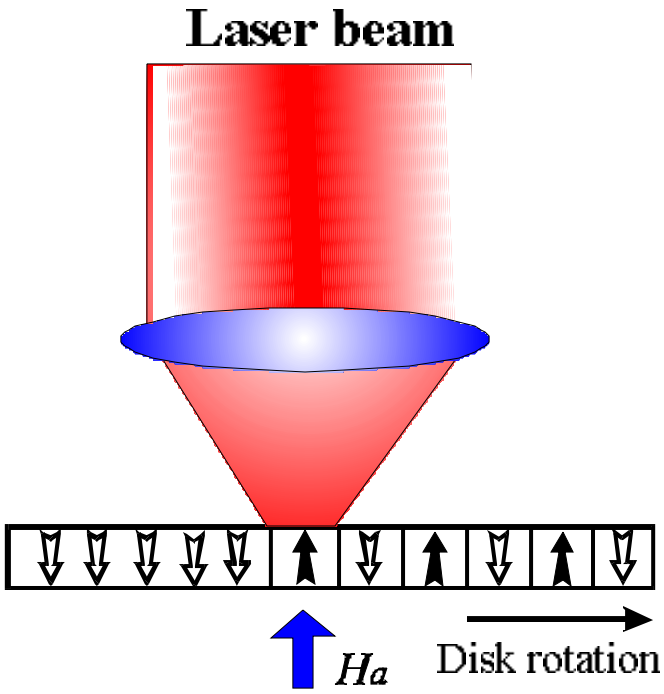

Fig. 3.11: Schematic diagram of writing mechanism in MO recording [22].

Two distinct means of thermo-magnetic recording were adopted to record the signals in MO drives: laser light intensity modulation (LIM) and magnetic filed modulation (MFM) [24]. In LIM recording, the electromagnet produces a constant field, while the power of the laser beam is modulated to record signals. As the disk rotates under the focused spot, the on/off laser-pulses create a sequence of up/down domains along the track, as shown in Fig. 3.12(a). The domains are highly stable and may be read over and over again without significant degradation. Besides, the electromagnet need not be capable of rapid switching. However, the disadvantage of LIM is its lack of direct overwriting capability because of the writing field with the constant direction. Therefore, the disk in the LIM recording should be erased by a field with the opposite direction to the writing field before writing new

domains in the track with the old marks. In addition, the tear-shaped domains limit the linear density of the disk [23].

In 1992, Sony Corp. produced the first MiniDisc (MD, 2.5") [25] with implementation of direct overwriting scheme by MFM technique, where laser power was in DC or pulse mode, but magnetic field was modulated by data pattern, as shown in Fig. 3.12(b). In MFM, the old domains are erased and new domains are written in the same run. The manner yields the crescent-shaped domains which leads to domain wall positioned along the track, being rather in sensitive to defocus and to laser power fluctuations [26-27]. The shape also allows higher linear density than LIM recording. However, the data rate of MFM recording is slower than LIM because laser-power switching is much faster than field modulation limited by the heat production in the coil.

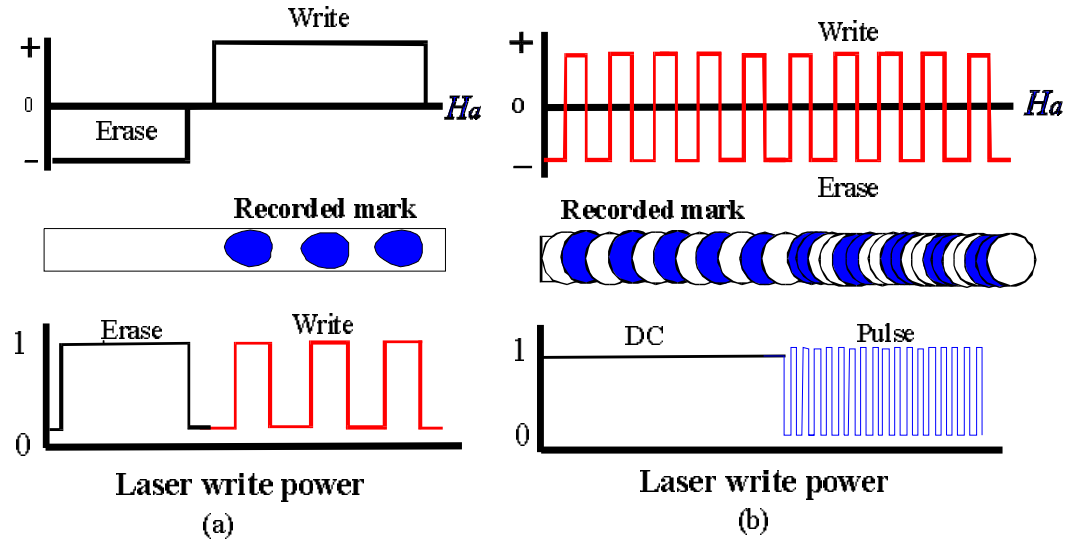

Fig. 3.12: Illustration of (a) LIM and (b) MFM recording in MO storage [27].

3.3.a.2 Reading Mechanism

The signals in the MO disks are read out by Kerr effect [29]. During the signal reading, a low power laser beam is focused upon the recording layer and the reflective beam becomes elliptically polarized with its major axis rotating clockwise or counterclockwise depending on whether the magnetization component along the beam direction is parallel or anti-parallel to the incident beam direction, as illustrated in Fig. 3.13. The polarization modulation of the reflected beam is detected by a photo-detector and transformed into the signal current. Besides, the intensity of incident laser beam focused on the magnetic film during reading is lower than that for writing. Thus, the temperature of the film increases and the coercivity decreases during reading would not change the direction of magnetization.

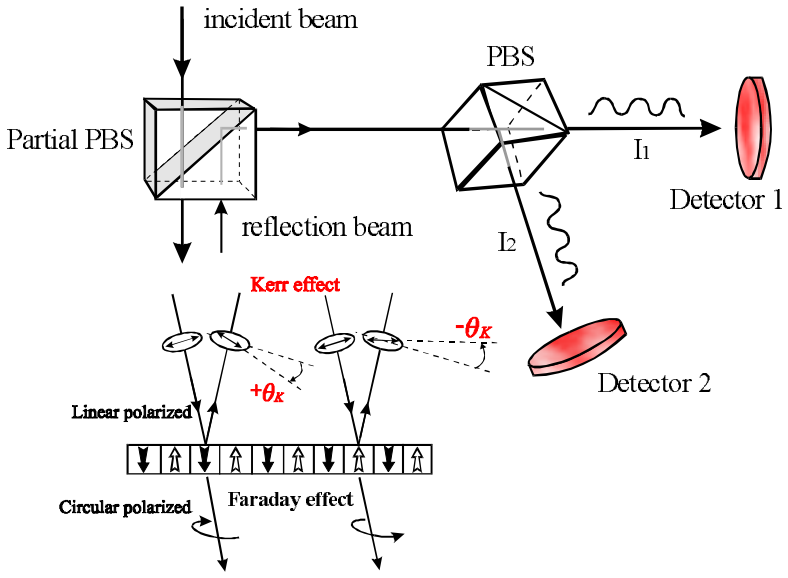

Fig. 3.13: Schematic diagram of reading mechanism in MO recording [22].

3.3.a.3 Magnetically Induced Super-resolution (MSR)

A large capacity memory has been required and is expected to store various kinds of massive data, such as moving picture, audio, text, and graph data. The capacity of the optical disks is not large enough to meet the requirement because the recording density is limited by the size of readout focused laser beam spot. A written mark with size smaller than diffraction limit, determined by the numerical aperture of object lens and laser wavelength, cannot be detected in conventional optics. Several magnetically induced super-resolution (MSR) detection schemes, such as Front Aperture Detection (FAD), Rear Aperture Detection (RAD), and Center Aperture detection (CAD), have been developed to enable the detection limit of small domains beyond the optical diffraction limitation [5, 30-32]. As indicated in Fig. 3.14, the disks in those MSR schemes are composed of RE-TM multilayers in which the composition of the layers should be specified to control their Curie temperature. By strong exchange coupling between the RE-TM films, the signals can be reliably recorded and detected.

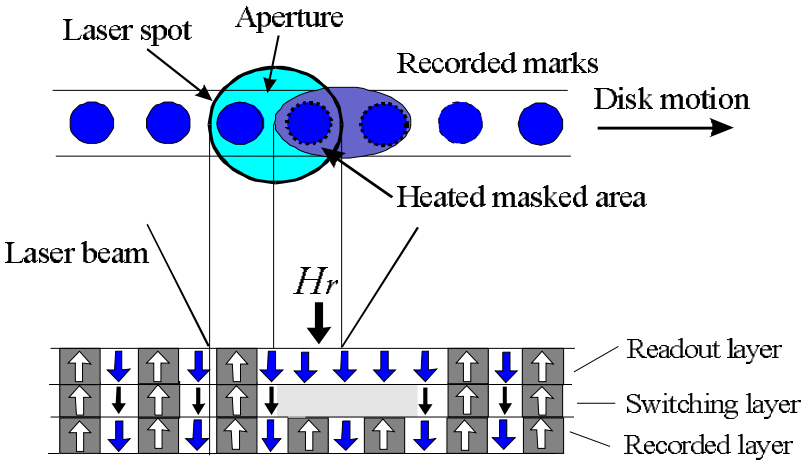

(a)

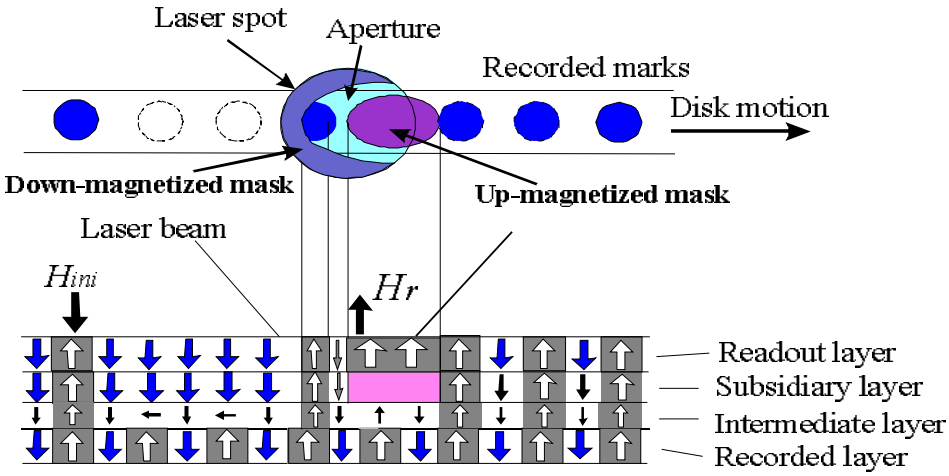

(b)

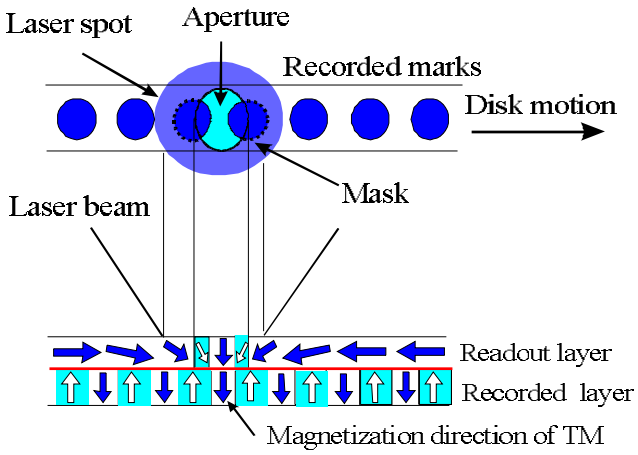

(c)

Fig. 3.14: Description of magnetically induced super resolution schemes (a) FAD, (b) RAD, and (c) CAD [5, 30-32].

3.3.b Thermomagnetic-Writing/ Magnetic-Flux-Reading Recording (Hybrid Recording)

As mention in the above, magneto-optical (MO) recording media have the potential to form domains with dimensions of less than 40 nm by the mechanism of thermally-assisted writing [33]. However, the recording density is restricted by the diffraction limited size of a readout laser beam spot. Although several MSR techniques and short-wavelength-laser recording [34] have been proposed to increase the sensitivity of signal readout, the Kerr-effect signal from small magnetic domain of tens nm is too low to be detectable in the recording density more than 100 Gb/in^2. On the other hand, the recording density in magnetic hard-disk recording maintains a high growth rate of 60 % per year (recently 100 %) since 1997. The increase is mainly attributed to the use of giant magnetoresistance (GMR) sensor in reading heads. However, continuous growth in area density of hard disks is limited by instability of small marks because of thermal fluctuation of magnetic spins [35], known as “superparamagnetic effect”. To overcome the thermal effect, high-coercivity media should be adopted, nevertheless, resulting in that writing field is insufficient to reliably record a domain.

Combining the advantages of thermo-magnetic writing and perpendicular RE-TM media in MO recoding, and magnetic flux detection in magnetic recording, hybrid recording reveals great potential for high-density storage [36-37]. Fig. 3.15 shows the configuration of

the hybrid recording. Similar with MO recording, the laser and magnetic coil are used to heat the media and determine the direction of domain magnetization in the writing process. GMR heads are utilized to read out the signal by detecting the direction of stray field from magnetic domains over the media surface. In the Chapter 6, the recording media in hybrid recording will be discussed in details.

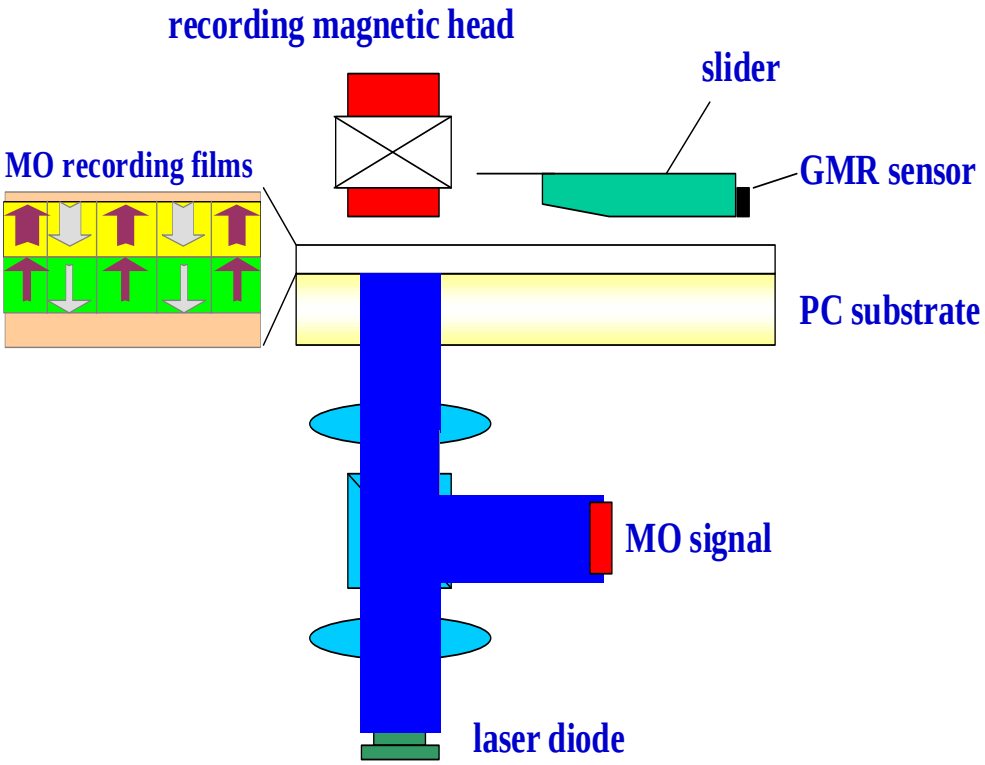

Fig. 3.15: Configuration of hybrid recording [36-37].

Chapter 4
Film Deposition and Measurement

In this Chapter, the depositions of films are introduced, including the sputtering system, the composition-adjusting method in RE-TM films and fabrication of Si/ SiO_2 substrates with various roughnesses. Then, the measurements of magnetic properties, such as magnetization, coercivity, Curie temperature, and perpendicular anisotropy constant, are describes. In addition, the observation of surface morphology and magnetic domains are interpreted. Finally, the analysis of X-ray magnetic circular dichroism in (XMCD) is introduced.

4.1 Sputtering System

All the films and disks in the dissertation were fabricated by an SFI sputtering system with six magnetron sputtering gun [1], as depicted in Fig. 4.1. Both of main chamber and load-lock chamber possess a mechanical pump and a turbo molecular pump, and a disk loader is utilized to load the samples between these two chambers separated by a chamber isolator. By the pumping system, the main chambers can be vacuumed to a base pressure of 3×10^{-7} torr. A cold trap is applied to adsorb the residual gas like O_2 and H_2O by filling with the liquid nitrogen, resulting in 1×10^{-7} to 2×10^{-7} torr of the base pressure in the main chamber. The base pressure of main chamber was monitored by a Bayard-Alpert

ionization gauge with an accurate range of 10^{-4} to 10^{-9} Torr. Under the deposition process, the evacuated chamber is filled with an inert gas (commonly Ar) at a working pressure of 1 to 10 mTorr. The working pressure within this range can be monitored accurately by a capacitance gauge, such as MKS 270C, with high sensitivity in the range of 10^{-1} to 10^{-4} torr. Besides, the gas flow rates of the inert and the reactive gases are controlled by flow potentiometers. Taking the uniformity consideration of film thickness, a planetary rotating mechanism is adopted to rotate the six sample holders in a circular dish in the deposition process. As the distance between the sample holder and the sputter guns keeps at 8.5 cm, the film uniformity can be better than 5 % in a disk with the diameter of 6.2 cm.

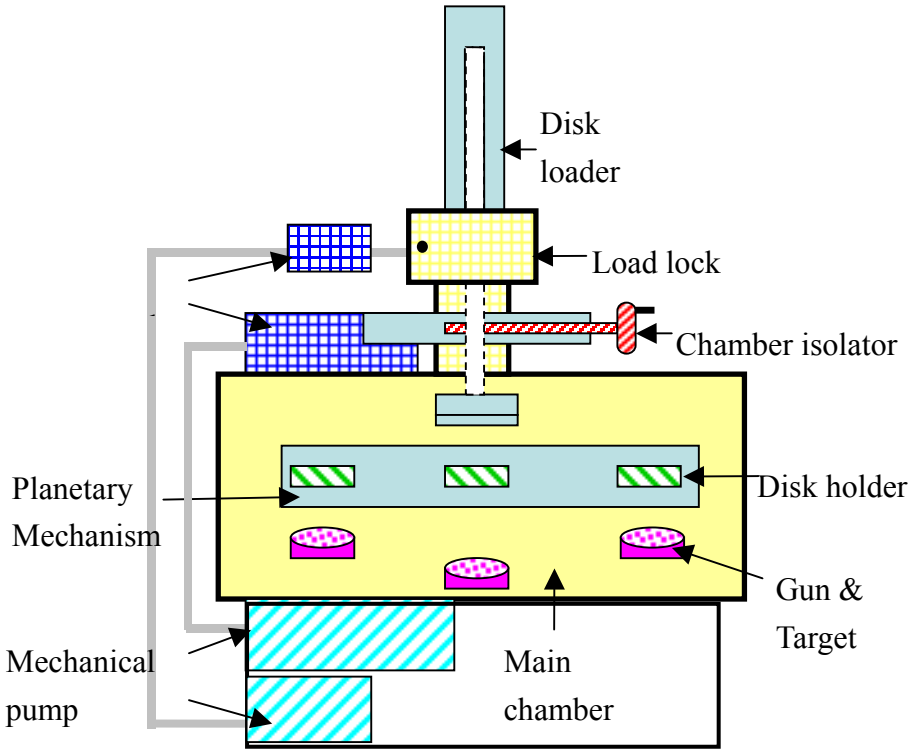

Fig. 4.1: Configuration of the sputtering machine in the experiments.

4.2 Deposition of RE-TM Films

The RE-TM films were deposited by co-sputtering method at the Ar pressure of 1.5 – 4 mtorr. The film composition was controlled by the sputtering rate of RE and TM targets where the following equation should be fulfilled [1].

$$\text{Atomic ratio} = \text{RE} : \text{TM} = \frac{R_{RE}}{r_{RE}^{\,3}} \cdot \frac{R_{TM}}{r_{TM}^{\,3}} \qquad (4.1)$$

Here, R and r respectively denote the sputtering rate and atomic radius. The Rutherford backscattering spectrometry (RBS) was utilized to calibrate the composition. The difference between the compositions obtained from the sputtering-rate calculation and RBS measurement is less than 0.5 atomic percentages. The RE-TM films were sandwiched by SiNx layers to prevent from the oxidation. The SiNx films were fabricated by RF-reactive sputtering at a mixed gas of 4 mtorr with the ratio of Ar to N_2 of 6.

4.3 Fabrication of Si/SiO_2 Substrates with Various Roughnesses

To investigate the dependence of exchange bias on the interfacial roughness in magnetic bilayers, Si/SiO_2 substrates with various roughnesses were fabricated. First, by using the wet oxidizing method, a 300-nm thick SiO_2 film was grown on a Si (100) substrate. Then we utilized hydrofluoric acid (HF) solutions with varying concentration to etch the Si/SiO_2 substrates for different minutes. The roughness of the Si/SiO_2 substrates was varied in the range of 3.4 to 10.4 Å. Fig. 4.2 shows the etching conditions and the roughness of the corresponded Si/SiO_2 substrates.

	Etching conditions	Roughness (Å)
Sample 1	No etching	5.1
Sample 2	1:10 HF over-etching	13.4
Sample 3	1:10 HF etching for 1min	14.4
Sample 4	1:10 HF etching for 2mins	10.5
Sample 5	1:10 HF etching for 3mins	8.2
Sample 6	1:20 HF etching for 3mins	7.5
Sample 7	1:30 HF etching for 3mins	3.7

Fig. 4.2: Etching conditions and roughnesses of the corresponded SiO_2/Si substrates.

4.4 Vibrating Sample Magnetometer (VSM)

The magnetic properties of RE-TM films, such as magnetization $M_s(T)$, coercivity $Hc(T)$, compensation temperature, and Curie temperature, were accurately measured by vibrating sample magnetometer (VSM) [2-3]. The schematic diagram of a typical VSM is shown in Figure 4.3. The large electromagnet provides a uniform DC field to the magnetic sample. The emanating magnetization is then measured by vibrating the sample to produce a flux change and therefore to induce a voltage in the pickup coils mounted on both sides of the magnet pole pieces. The coil output voltage is combined with the output from the displacement transducer to produce a magnetization signal. As a result, variations in vibration amplitude and frequency are canceled out. Then, the electromotive-force signal is detected, by a lock-in amplifier, and transmitted along with the applied field signal to a computer to generate a hysteresis loop.

The VSM in the studies, produced by DMS (Digital Measurement Systems, INC), has many special features, such as computer control, automatic data acquisition, and temperature-controlled measurement. The samples can be measured within the temperature range of 100 to 1000 K. A magnetic field up to 16 kOe can be applied to the sample in the measurements. In addition, the VSM system is well suited for measuring major and minor hysteresis loops, initial magnetization curves, and remanent magnetization curves.

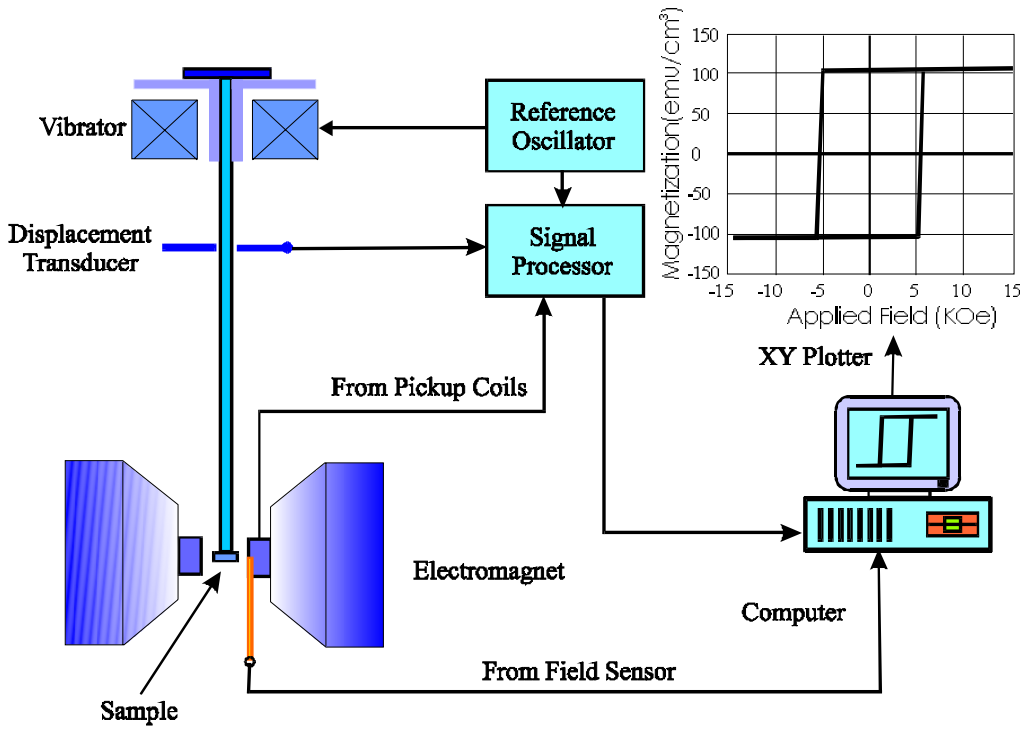

Fig. 4.3: Schematic diagram of VSM [2-3].

4.5 Kerr-loop Tracer

A Kerr-loop tracer was utilized to measure the out-of-plane hysteresis loops. Fig. 4.4 illustrates the experimental setup. The tracer utilized a polarized He-Ne laser with $\lambda = 632.8nm$ passing though a beam splitter. By detecting the signal of the reflected light from the magnetic films, the relative Kerr rotation angle can be derived. As the axis of the Wollaston prism is set at 45° relative to the polarization of the incident beam, the Kerr angle θ_K can be obtained by following equation [4]:

$$\theta_K = \frac{1}{2}\tan^{-1}\frac{I_1 - I_2}{I_1 + I_2}, \qquad (4.2)$$

where I_1 and I_2 denote the light intensity of two split beams. In addition, the Kerr-loop measurement can be used to distinguish that the RE-TM films is TM-rich or RE-rich by the tendency of hysteresis loops [5]. As mentioned in the paragraph 3.1.e, the Kerr effect in RE-TM films is mainly contributed by TM subnetwork. If upward and downward TM spins respectively lead to the Kerr angles of $+\theta_K$ and $-\theta_K$, we can obtain the hysteresis loop of the TM-rich RE-TM film in which the Kerr angles are $+\theta_K$ and $-\theta_K$ at positive and negative saturation field, respectively, as shown in Fig. 4.5(a). In contrast, the loop of RE-rich film can be expected as that in Fig. 4.5(b). Besides, the sample holder is also designed with a heating stage, thus the Curie temperature can be measured in the instrument.

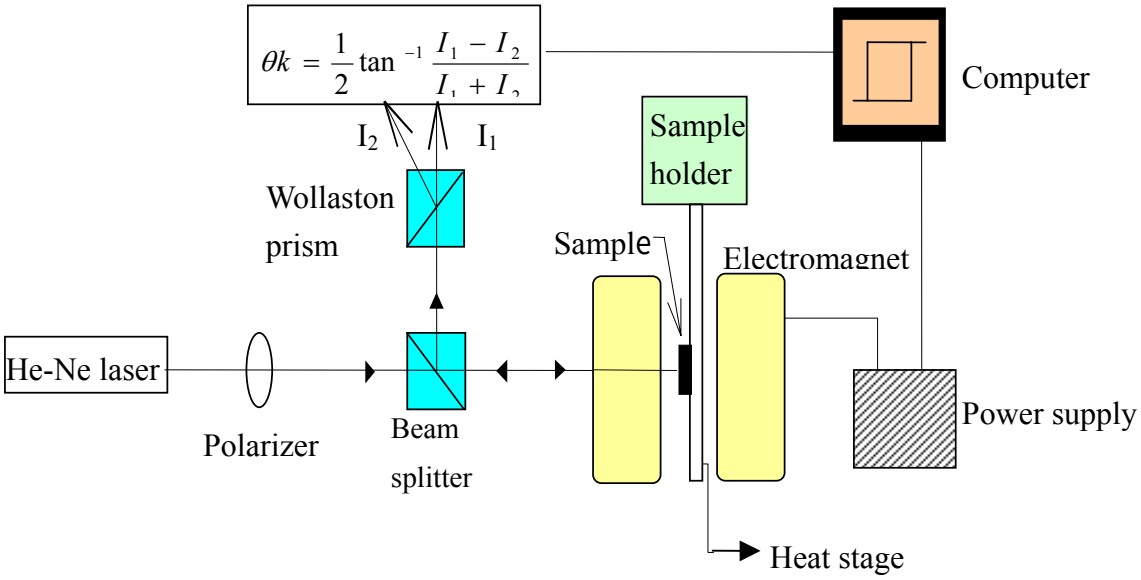

Fig. 4.4: Schematic diagram of Kerr-loop tracer.

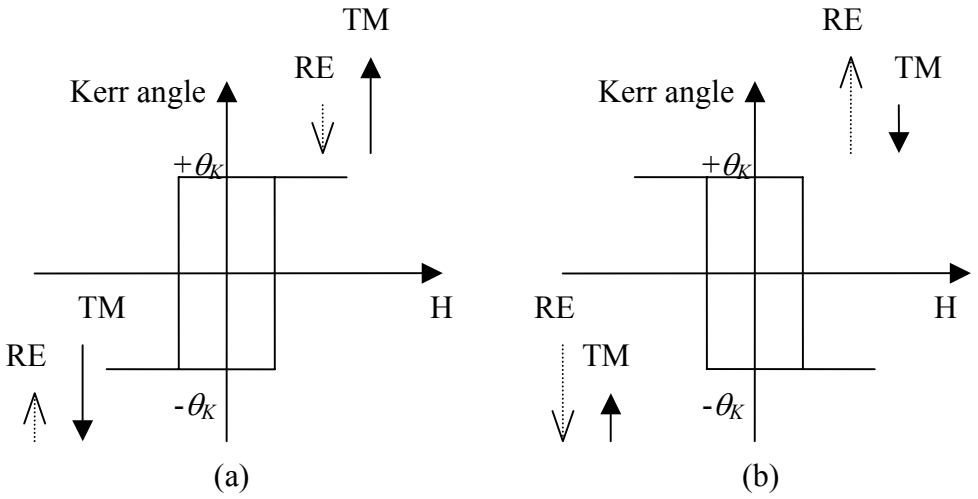

Fig. 4.5: Kerr loops of (a) TM-rich and (b) RE-rich RE-TM films.

4.6 Measurement of Perpendicular Anisotropy Constant Ku

The perpendicular anisotropy constant Ku of RE-TM film was obtained by the measurement of extraordinary Hall Effect. As indicated in Fig. 4.6, if the current is flowing along x axis from a to b in the films with out-of-plane magnetization, an electric field is produced in the Y axis, called "extraordinary Hall Effect" (EHE). Different from the ordinary Hall Effect originating from the deflection of flowing electrons in a magnetic field, the EHE is related with the scattering of incident electrons by magnetic spins [6-7].

The amorphous RE-TM films exhibit the large EHE [8], which is utilized in the measurement of Ku [9-10]. In the experiments of this dissertation, the dependence of the in-plane field on the EHE was

measured. Fig. 4.7 shows the magnetization orientation in a RE-TM film with perpendicular anisotropy under an in-plane applied field. We can expect the relation [7] as

$$V_H \propto M\cos\theta, \tag{4.3}$$

where V_H and θ are the Hall voltage and the angle of the magnetization from the film normal. On the other hand, if we take the Stoner-Wohlfarth (SW) model [11] under the assumption of coherent magnetization rotation, the total magnetic energy of the film is written as,

$$E_{total} = -HM_s\cos(\alpha-\theta) - 2\pi M_s{}^2\sin^2\theta + K_u\sin^2\theta, \tag{4.4}$$

where the three terms respectively are the external field energy, the demagnetizing energy, and the uniaxial anisotropy energy. The œ, the angle of applied field from the film normal, is 90 degree in the measurement. One can obtain Ku from the energy minimum condition, namely,

$$\frac{\partial E_{total}}{\partial\theta} = -HM_s\sin(90-\theta) + (K_u - 2\pi M_s{}^2)\sin 2\theta = 0. \tag{4.5}$$

To get higher accuracy, one usually measures a series of data with varies H and uses the SW solution to best fit the curve by adjusting Ku [9-10]. In the experiments, we measured the variation of V_H in

single-layer RE-TM films with in-plane applied field, as shown in Fig. 4.8. By combing the Eqs. (4.3) and (4.5), the V_H-H curve can be theoretically derived by the formula,

$$V_H = A\frac{MsH}{2(K_u - 2\pi M_s^2)}, \tag{4.6}$$

where A, a constant associated with the incident current and the film materials, can be eliminated by normalizing the V_H at H=0. By adjusting the Ku values, we can best fit measured curves to the theoretical V_H-H curves to obtain the Ku of RE-TM films, as indicated in Fig. 4.9.

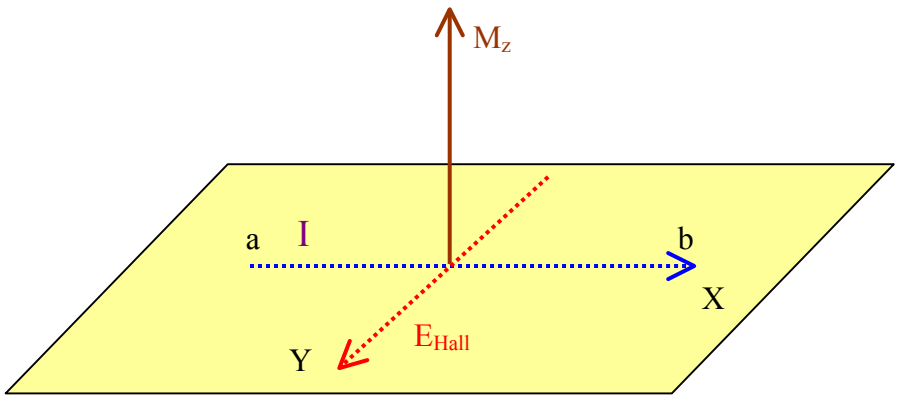

Fig. 4.6: Illustration of extraordinary Hall Effect.

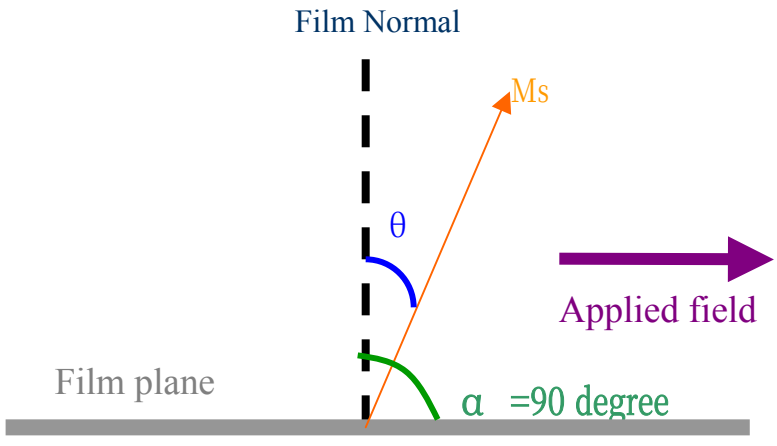

Fig. 4.7: Magnetization orientation in a RE-TM film under an in-plane applied field.

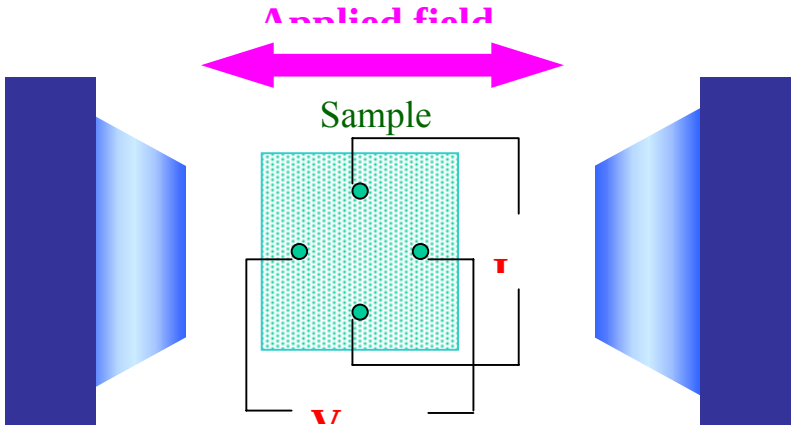

Fig. 4.8: Illustration of Hall-Effect measurement of RE-TM films under in-plane applied

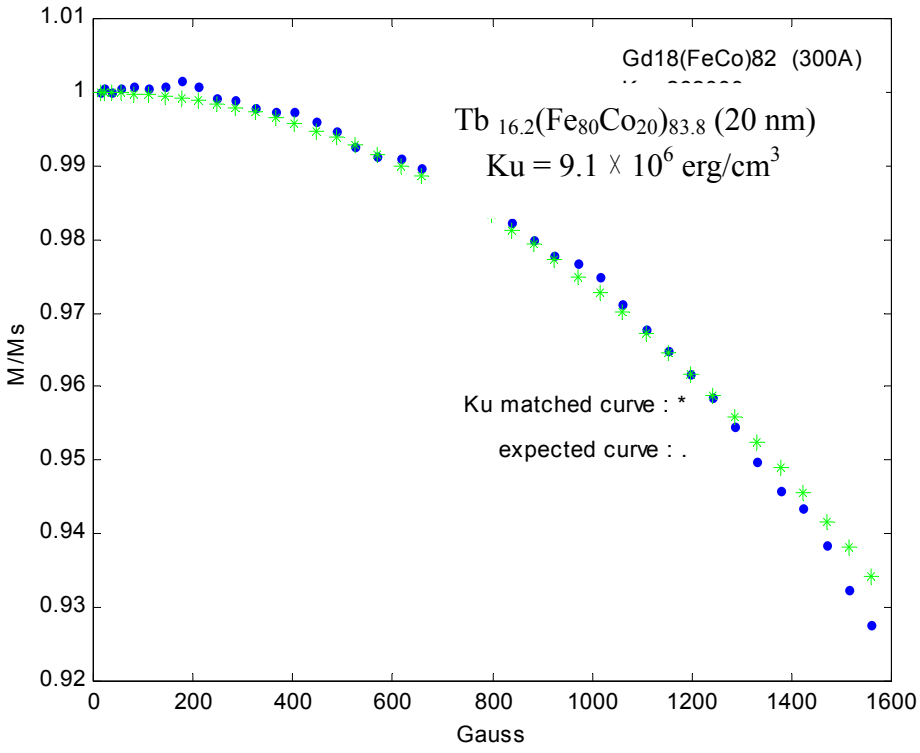

Fig. 4.9: Ku-matching curves.

4.7 Observation of Surface Morphology and Magnetic Domains

A multiple scanning probe microscopy (SPM, Digital Instrument 3100 model) was employed for characterizing the surface morphology of the films and the magnetic domains [12]. It was quipped with various modes, such as contact mode atomic force microscopy (AFM), tapping AFM, electric force microscopy (EFM), scanning tunneling microscopy (STM), and magnetic force microscopy (MFM) mode etc. In this study, we use the tapping mode AFM, and MFM function of SPM, and they are described in the following.

The tapping mode AFM is operated by scanning a tip attached to the end of an oscillating cantilever across the sample surface, shown in Fig. 4.10. The cantilever is oscillated at or near its resonance frequency with amplitude ranging typically from 20 to 100 nm. The frequency of oscillation can be at or on either side of the readout frequency. The tip lightly “taps” on the sample surface during scanning, contacting the surface at the bottom of its swing. The feedback loop maintains constant and oscillatory amplitude by maintaining a constant RMS of the oscillation signal acquired by a quad-photodiode. The vertical position of scanner at each (x,y) data point to maintain a constant “setpoint” amplitude is stored by computer to form the topographic image for

sample surface. By maintaining the amplitude of constant oscillation, a constant tip-sample interaction is maintained during imaging. Finally, the thin film's morphology was observed by employing an AFM. In addition, the surface roughness of thin films can be quantitatively determined by the instrument.

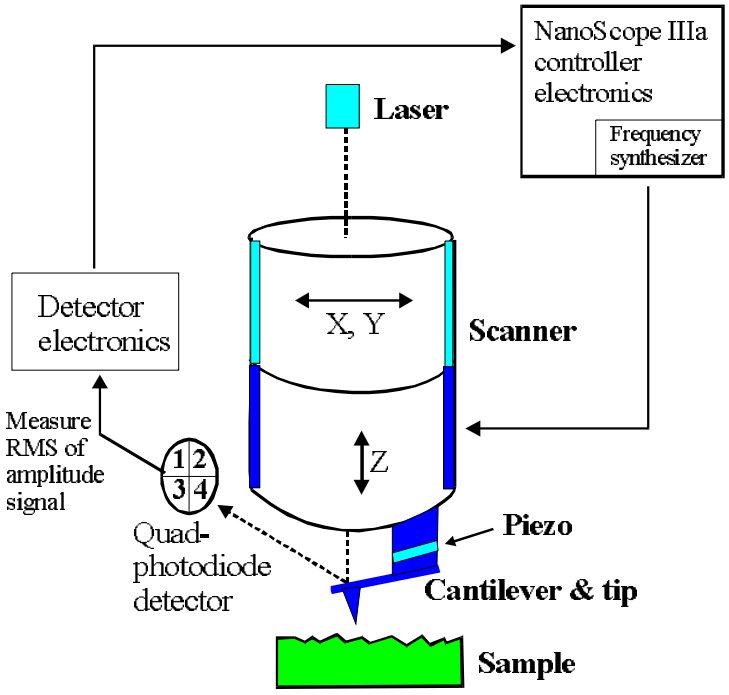

Fig. 4.10: Schematics diagram of tapping mode AFM [12].

MFM imaging utilizes the interleave- and lift-mode of AFM. Best results will be obtained with Digital Instruments Nanoscope extender electronics module. This hardware unit allows phase detection and frequency modulation for optimal MFM imaging. In addition, the magnetic tip with a CoCr-coated Si tip magnetized along the tip axis was used to scan the magnetic domain structures in tapping-lift mode [13].

In MFM, a tapping cantilever equipped with a special tip is first scanned over the surface of the sample to obtain topographic information.

Using lift-mode, the tip is then raised just above the sample surface. The surface topography is scanned while being monitored for the influence of magnetic forces. These influences are measured using the principle of force gradient detection. In the absence of magnetic forces, the cantilever has a resonant frequency f_0. This frequency is shifted by an amount f, which is proportional to vertical gradients of the magnetic forces on the tip. The shifts of resonant frequency tend to be very small, typically in the range 1-50 Hz for cantilever with a resonant frequency f_0 ~100 MHz. These frequency shifts can be detected in three ways: phase detection, which measures the cantilever's phase of oscillation relative to the piezo; amplitude detection, which tracks variations of oscillation's amplitude; and frequency modulation, which directly tracks shifts in resonant frequency. Phase detection and frequency and frequency modulation produce results that are generally superior to amplitude modulation. By employing magnetic force microscope, the morphology and magnetic domain structure of thin films can be observed, as shown in Fig. 4.11. The land and groove profiles of an optical disk are shown in Fig. 4.11(a), and the recorded marks of ECDL RE-TM disks written by magnetic-field-modulation are shown in Fig. 4.11(b).

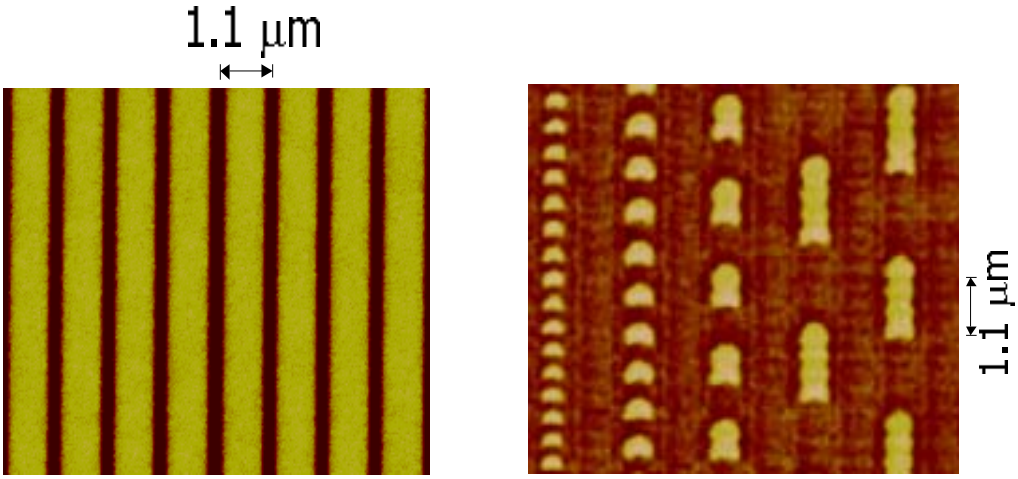

(a) (b)

Fig. 4.11: (a) the morphology of the optical disk observed by tapping-mode AFM and (b) the recording domains observed by MFM.

4.8 X-Ray Magnetic Circular Dichroism (XMCD) Spectroscopy

X-ray Magnetic Circular Dichroism (XMCD) is considered to be one of the most important discoveries in the field of magnetism in the last two decades. It was first suggested by Erskine and Stern in 1975 [14]. The first experiments with circularly polarized x-rays are performed in the high energy range by Schütz *et al*. in 1987 [15]. The XMCD measurement has several capabilities that are not afforded by traditional magnetic analysis techniques. Its foremost strengths are the element-specific, quantitative determination of spin and orbital magnetic moments and their anisotropies [16]. Other strengths are the chemical

sensitivity [17], the element-specific imaging capability [18], and its high sensitivity [19-20].

In the XMCD measurement of transition metals, typically, *L-edge* X-ray spectrum was detected, which can best probe the properties of 3d electrons. As shown in Fig. 4.12 [20], the *L*-edge spectrum contains two main absorption peaks of L_3- and L_2-edges which are respectively associated with excitation of $2p_{3/2}$ and $2p_{1/2}$ core electrons to unfilled 3d states. The *L*-edge absorption spectra are characterized by strong absorption resonances, so-called white lines, near the L_3 and L_2 thresholds [20]. The sum of the L_3 and L_2 absorption intensities, denoted I_{L3} and I_{L2}, is proportional to the number of d holes related with the spin moments, as shown in Fig. 4.11. In addition, the spectrum detection affords the capability of element-specific measurement because the *L*-edge position depends strongly on atomic number.

The use of circularly polarized X-rays opens the door for X-ray-based spectroscopy studies of magnetic materials and structure. The basic concept of XMCD spectroscopy is easily understood if we assumed that the d shell has only a spin moment. To measure the difference in the number of d holes with up and down spins, we need to make the X-ray absorption process spin-dependent. Since spin flips are forbidden in electric dipole transitions, spin-up (spin-down) photoelectrons from the p core shell can only be excited into spin-up (spin-down) d hole states. Hence, if one could preferentially generate spin-up photoelectrons in one measurement and the spin-down in another, the difference of the transition intensity in the spectra would simply

reflect the difference between up and down holes in the d shell. i.e. the spin moment. This is done by use of right or left circularly polarized photons which transfer their angular momentum to the excited photoelectrons. Fig. 4.13 indicated the spectra of Fe in TbFe films obtained by the incidence of right- or left-circularly-polarized X-ray. The difference between the spectra of right- and left-circularly-polarized X-ray is the XMCD spectrum. [20-21].

The XMCD effect is quantitatively related to the amounts of magnetic moments and to the anisotropies of the spin density and orbital moments [20, 22-23]. The maximum dichroism effect is observed if the photon spin direction and the magnetization directions are parallel or anti-parallel. When the photon spin and the magnetization directions are perpendicular, the resonance intensities at the L_3 and L_2 edges lie between those obtained for parallel and anti-parallel alignments. Thus, the size of the dichroism effect can be considered as a function of cos θ, where θ is the angle between the photon spin and the magnetization direction. The L_3 and L_2 resonance intensities and their differences for parallel and anti-parallel orientation of photon spin and magnetization directions are quantitatively related by sum rules [20-21] to the number of d holes and the size of the spin and orbital magnetic moments. Angular-dependence measurements in external magnetic fields give the anisotropies of the spin density and orbital moment. In the Chapter 7, the XMCD measurement will be further discussed.

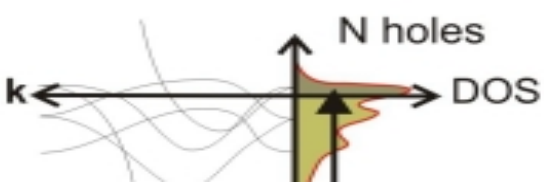

Fig. 4.12: Electronic transitions in conventional L-edge x-ray absorption [20].

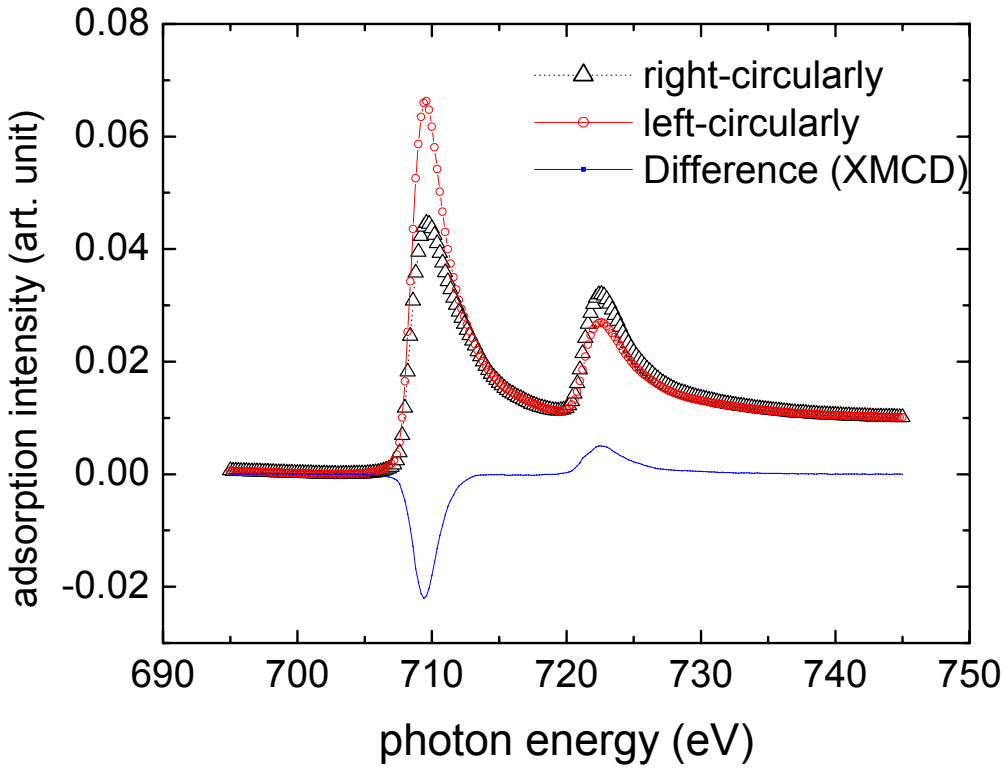

Fig. 4.13: X-ray absorption spectra of Fe in TbFe films by using right- and left-circularly-polarized X-ray. The difference of the two spectra is so-called the XMCD spectrum.

Chapter 5

High Interfacial Energy in TbFeCo Exchange-bias Films with Perpendicular Anisotropy

5.1 Introduction

Exchange-bias (EB) between an antiferromagnet (AFM) and a ferromagnet (FM) was discovered more than 40 years ago by Meiklejohn and Bean [1]. Because of its fundamental interest and important technological applications, extensive efforts had been devoted to develop a full understanding of this phenomenon in last two decades [2-6]. The simplest model [1-2], assuming an ideal uncompensated plane at FM/AFM interface, predicts bias fields of orders of magnitude larger than those observed. Mauri et al. [3] provided an explanation for the reduced bias field by introducing formation of domain walls parallel to the interface. Malozemoff interpreted EB in terms of a random field at the interface which causes the AFM to break up into domains [4]. The experimental correlation between the interfacial uncompensated CoO spins and the exchange field in CoO/NiFe bilayer was demonstrated by Takano [5]. The low density of uncompensated interfacial spins are responsible for a low exchange field observed compared to the ideal interface model [1].

Except FM/AFM systems, exchange bias also exists in ferrimagnet (FI)/ FI [6] and ferromagnet (FM)/ FM bilayer. Amorphous rare-earth-

transition-metal (RE-TM) multilayers, possessing perpendicular anisotropy, exhibited strong exchange-coupling [7]. A micromagnetic analysis [8], conducting the concept of a Block wall existing at the interface between magnetic layers, has been performed to interpret the strong EB. In this study, we studied the difference of exchange-coupling strength among FI/FI, FM/ FM, and FM/ AFM bilayers, based on the view of spin-spin coupling at interface. By exploring the EB dependence on interface roughness, on spin-spin coupling states, and on the Ku of pinning layers, a highly-uncompensated-spin interface model is proposed to explain the ultra high interfacial coupling between perpendicular TbFeCo layers.

5.2 Experimental Procedures

Films were deposited by using magnetron sputtering at backing pressure of 3×10^{-7} Torr onto Si or Si/SiO_x substrates. The TbFeCo layers were sandwiched by SiN_x protective layers to prevent from oxidation. The composition of TbFeCo films was controlled by the sputtering rate of Tb and $Fe_{80}Co_{20}$, and calibrated by Rutherford backscattering spectrometry. To induce exchange-bias fields, IrMn/NiFe films were post-annealed at 200 ℃ for 10 mins at a field of 1000 Oe. The crystal structure was characterized by X-ray diffraction. To explore the effects of interface roughness on exchange bias, we deposited films on substrates with different roughness. To prepare these substrates, we grew SiO_x of 300 nm on Si wafers by furnace oxidation and then dipped the wafers in the HF solution with distinct concentrations. The roughness of substrates and films was identified with an atomic force microscope. The r. m. s. roughness of substrates varied from 0.3 to 1.5 nm, and the wavelength changed from 18 to 39 nm. A vibrating sample magnetometer (VSM) and Kerr-effect Tracer were used for measuring the magnetic properties. In addition, the Ku of single-layer TbFeCo was derived from the measurement of Hall Effect with an in-plane external field [9], mentioned in the paragraph 4.6.

5.3 Results and Discussion

5.3.a Strong Exchange Coupling in TbFeCo Bilayers

Ultra strong exchange coupling was found in amorphous TbFeCo bilayers with perpendicular Ku. Figure 5.1 shows the full and minor hysteresis loops of TbFeCo bilayers with TM-rich compositions by applying the field in the out-of-plane direction. The layer with the composition of $Tb_{16.2}$ $(Fe_{80}Co_{20})_{83.8}$ can be considered as a pinned layer because of its lower coercivity than the other. The interfacial exchange energy (σ_w) of the TbFeCo bilayers is derived from

$$\sigma_w = H_b M_s t. \qquad (5.1)$$

Here, H_b, Ms and t are the biasing field, saturation magnetization and thickness of pinned layer $Tb_{16.2}$ $(Fe_{80}Co_{20})_{83.8}$. Typically, the σ_w in FM/AFM bilayer is calculated by the slope of H_b vs. $(1/t_F)$. However, the saturation magnetization and the anisotropy constant of TbFeCo vary with film thickness [10], so the σ_w of TbFeCo bilayers can only be estimated at the specific thickness. The σ_w of the sample of $Tb_{22.1}(Fe_{80}Co_{20})_{77.9}$ 200 nm/ $Tb_{16.2}$ $(Fe_{80}Co_{20})_{83.8}$ 100 nm, estimated from Figure 5.1, is about 5.3 erg/cm^2, which is one or two order of magnitude higher than that in the FM/AFM systems [11]. A non-magnetic SiN_x layer was inserted between two TbFeCo layers to examine the origin of the strong exchange coupling. When the SiN_x of 1.5 Å was inserted, the

EB of pinned layer decreased for 95 %, as indicated in Fig. 5.2. With further increasing SiN_x layer to 6 Å, the bias field completely disappeared. The results imply that the high interfacial energy mainly resulted from short-range exchange coupling instead of dipolar interaction.

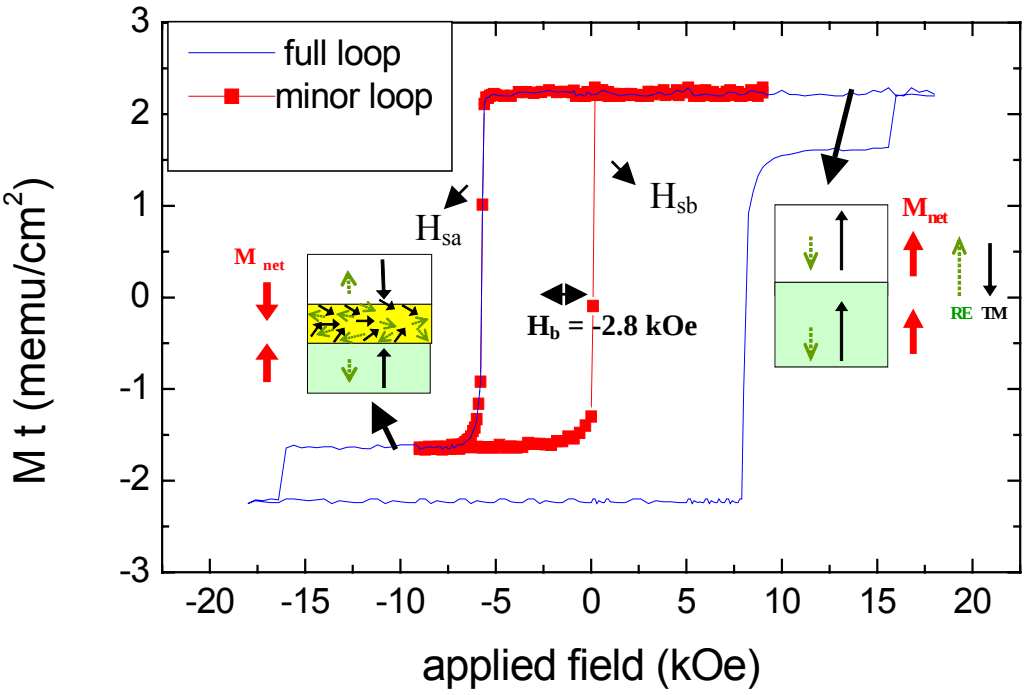

Fig. 5.1: Full and minor loops of the TbFeCo bilayers with a pinning layer $Tb_{22.1}(Fe_{80}Co_{20})_{77.9}$ (200 nm)/ a pinned layer $Tb_{16.2}$ $(Fe_{80}Co_{20})_{83.8}$ (100 nm).

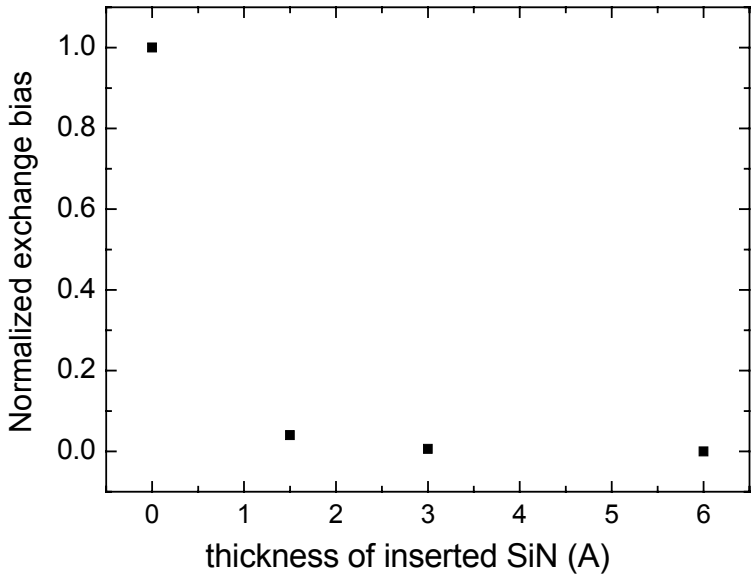

Fig. 5.2 Effect of inserted SiNx thickness on exchange bias in the magnetic films $Tb_{22.1}(Fe_{80}Co_{20})_{77.9}$ (200 nm)/ SiNx X nm/ a pinned layer $Tb_{16.2}$ $(Fe_{80}Co_{20})_{83.8}$ (100 nm).

5.3.b Negative and Positive Exchange Bias in TbFeCo Bilayers

The minor loop in Fig. 5.1 also exhibits a negative EB of pinned layer in the TbFeCo films with TM-rich compositions, similar with that in typical FM-AFM bilayers. However, the EB field of TbFeCo bilayers shifted from the negative to the positive as Tb content of pinning layer varied from 22.1 % (TM-rich) to 27.5 % (RE-rich), as shown in Figure 5.3. As mentioned in the chapter 3, the TbFeCo bilayers in Fig 5.1 and 5.3 respectively are of P-type and A-type [12]. Before the minor-loop measurement of the pinning layer in the TbFeCo bilayers, the net-magnetization direction of the pinning layer with high coercivity was

set in the upward direction by a positive saturation field, and was fixed during the measurement. In the case of P-type bilayers, the TM (RE) spins in the two TbFeCo layers align parallel under the positive saturation field while the net magnetizations follows the direction of the applied field. With variation of the field from positive to negative, the magnetization of the pinning layer reversed from upward to downward at a the field H_{sa}. Simultaneously, a Block wall was form at the interface between pinning and pinned layers because the TM (RE) spins in the two TbFeCo layers are antiparallel while the net magnetizations of the two layers are opposite, as illustrated in Fig. 5.1. The H_{sa} can be given by [12]

$$H_{sa} = -Hc_1 - H_b = -Hc_1 - \frac{\sigma_w}{2M_1 t_1}, \tag{5.2}$$

where 1 denotes the pinned layer. In addition, the other switching field (H_{sb}) in the minor loop of the pinned layer in the P-type bilayer can be provided by

$$H_{sb} = +Hc_1 - H_b = +Hc_1 - \frac{\sigma_w}{2M_1 t_1}. \tag{5.3}$$

From the Eqs. (5.2) and (5.3), the minor-loop center of the pinned layer was shifted to the negative side by an exchange bias of $\sigma_w / M_1 t_1$ through the exchange coupling between two TM-rich TbFeCo layers.

On the other hand, as illustrated in Fig. 5.3, a Block wall was formed at

the interface of the A-type bilayers at the positive saturation field, resulting from the opposite direction of RE-RE and TM-TM spins between two layers. In the A-type bilayers, the two switching field in the minor loop of the pinned layer can be respectively given by

$$H_{sa} = -Hc_1 + H_b = -Hc_1 + \frac{\sigma_w}{2M_1 t_1} \tag{5.4}$$

And

$$H_{sb} = +Hc_1 + H_b = -Hc_1 + \frac{\sigma_w}{2M_1 t_1}. \tag{5.5}$$

Therefore, a positive shift of the hysteresis loop of the pinned layer occurred in the A-type TbFeCo bilayers, seldom observed in F/AF systems.

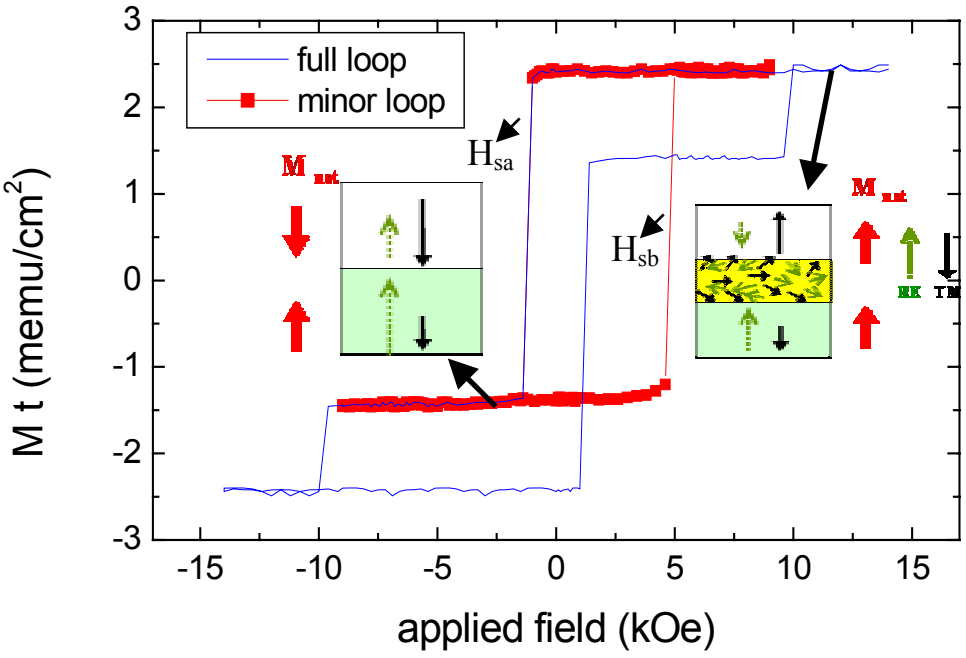

Fig. 5.3: Full and minor loops of the TbFeCo bilayers with a pinning layer $Tb_{27.5}(Fe_{80}Co_{20})_{72.5}$ (200 nm)/ a pinned layer $Tb_{16.2}$ $(Fe_{80}Co_{20})_{83.8}$ (100 nm).

5.3.c Highly-uncompensated-spin Interface in TbFeCo Bilayers

A highly-uncompensated-spin interface is proposed to explain the strong EB in TbFeCo bilayer systems. At the interface of TbFeCo bilayers, the adjacent spins of the same atoms, Tb-Tb and Fe (Co)-Fe (Co), are ferromagnetically coupled, and AF-coupling only occurs between heterogonous atoms, as shown in Fig. 5.4(a). Namely, no spin-compensation occurs, regardless of interfacial roughness, between magnetic atoms, leading to high σ_w. In FM/AFM systems, such as IrMn/NiFe, adjacent Mn-Mn spins in the IrMn layer prefer AF-coupling, resulting in the compensated spins at interface due to roughness or defects, as shown in Fig. 5.4(b), and thus low σ_w.

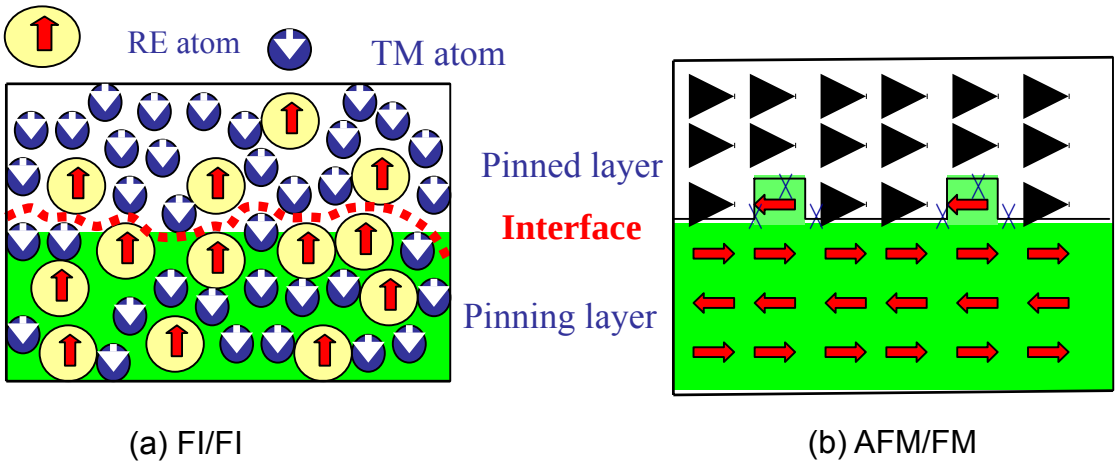

Fig. 5.4 Schematic diagrams of spin-spin coupling states at the interface of (a)FI/FI and (b)AFM/FM bilayers.

To explore the importance of uncompensated-spin interface to EB strength, we studied the poly-IrMn/NiFe and SmCo/NiFe (FM/FM) exchange-bias films, with in-plane anisotropy, for comparison. The σ_w values of the bilayer films were derived from VSM measurement by applying the in-plane field. The maximum σ_w of NiFe/IrMn bilayer in our experiments is 0.10 erg/cm^2 by varying interface roughness. Generally, single hysteresis loop was observed in the bilayers of hard-FM/ soft-FM. By increasing thickness of magnetic layers to satisfy the Eq. (5.1) [12], double loops were observed in SmCo 100 nm/ NiFe 200 nm, as shown in Fig. 5.5

$$\sigma_w (1/M_h t_h + 1/M_s t_s) > Hc_h - Hc_s, \qquad (5.6)$$

where h and s denote the hard and soft FM layers. Unlike the antiferromagnetic coupling in IrMn, the coupling between spins of Sm-Sm, Co-Co, and Sm-Co in SmCo prefers ferromagnetic one, leading to uncompensated-spin interface in SmCo/NiFe systems. Thus, the strong exchange interaction exists between SmCo and NiFe layers, and σ_w of 0.44 erg/cm^2 was obtained, several factors of magnitude higher than that in IrMn/NiFe. On the other, the in-plane and out-of-plane loops of the SmCo layer in Fig. 5.6 indicates a low in-plane anisotropy in SmCo, which causes lower σ_w than that in TbFeCo bilayers. We will further discuss how the Ku affects EB in the magnetic bilayers later.

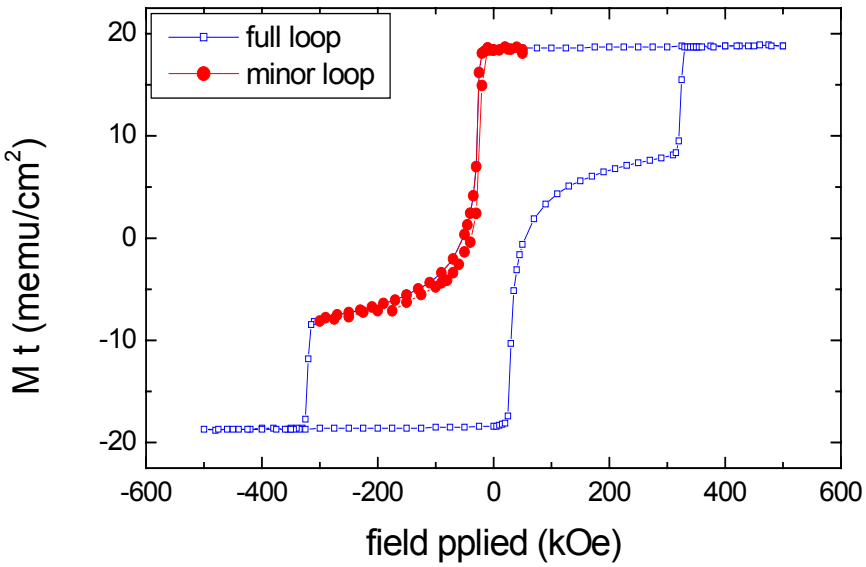

Fig. 5.5: Hysteresis loop of SmCo 100 nm/ NiFe 200 nm in the easy axis in the plane.

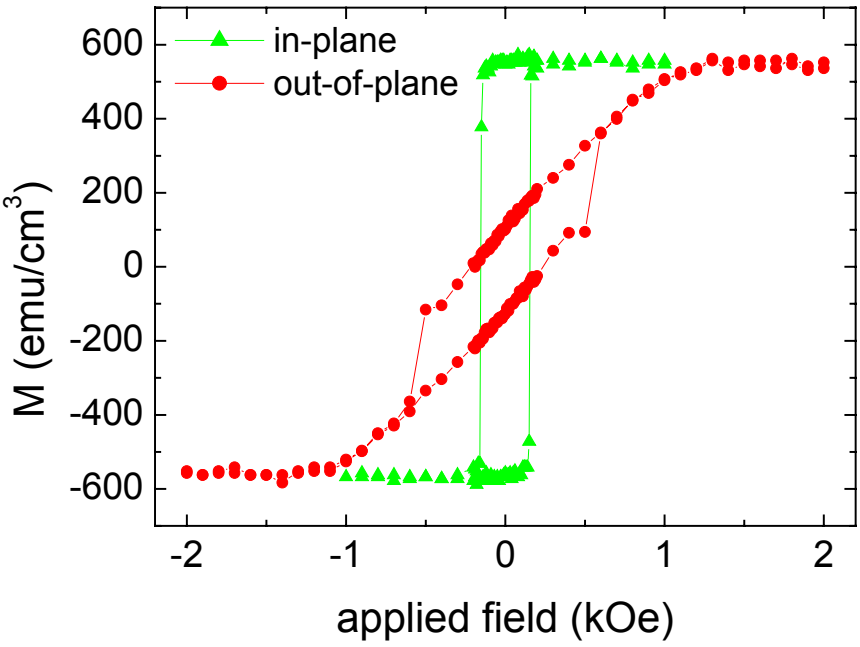

Fig. 5.6: In-plane and out-of-plane loops of SmCo 100 nm/ NiFe 200 nm.

5.3.d Dependence of Surface Morphology on Exchange Bias

To further illustrate the difference of spin compensation between TbFeCo bilayers and IrMn/NiFe, we investigate the roughness dependence on EB. TbFeCo bilayers and IrMn/NiFe films were deposited on the substrates with varied r. m. s. roughness. From the AFM analysis, we have confirmed that the film roughness can be manipulated by the substrate roughness. Figure 5.7 shows EB dependence of TbFeCo bilayers and IrMn/NiFe films upon r.m.s. roughness. Notice that the wavelength of the roughness also varies from 18 to 39 nm with increasing r.m.s. roughness. Even though the r. m. s. roughness varies from 0.34 to 1.55 nm, σ_w in TbFeCo bilayers almost keep constant. However, σ_w of IrMn/NiFe exhibits a strong function of r.m.s. roughness and wavelength, that is, the σ_w depends on the interfacial morphology. As mentioned above, the adjacent spins of the same atoms are ferromagnetically coupled and AF-coupling occurs between heterogonous atoms in TbFeCo bilayers. The magnetic interface, which is associated with spin-spin coupling, of TbFeCo bilayer is continuous and homogeneous no matter how the interface morphology or roughness changes. In contrast, the amount of uncompensated-spin pairs in FM/AFM systems changes with interface morphology, leading to that exchange coupling strongly depends upon the r.m.s. roughness and the wavelength. Based on these experiment results, we suggest that the enhancement of EB in FM/AFM by adjusting the interfacial roughness

and wavelength may be attributed to increasing the amount of uncompensated spins at the interface of FM/AFM.

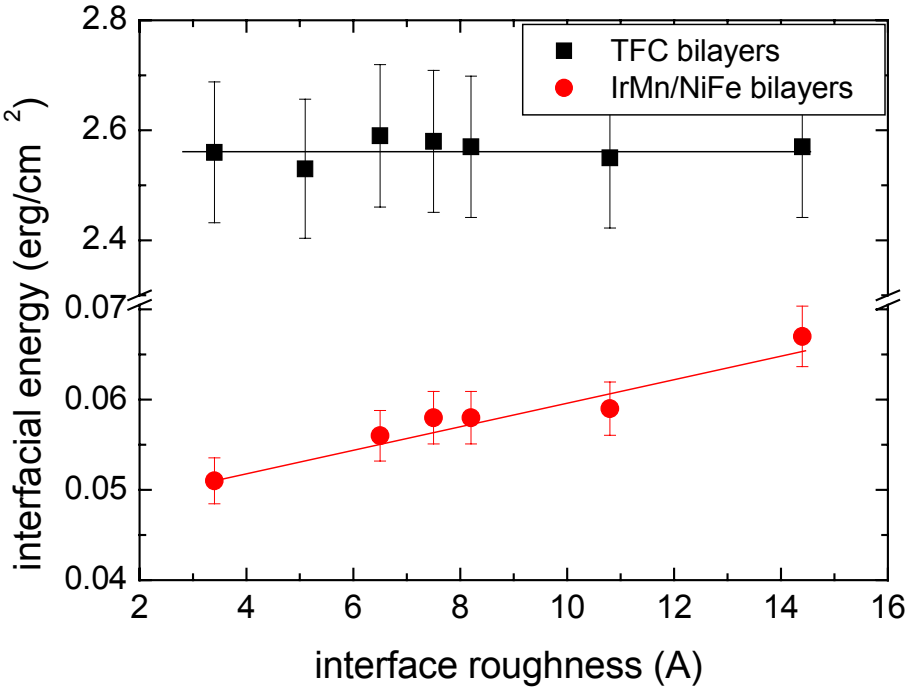

Fig. 5.7 Roughness dependence on σ_w of the bilayers of $Tb_{26.1}(Fe_{80}Co_{20})_{73.9}$ (20 nm)/ $Tb_{16.2}(Fe_{80}Co_{20})_{83.7}$ (20 nm) and IrMn (9 nm)/ NiFe (20 nm). Notice that the wavelength of the roughness also varies from 18 to 39 nm with increasing r.m.s. roughness.

5.3.e Dependence of Magnetic Anisotropy on Exchange Bias

In addition to spin compensation, the anisotropy of pining layer plays an important role for EB. Unfortunately, in typical FM/AFM systems, the magnetic anisotropy of AFM is hard to be measured and manipulated. In the TbFeCo system, the anisotropy can be easily varied by composition,

which enables us to study the effects of the anisotropy on EB. We adjusted the composition of TbFeCo layers, and investigated the dependence of EB on anisotropy of pinning layers. We fabricated the EB bilayers with the structure of pinning layer $Tb_x(Fe_{80}Co_{20})_{(100-x)}$ 20 nm/ pinned layer $Tb_{16.2}(Fe_{80}Co_{20})_{83.8}$ 20 nm, where x varied from 25.5 to 38.5. Fig. 5.8(a) shows the Ku of single TbFeCo layer with different composition, obtained by the measurement of Hall Effect with an in-plane external field [9]. The pinned layer of $Tb_{16.2}(Fe_{80}Co_{20})_{83.8}$ possesses higher Ku than pinning layers. σ_w of TbFeCo bilayers decreases with increasing Tb content of pinning layers, as indicated in Figure 5.8(b). Based on the concept of Block-wall formation in FI/FI bilayer, the theoretical values of σ_w can be expressed by [12-13]

$$\sigma_w = H_b Mt = \triangle\sigma/2 = 2(A \times Ku)^{1/2}, \qquad (5.7)$$

where A and $\triangle\sigma$ denote exchange stiffness and Block-wall energy, respectively. By assuming a typical value of A (2.0×10^{-7} erg/cm) and substituting Ku value into Eq. (2), we can derive the theoretical σ_w, which approximately agrees with the experimental value. This consistency implies that the Bloch wall was formed, similar to the AF domain wall model of Mauri et al. in FM/AFM systems [3].

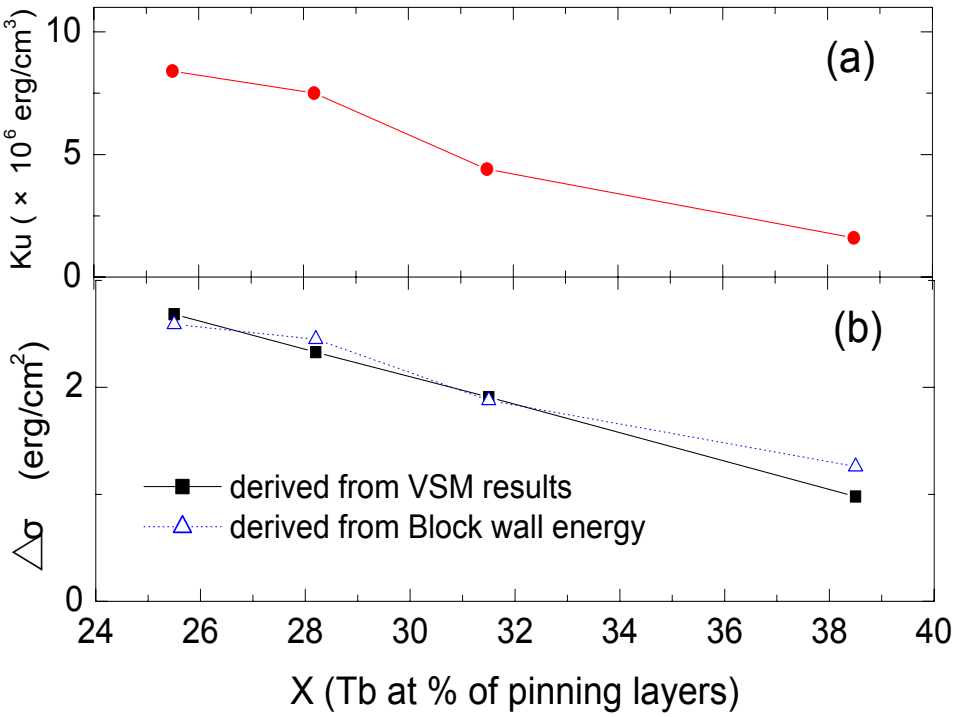

Fig. 5.8 (a) Variation of Ku of TbFeCo single layer with Tb content; (b) Dependence of experimental σ_w and the σ_w theoretically derived from Bloch-wall energy on Tb content of pinning layer in TbFeCo bilayers

5.4 Conclusion

The exchange-bias films of ferrimagnetic/ ferrimagnetic, ferromagnetic/ ferromagnetic, and ferromagnetic/ antiferromagnetic bilayers were fabricated to investigate their interfacial exchange energy σ_w. We have demonstrated high interfacial exchange energy (>5 erg/cm^2) in TbFeCo bilayers. A highly-uncompensated-spin interface is proposed to explain the strong EB in TbFeCo bilayer systems. IrMn/NiFe exhibited weaker EB than SmCo/NiFe due to the AF-coupling between the adjacent Mn-Mn atoms, verifying the importance of an uncompensated-spin interface to EB. In the bilayers with highly-uncompensated-spin interface, as TbFeCo films, the amount of uncompensated spins is a weak function of interface roughness, leading to less dependence of σ_w upon interfacial morphology. By adjusting the composition of TbFeCo films, we further demonstrated that the high Ku of pinning layer significantly enhances the σ_w.

Chapter 6

High Magnetization Exchange-Couple Double-Layer TbFeCo for Hybrid Recording

6.1 Introduction

As mentioned in the chapter 3, amorphous rare-earth transition-metal (RE-TM) films have been considered as a candidate for ultra-high density storage media because of amorphous structure, high perpendicular anisotropy, temperature-dependent magnetic properties, and simple deposition processes at room temperature [1-3]. In conventional magneto- optical (MO) recording, to reach higher recording density, shorter wavelength laser beams are needed for detecting small size marks; however, the readout signal level is still low due to the small mark size [1]. On the other hand, the GMR readout sensor in hard disk drive has much higher sensitivity in reading small marks, promoting a high growth rate of 60 % per year since 1997 [4]. Unfortunately, as the size of recording bits of longitudinal media decreases to several tens nm, the magnetic moments become unstable due to super-paramagnetic effect [4]. To overcome the thermal instability of magnetic domains, the media should possess high coercivity; however, the writing field may be insufficient to reliably record magnetic domains. Combining the

advantages of thermo-magnetic writing, magnetic flux detection, and the amorphous characteristics, the use of RE-TM films with perpendicular anisotropy in hybrid recording renders great potential for high-density storage [5-6].

For the magnetic flux reading, high magnetization media are desired to yield large flux density for GMR sensing. To ensure adequate stability of small size domains, the media for hybrid recording should possess large coercivity. However, the single-layer RE-TM film commonly used can not meet these requirements of high magnetization and coercivity simultaneously [2]. On the other hand, RE-TM exchange-coupled dual-layer (ECDL) films have been widely investigated as conventional MO recording media [7-8]. The RE-TM dual-layer media possess high CNR, wide power margin and high recording sensitivity in typical MO recording [8]. In addition, as discussed in the chapter 5, a strong exchange coupling also exists in the RE-TM bilayers. Therefore, ECDL RE-TM films were proposed to enhance the coercivity of high magnetization films through exchange-coupling between magnetic layers for the hybrid-recording media. At first, we designed, fabricated, and examined the dual-layer TbFeCo media, composed of readout and memory layers, with high magnetization and coercivity. The enhanced coercivity and the interfacial exchange energy in the TbFeCo dual layers with various compositions and thicknesses were explored. Then, the various magnetization-switching mechanisms in ECDL films were investigated. To further evaluate the feasibility of RE-TM films applied for the

magnetic-flux-reading, the single-layer RE-TM media were examined by GMR sensors in a dynamic tester of hard disks.

6.2 Experimental Procedures

The dual-layer TbFeCo media composed of readout and memory layers with various compositions and thicknesses were fabricated by using magnetron sputtering onto Si wafers, shown schematically in Fig. 6.1. The active layers were sandwiched by SiN_x layers to prevent TbFeCo from oxidation. The composition of ferrimagnetic films was controlled by the sputtering rate of Tb and $Fe_{80}Co_{20}$ targets to adjust the magnetic properties, including magnetization, coercivity, Cuie temperature, and magnetic anisotropy. The composition was calibrated by Rutherford backscattering spectrometry. A vibrating sample magnetometer (VSM) was applied to measure the hysteresis loops of the media. By using perpendicular Kerr-effect Tracer, the reversal of readout and memory layers in the hysteresis loops was identified. In addition, the Ku of single-layer TbFeCo was derived from the measurement of Hall Effect with an in-plane external field [9-10].

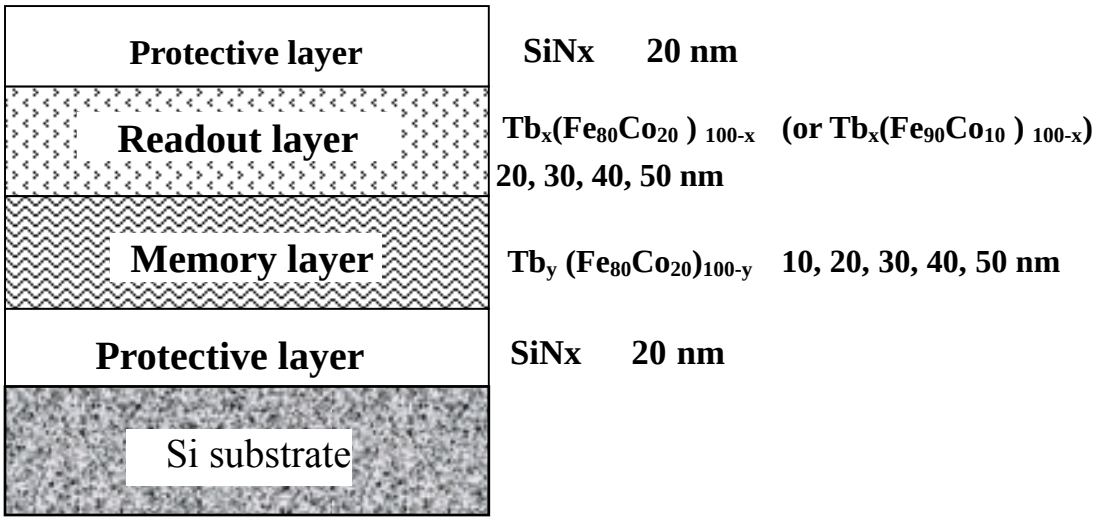

Fig. 6.1: Structure of TbFeCo dual-layer media.

To test thermomagnetic writing, the A-type media deposited on 3.5″ polycarbonate substrates were examined by a MO-disk tester using light intensity modulation (LIM) at a laser wavelength of 785 nm and an objective lens with NA = 0.55. Magnetic force microscope (MFM) was utilized to observe the recorded magnetic marks. In the magnetic-flux-detection testing, the TbFeCo films were deposited at different conditions on 1″ glass substrates. The media noises of the TbFeCo disks were examined by a GMR sensor in a commercial hard-disk tester (Guzik S1701B SpinStand). The testing conditions are listed as followed,

1. Read width: 0.32 um (min);
2. Write width: 0.72 um (max);
4. Flying height: 0.75 uinch;
5. Read bias: 5 mA;

6. Write current: 60 mA;

7. Testing radius: 0.255 inch from disk center;

8. RPM: 4500.

To clarify the factors affecting the media noise, a dynamic Kerr microscope was utilized to observe the coercivity uniformity of TFC films.

6.3 Results and Discussion

6.3.a Coercivity Enhancement in ECDL TbFeCo Films

The use of dual-layer films greatly enhances coercivity of high magnetization media because of strong exchange coupling at the interface between two active layers. The TbFeCo media with the composition diverged far from the compensation point were adopted as readout layers in ECDL films because of their high magnetization. Fig. 6.2 depicts the hysteresis loop of a single layer of 20 nm with the TM-rich composition of $Tb_{16.3}(Fe_{80}Co_{20})_{83.7}$, as a readout layer, possessing the saturation magnetization of 285 emu/cm^3 and the low coercivity of 1.7 kOe. When a RE-rich memory layer ($Tb_{25.5}(Fe_{80}Co_{20})_{74.5}$) of 20 nm was added at the bottom, the effective coercivity (Hc_{eff}), corresponding to the switching field, of readout layer increased greatly from 1.7 kOe of a single layer to 7.5 kOe in the A-type medium, as shown in Fig. 6.3. In

addition, the hysteresis loop also shows the two-step magnetization switching as a field varies from positive to negative saturation. A micromagnetic model established by Kobayashi et al. has been widely employed to theoretically analyze the magnetization reversal mechanism of RE-TM exchange-coupling dual-layer (ECDL) films [11]. Phenomenally, the magnetization reversal of the A-type media in Fig. 6.3 followed the switching mechanism in Kobayashi model specified by the condition:

$$H_{c1} + H_{c2} > \frac{\Delta\sigma}{2M_1 t_1} - \frac{\Delta\sigma}{2M_2 t_2} > H_{c1} - H_{c2} \quad . \tag{6.1}$$

Here, 1 and 2 respectively for readout and memory layers, Hc is coercive field, M is magnetization, t is layer thickness, and $\triangle\sigma$ is interfacial-wall energy. The coercivity enhancement in the A-type ECDL film with high magnetization results from the formation of interface wall at saturation field to relax the increase in exchange coupling energy for 3d-3d and 4f-4f subnetworks after readout layer reverses. In the Fig. 6.3, the effective coercivity or the switching field for transition "C" of readout layer Hc_R is given by:

$$Hc_R = Hc_1 + \triangle\sigma/2M_1t_1 \tag{6.2}$$

Also, the switching fields Hs_A and Hs_B for the transitions of "A" and "B" are given as:

$$Hc_A = Hc_2 + \triangle\sigma/2M_2t_2 \tag{6.3}$$

and

$$Hs_B = -Hc_2 + \triangle\sigma/2M_2t_2 \tag{6.4}$$

Combining Eqs. (6.3) and (6.4), we can derive the equations

$$\Delta\sigma = M_2t_2(Hs_A + Hs_B) = M_2t_2(\frac{H_{b2}}{2}) \tag{6.5}$$

and

$$H_{b2} = \frac{(Hs_A + Hs_B)}{2}. \tag{6.6}$$

where H_{b2} is the shifting field of memory layer due to the exchange coupling from readout layer. By obtaining the values of M, t, and switching fields in VSM measurement, the $\triangle\sigma$ can be experimentally derived.

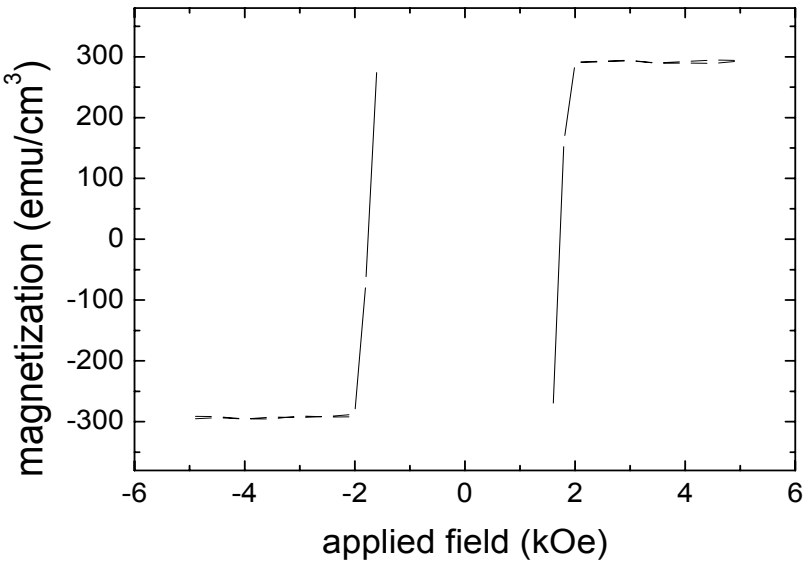

Fig. 6.2: Hysteresis loop of single layer of 20nm with TM-rich composition of $Tb_{16.3}(Fe_{80}Co_{20})_{83.7}$.

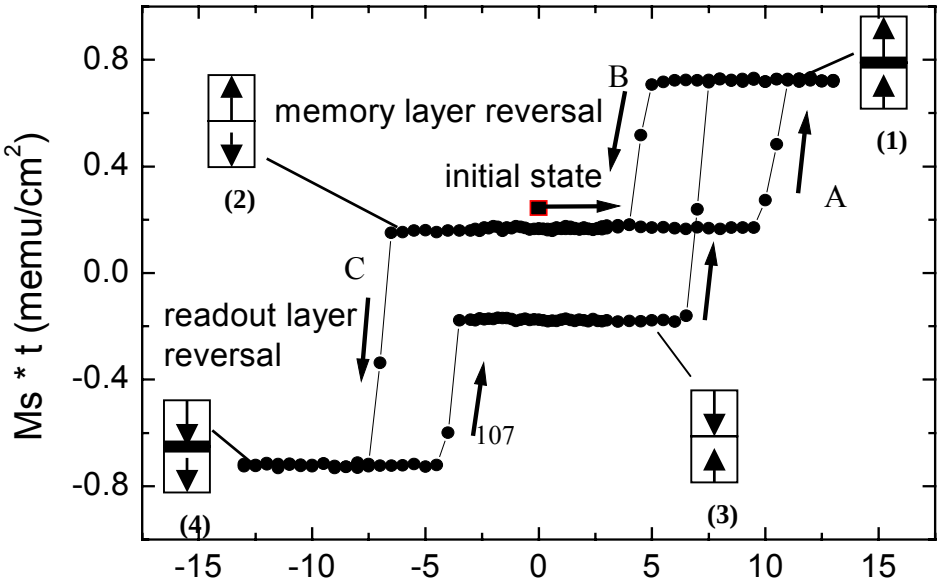

Fig. 6.3: VSM measurement of A-type ECDL film with 20 nm memory layer (RE-rich)/20 nm readout layer (TM-rich). The initial state is in state (2). The field was applied following the ABCDE sequence indicated by the arrows.

On the other hand, the coercivity enhancement was also observed in P-type films. Fig. 6.4 shows the hysteresis loop of P-type dual-layer media composed of TM-rich memory layer 20 nm $(Tb_{20.5}(Fe_{80}Co_{20})_{79..5})$/ TM-rich readout layer 20 nm $(Tb_{16.3}(Fe_{80}Co_{20})_{83.7})$. In this film, the magnetizations in two magnetic layers coherently switch with the variation of applied fields, consistent with the switching mechanism in Kobayashi model designated by the condition,

$$\frac{\Delta\sigma}{2M_1t_1}+\frac{\Delta\sigma}{2M_2t_2}>\left|H_{c1}-H_{c2}\right| . \qquad (6.7)$$

Because of strong exchange coupling between the RE-TM bilayers, the interfacial-wall energy in the film is higher than the coercive energy of magnetic layers. While one of the two layers reverse and their net magnetizations of two TM-rich TbFeCo layers are antiparallel, the formation of interfacial-wall in the films is a high-energy state, not a preferred state. Therefore, the mechanism of coherent

magnetization-switching without the interfacial-wall formation is adopted in the P-type film. As described in the Section 3.2.b, the switching field Hs can be given by

$$H_s = -\frac{M_2 t_2 H_{c2} + M_1 t_1 H_{c1}}{M_2 t_2 + M_1 t_1} \tag{6.8}$$

As shown in Fig. 6.4, the effective coercivity of readout layer in the P-type film is only 4.1 kOe, less than that in the above A-type.

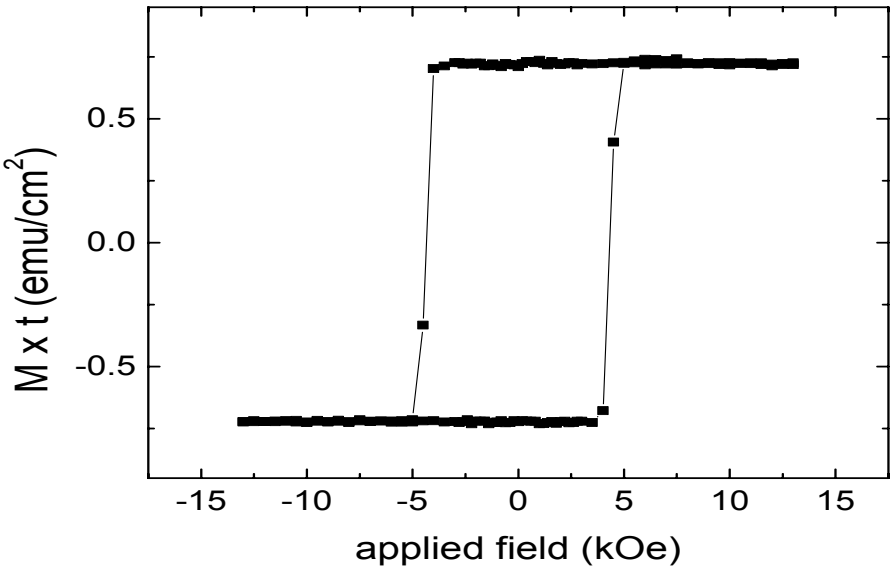

Fig. 6.4: VSM measurement of P-type ECDL film with 20 nm memory layer (TM-rich)/20 nm readout layer (TM-rich).

6.3.b Dependence of TFC-layer Composition on Enhanced Coercivity

The enhanced coercivity of readout layer in ECDL media is significantly affected by the composition of TbFeCo layers. In the experiments, two sets, A and B, of dual-layer TbFeCo media consisting of 20 nm readout and 20 nm memory layers were fabricated on Si substrate. The readout layers were made of a TM-rich layer of composition A ($Tb_{16.3}(Fe_{80}Co_{20})_{83.7}$, Ms = 285 emu/cm^3, Hc = 1.7 kOe) in set A or of an RE-rich layer of composition B ($Tb_{40.5}(Fe_{80}Co_{20})_{59.5}$, Ms = 253 emu/cm^3, Hc = 0.8 kOe) in set B. The memory layers were $Tb_x(Fe_{80}Co_{20})_{(100-x)}$ with x varying from 19 to 38.5. The dependence of the Hc_{eff} of readout layer and the $\triangle\sigma$ on the composition of memory layer for the media in set A and B is shown in Fig. 6.5. As indicated in Figure 6.5(a), the P-type media in set A with both TM-rich readout and memory layers exhibit slightly larger coercivity than the single readout layer, resulting from the biasing effect. In contrast, the Hc_{eff} of readout layer can increase significantly from 1.7 kOe of single-layer TFC to 7.5 kOe in the A-type media with memory layer $Tb_{25.5}(Fe_{80}Co_{20})_{74.5}$. With further increasing Tb content, the Hc_{eff} of readout layer gradually decreases. In addition, the $\triangle\sigma$ of A-type media in set A, derived from the Eq. (6.5), also reduced with increasing Tb contents, directly interpreting the variation of the Hc_{eff} of readout layer with the composition of memory layer. On the other hand, Fig. 6.5(b) indicates the $\triangle\sigma$ of A-type media in set B is much lower than those in set A, leading to the low coercivity enhancement.

To further clarifying the above argument, the Ku in the $Tb_x(Fe_{80}Co_{20})_{100-x}$ film was obtained from the measurement of Hall Effect

[3.9-3.10] shown in Fig. 6.6. As described in the previous chapter, the $\triangle\sigma$ is associated with exchange coupling between active magnetic layers and can be given by [12]

$$\triangle\sigma = 4\sqrt{AK_u}\ . \tag{6.9}$$

Here, Ku and "A" respectively indicate the magnetic anisotropy constant and exchange stiffness coefficient of the one of two adjacent TbFeCo layers with lower anisotropy.

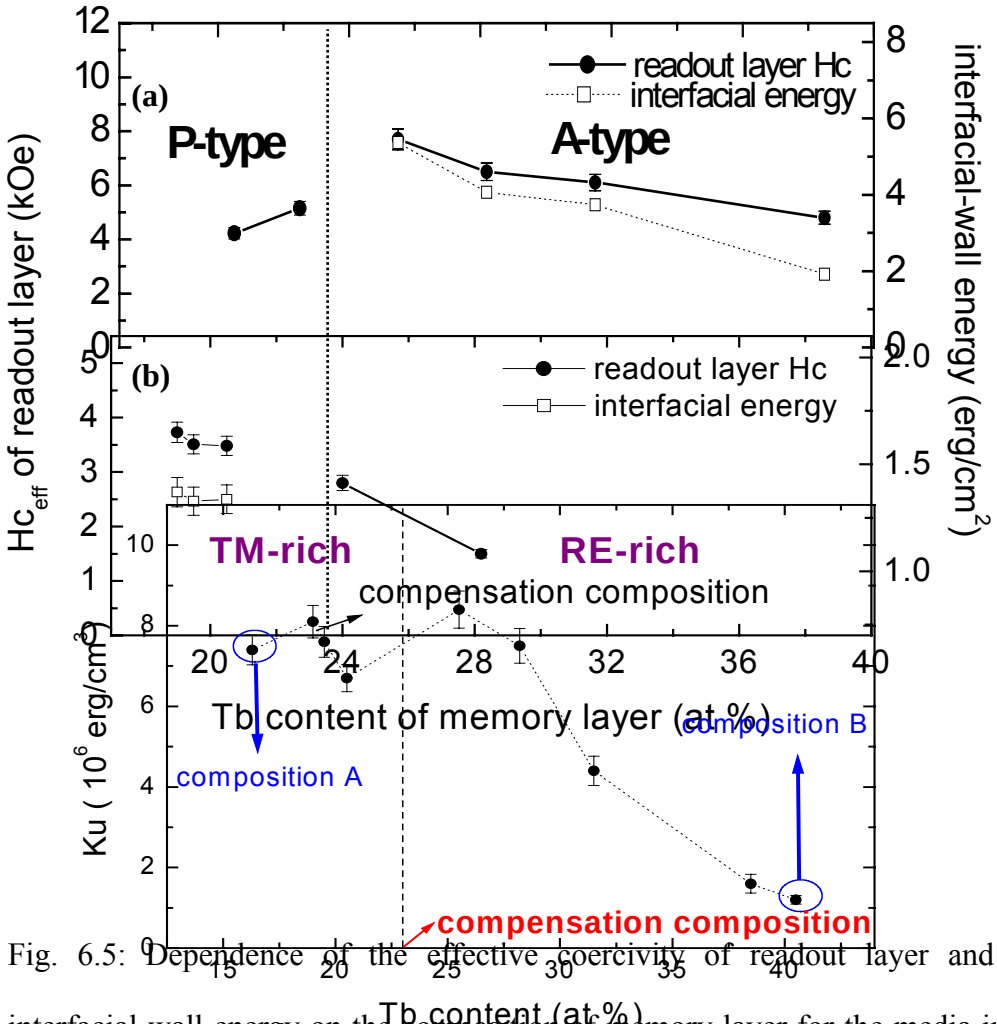

Fig. 6.5: Dependence of the effective coercivity of readout layer and the interfacial-wall energy on the composition of memory layer for the media in (a) set A and (b) set B.

Fig. 6.6: Variation of anisotropy constant Ku with Tb content in $Tb_x(Fe_{80}Co_{20})_{100-x.}$

6.3.c Thickness Dependence on Enhanced Coercivity

Magnetic properties of A-type ECDL films strongly depend upon thickness of active magnetic layers. To explore how thickness of active layers affects effective coercivity and interface energy, a series of the media with different thickness were fabricated and examined. Here, the readout layer with TM-rich composition of $Tb_{16.5}(Fe_{90}Co_{10})_{83.5}$ possesses Ms = 370emu/cm^3 , Hc = 0.95 kOe, and Curie temperature (T_{Curie})=200 ^oC; the memory layer with RE-rich composition of $Tb_{27.5}(Fe_{80}Co_{20})_{72.5}$ has Ms = 113 emu/cc, Hc = 4.6 kOe, and T_{Curie} = 250 ^oC. First, at 20 nm of readout layer, coercivity and interface energy as a function of memory-layer thickness are shown in Figs. 6.7 and 6.8. The thickness of memory layer (t_M) significantly affects the magnetic properties of the above media, as revealed in Fig. 6.7. At t_M = 10 nm,

the hysteresis loop exhibits larger Hc than that of single TM-rich layer because of biasing effect from the RE-rich layer. When t_M > 10 nm, RE-rich memory layer exhibits its own properties that results in further coercivity enhancement, where the coercivity of readout layer increases from 0.95 kOe in single-layer medium to 6 kOe in dual-layer media with 20 nm memory layer. As mentioned in the above, the larger coercivity of TM-rich layer is due to the formation of domain wall at the interface of the double-layer under a saturation field. When t_M > 20 nm, readout layer coercivity almost keeps constant as shown in Fig. 6.8. On other hand, interfacial-wall energy exhibits less dependent on thickness and maintains the value around 4.1 erg/cm^3, implying that the energy mainly be related with exchange interaction at the interface for ECDL films. Once the interface wall can be formed in the layers with sufficient thickness, further increase in memory layer no longer affects the exchange interaction at the interface. As a result, readout layer coercivity becomes constant. For comparison, the dependence of interface energy and coercivity on readout-layer thickness is plotted in Fig. 6.9, where readout layer coercivity is smaller for thicker films. It results from the coercivity enhancement is inversely proportional to thickness and the interface energy less depends on readout-layer thickness, as indicated in Eq. 6.2.

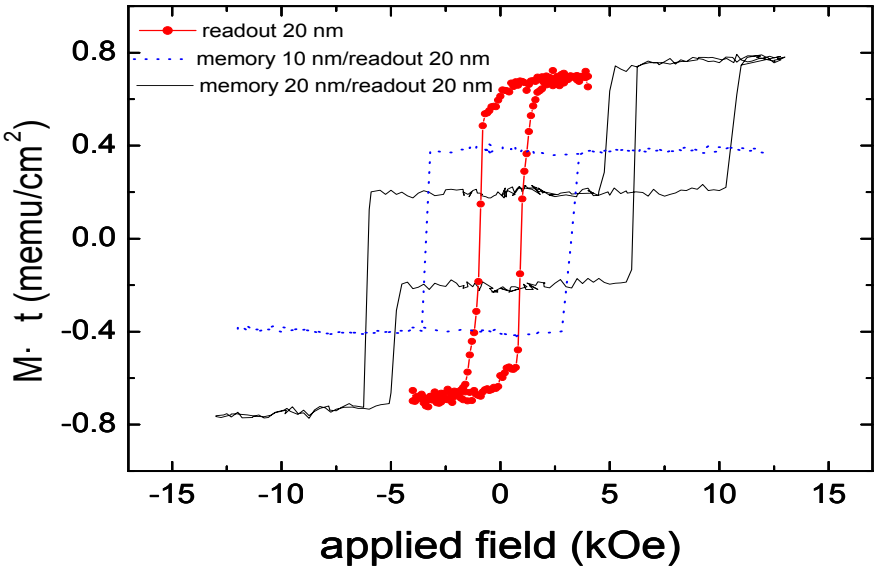

Fig. 6.7: VSM measurement of dual-layer media with different memory layer thickness.

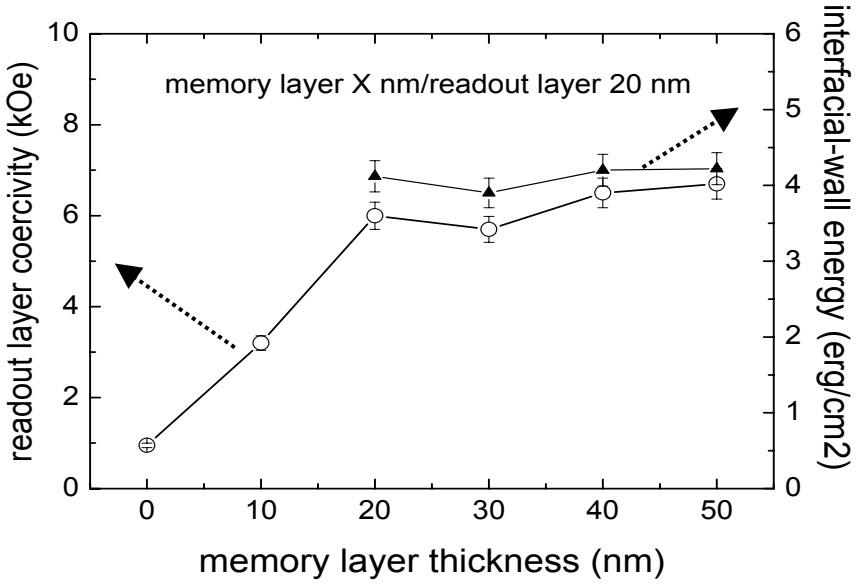

Fig. 6.8: Memory-layer thickness dependence of readout layer coercivity and interface energy.

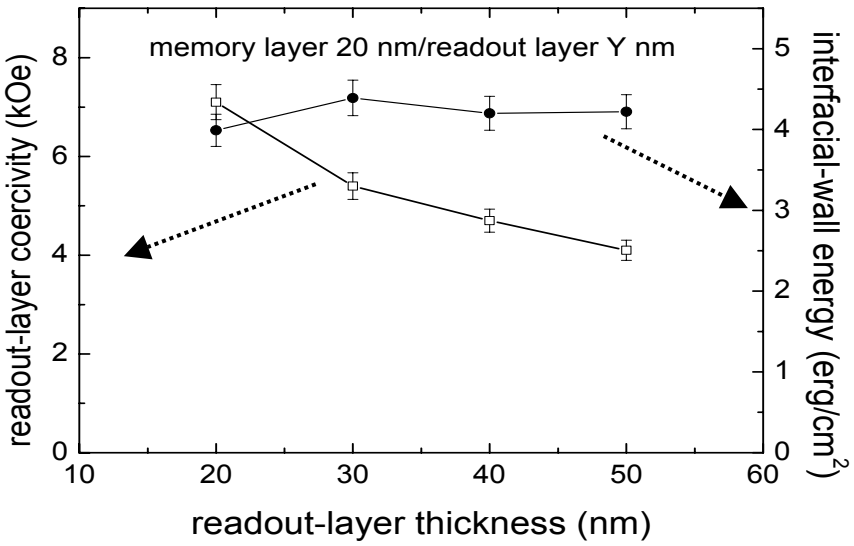

Fig. 6.9: Readout-layer thickness dependence of readout-layer coercivity and interface energy.

6.3.d Thermomagnetic Properties of A-type ECDL Media

Since the signal-recording in hybrid recording is achieved by thermomagnetic-writing mechanism, the thermomagnetic properties in A-type ECDL TbFeCo films should be seriously taken into the consideration. In the experiments, the magnetic properties of A-type ECDL media are strong functions of temperature. As indicated in Fig. 6.10, the interfacial-wall energy in an A-type media, consisting of the readout layer with T_{Curie} = 200 ^{o}C and memory layer with T_{Curie} = 270 ^{o}C, decreases with increasing temperature because of thermal fluctuation of magnetic spins. As temperature is up to the T_{Curie} of readout layer, the exchange coupling between magnetic layers disappears. Therefore, the

single hysteresis loop is observed at the T_{Curie} of readout layer. Fig. 6.11 shows the Kerr loops of an A-type medium at different temperature. In addition, as indicated in Fig. 6.11, the magnetization-switching mechanism in the A-type medium also varies with temperature. Within 25 ^{o}C and 50 ^{o}C, two-step transition is adopted as the field varies from positive to negative saturation, resulting from the condition of Eq. (6.1) is satisfied [11]. However, the variations of interfacial-wall energy and the magnetizations of readout and memory layers with temperature lead to the following switching mechanism specified by Eq. (6.10) at high temperature.

$$\frac{\sigma_w}{2M_1 t_1} - \frac{\sigma_w}{2M_2 t_2} > H_{c1} + H_{c2} \tag{6.10}$$

Therefore, magnetization-switching mechanism of three-step transition becomes preferred at the temperatures of 80 ^{o}C and 190 ^{o}C, as exhibited in Fig. 6.11. Although the switching mechanism varies with temperature lower than the T_{Curie} (200 ^{o}C) of readout layer, it does not affect the signal-writing performed near the T_{Curie} (270 ^{o}C) of memory layer. The thermomagnetic writing in the A-type TbFeCo media will be further discussed in the following section.

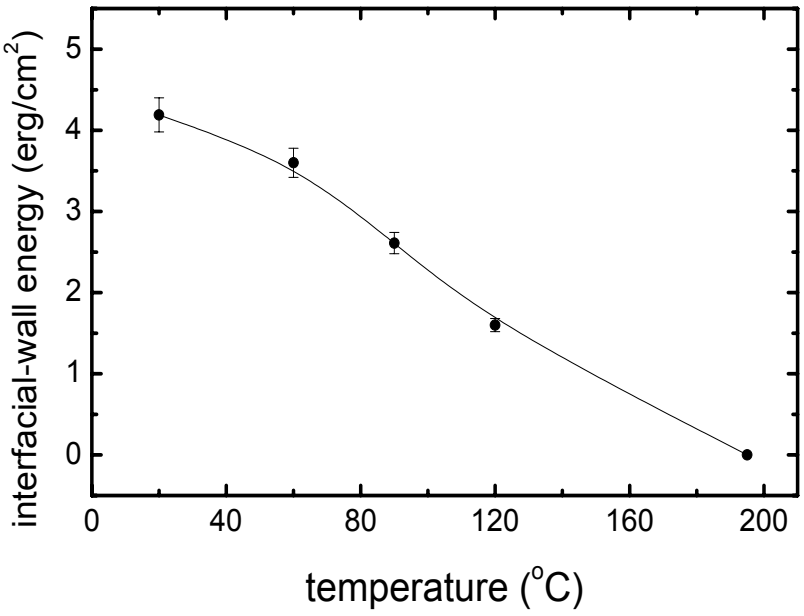

Fig. 6.10: Dependence of interfacial-wall energy on temperature in an A-type ECDL medium.

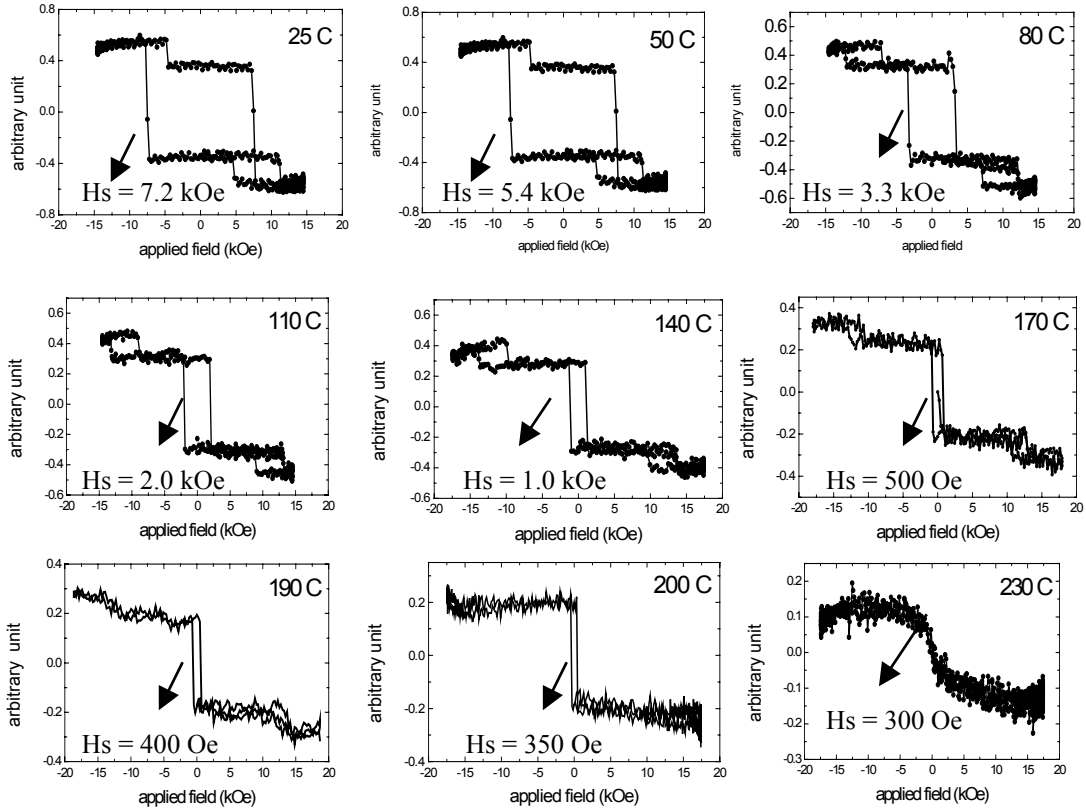

Fig. 6.11: Kerr loops of an A-type ECDL medium at different temperature.

6.3.e Simulating Thermomagnetic-Writing Process

Because of strong demagnetizing effect in the single-layer TbFeCo with high magnetization during the thermomagnetic-writing process, the subdomains are easily formed during cooling process in the media and recorded domains become irregular, leading to large media noise in the signal reading [13-14]. Therefore, to suppress the formation of the subdomain and the irregularity of the domain shape, the RE-rich memory layer with higher T_{Curie} and lower magnetization than TM-rich readout

layer was adopted in the proposed A-type ECDL TbFeCo media for hybrid recording. In the writing process, the A-type media was rapidly heated by laser incidence to the temperature around the T_{Curie} of memory layer (higher than the T_{Curie} of memory layer). Meanwhile, a magnetic field induced by a writing current is applied to determine the magnetization direction of recording domain in the memory layer while the moments of TM-rich readout layer align randomly. During cooling to room temperature after the laser moving away, the magnetization direction of readout layer in the A-type media is designated by that of the memory layer through strong exchange coupling between two magnetic layers. To explore the feasibility of the A-type media for hybrid recording, experiments were performed to simulate the thermomagnetic writing. The A-type ECDL TbFeCo films, consisting of the TM-rich readout layer with T_{Curie} = 200 ^{o}C and RE-rich memory layer with T_{Curie} = 270 ^{o}C, was first heated to 260 ^{o}C and a magnetic field of 200 Oe was applied to determine the magnetization direction of the memory layer. The film was subsequently quenched down to room temperature without a magnetic field, the residual magnetization of the A-type ECDL medium is the same as that of the medium initialized by a positive saturation field (10 kOe) at room temperature. The result strongly suggests that the magnetization direction of RE-rich layer determined at writing temperature can be effectively exchanged-coupled to the TM-rich layer for desired magnetization switching. In addition, the disk composed of the A-type ECDL films was examined in a MO-disk tester by using the manner of LIM recording. From the clear MFM images of the 1um and 0.5 um marks shown in Fig. 6.12, it can be further concluded the

magnetic signals could be successfully recorded in the proposed media of the A-type ECDL TbFeCo through thermomagnetic writing.

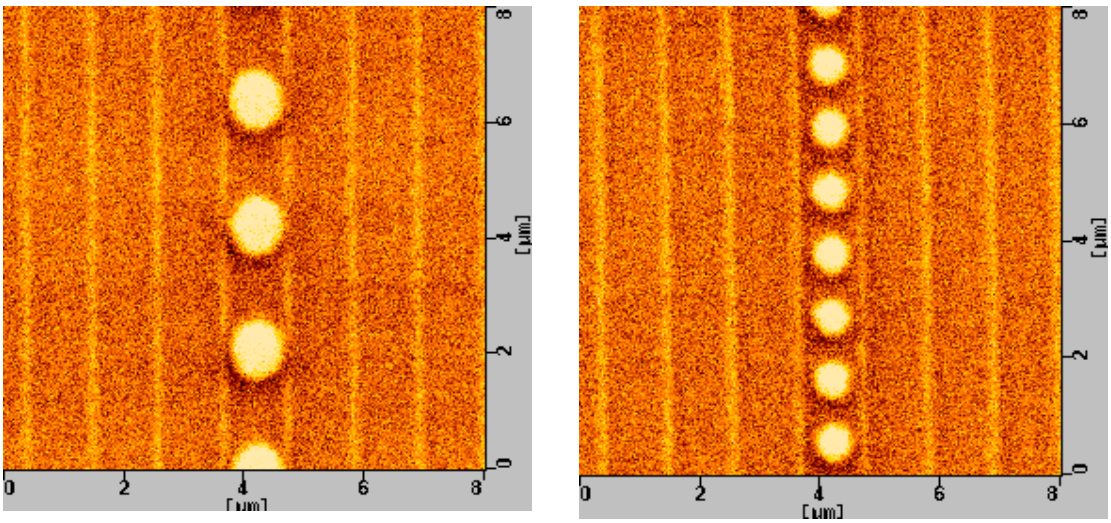

(a) 1μm marks (b) 0.5μm mark

Fig. 6.12: MFM observation of (a) 1 um and (b) 0.5 um marks in the A-type ECDL disk which were writing by MO-disk.

6.3.f Low Media-noise TbFeCo Disks

To evaluate the application of the RE-TM media to hybrid recording, the disks composed of readout layer of $Tb_{16.3}(Fe_{80}Co_{20})_{83.7}$ with high magnetization of 285 emu/cm^3 were fabricated in the clean room for the testing of signal reading by GMR sensor, as shown in Fig. 6.13. Because the out-of-plane writing field provided by the recording head in the commercial hard-disk tester is not large enough to saturate the A-type ECDL media, to fully saturate the readout layer to study the erased signal, the memory layer was skipped to reduce the saturation field in the tested

disks. In addition, the diamond-like carbide (DLC) layer is used to increase the hardness of disks against the striking of R&D heads, and the lubricant is used to decrease the friction between the disk and the head. The total thickness of upper SiN_x layer, DLC layer, and lubricant should be thin to reduce the spacing loss of readout signal. The media noise of TbFeCo disks, examined by GMR sensor after saturating the media by a writing head, was strongly affected by the fabrication parameters, like base pressure. Figs. 6.14 (a) and (b) indicate the erased signals of $Tb_{16.3}(Fe_{80}Co_{20})_{83.7}$ disks deposited respectively at the base pressures of 5 x 10^{-7} and 1.5 x 10^{-7} torr. Obviously, the noise in the disk (b) is lower than that in the (a) where irregular jumps appear in the erased noise. Comparing with the erased noise of commercial CoCr-based disk shown in Fig. 6.14(c), the TbFeCo disk deposited at relatively high vacuum exhibits the media-noise as low as the hard disks. To further explain the high media-noise in the TbFeCo disk deposited at relatively poor vacuum, a dynamic Kerr microscope was utilized to examine the film quality of TbFeCo disks. The coercivity distributions of the above TbFeCo disks are showed in Figs. 6.15 (a) and (b). Fig. 6.14(a) indicates the magnetization-switching was restricted in some area of the TbFeCo deposited at relatively poor vacuum, leading to the non-uniformity in coercivity distribution. It should result from the existence of the impurity or the TbOx formation in the films because of poor vacuum and easy-oxidation of Tb. In contrast, a uniform coercivity distribution and square hysteresis loop are observed in the TbFeCo disk deposited at high vacuum, leading to its low media noise. Therefore, the requirement of the base pressure in the fabrication of TbFeCo disks is strict for the

magnetic-flux-detection recording.

On the other hand, the dynamic recording characteristics of the single-layer TbFeCo disks deposited at high vacuum was also examined without heating procedure by using a recording head in the hard-disk tester. Fig. 6.16 shows the recording signals of the single-layer TbFeCo disk with H_c of 1.7 kOe at 1, 2, 4, and 8 MHz recording frequencies which respectively correspond with the recording- mark lengths of 3, 1.5, 0.75, and 0.225 um. As indicated in the reproduced-waveform figures, the signals at the frequency more than 4MHz are difficult to be reliably recorded in the TbFeCo disks. In addition to the insufficient out-of-plane writing field providing by the recording head, the strong exchange coupling between magnetic spins in the RE-TM films also lead to the difficulty in the signal writing [15-16].

Lubricant	1 nm
DLC layer	5 nm
Upper SiNx	2 nm
TbFeCo	20 nm
Bottom SiNx	30 nm
Glass substrate	

.

Fig. 6.13: Schematic diagram of TbFeCo disks for the dynamic testing of magnetic-flux detection.

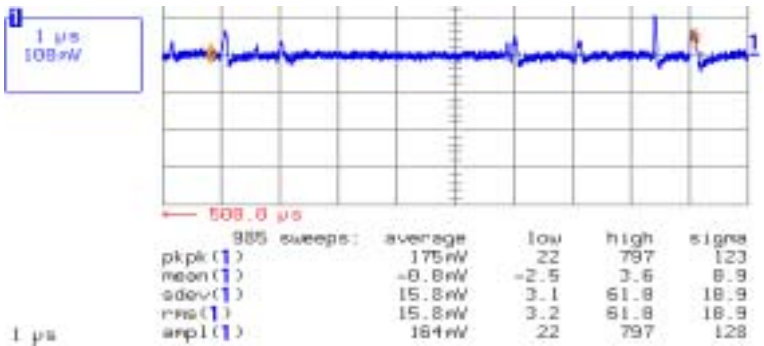

(a)

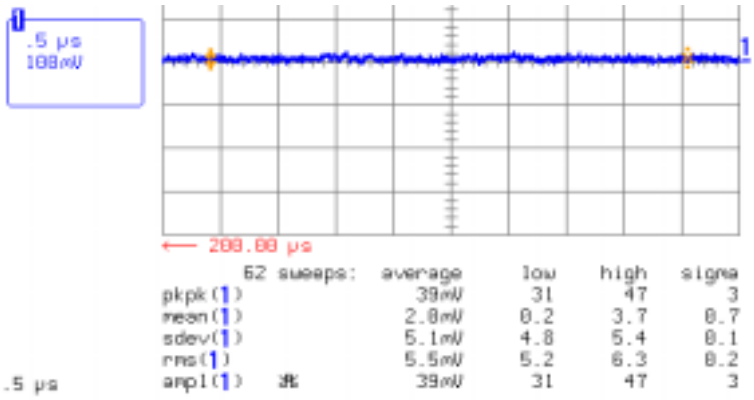

(b)

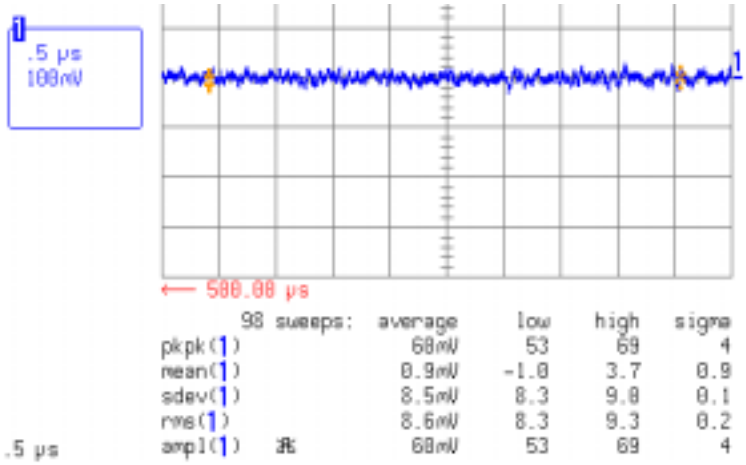

(c)

Fig. 6.14: Erased signals of TbFeCo disks deposited at the based pressure of (a) 5 x 10^{-7} torr and (b) 1.5 x 10^{-7} torr. The (c) is the erased signal of commercial CoCr-based disk.

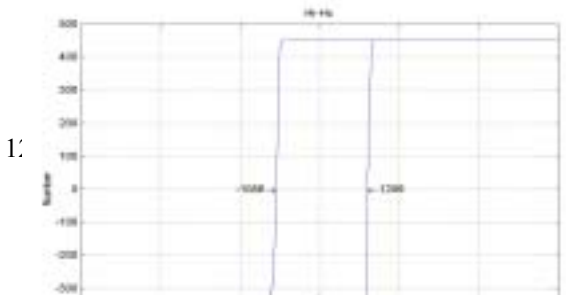

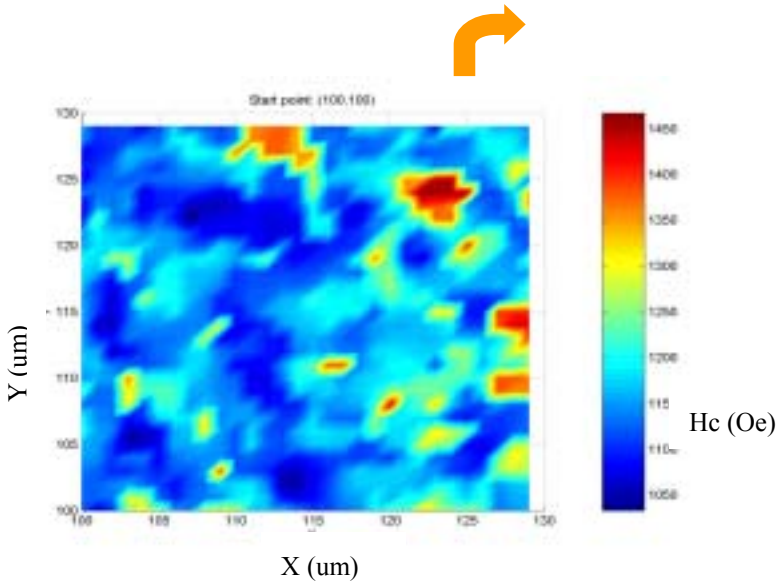

(a)

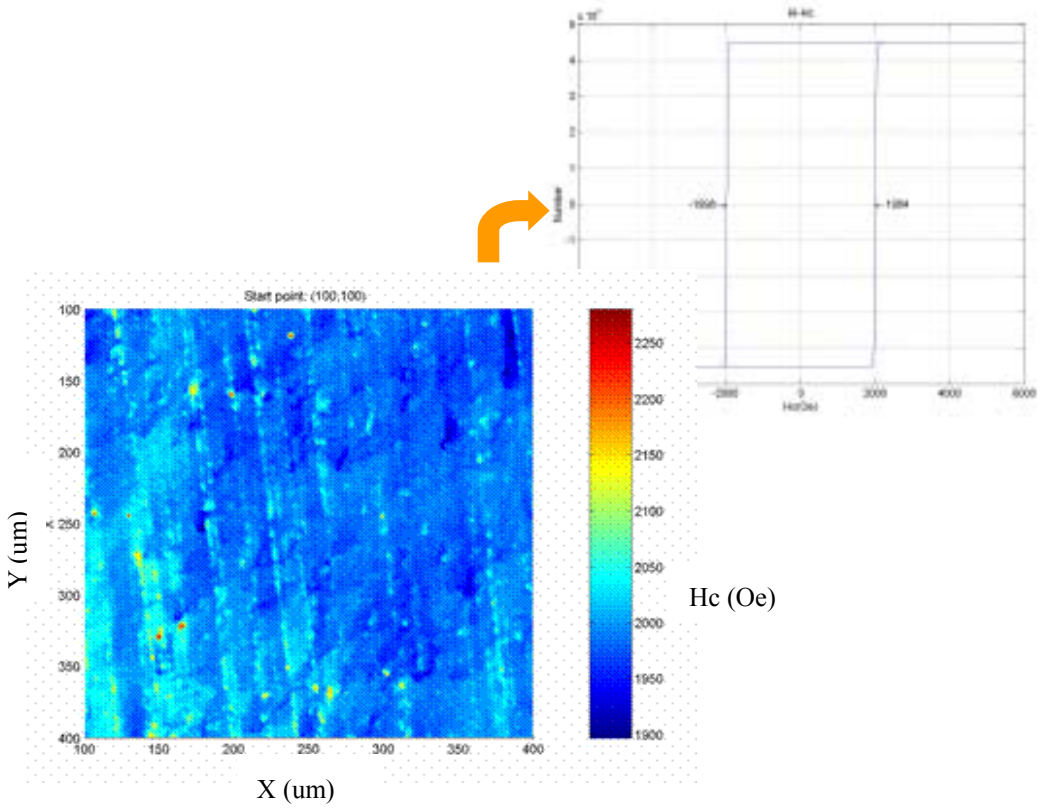

(b)

Fig. 6.15: Coercivity distribution of TbFeCo disks deposited at the based pressure of (a) 5 x 10^{-7} torr and (b) 1.5 x 10^{-7} torr.

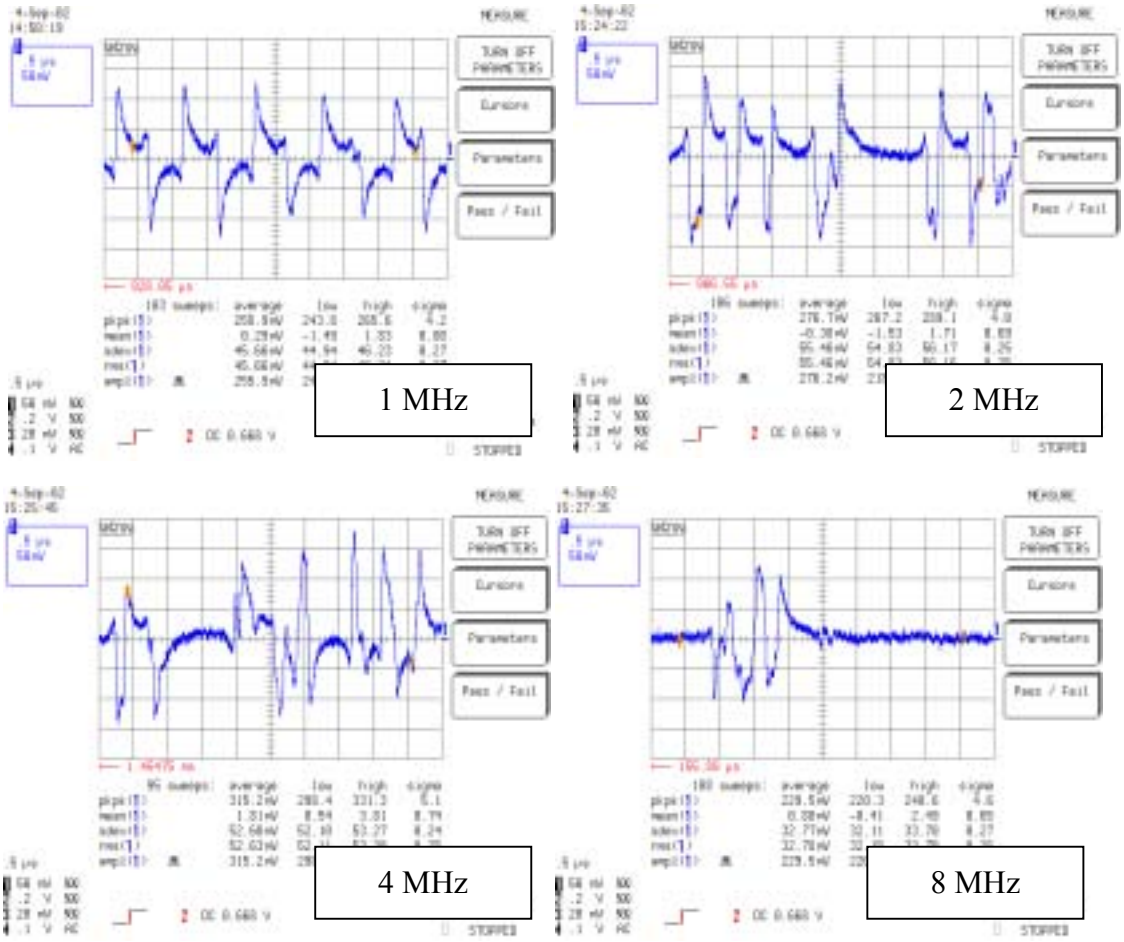

Fig. 6.16: Recording signal of single-layer TbFeCo disk with H_c of 1.7 kOe at 1, 2, 4, and 8 MHz recording frequencies which respectively corresponding with the recording- mark lengths of 3 , 1.5 , 0.75, and 0.225 um.

6.4 Conclusion

RE-TM exchange-couple dual layer media with high magnetization and large coercivity were investigated for hybrid recording. Through the strong exchange coupling between TbFeCo layers with perpendicular anisotropy, the coercivity of the TbFeCo with high magnetization of 370 emu/cm^3 could be greatly enhanced from 0.95 to 6 kOe. In addition, the A-type ECDL films exhibit larger coercivity enhancement than the P-type because of the interfacial-wall formation. The coercivity enhancement in the A-type media is proportional to interfacial-wall energy and, thus, magnetic anisotropy. Therefore, the A-type ECDL media composed of TM-rich readout layer and RE-rich memory layer with high magnetic anisotropy are preferred for the hybrid recording because of the consideration of high coercivity enhancement. Furthermore, the interfacial-wall energy in ECDL films is less dependent on thickness of readout and memory layer. Thin readout layer possesses high effective coercivity because the coercivity enhancement is inversely proportional to its thickness. In the thermomagnetic-writing testing, we can reliably record the marks in the A-type media with TM-rich readout layer by using MO-disk tester. In magnetic-flux-detection testing, the TbFeCo disks fabricated at high vacuum exhibit low media-noise examined by GMR sensor. Consequently, the A-type ECDL TbFeCo media with magnetization over 370emu/cm^3 and high stability are potentially applicable for hybrid recording of thermomagnetic writing and magnetic-flux readout.

Chapter 7

Investigation of Exchange Coupling

in TbFe/Co Exchange-coupled Bilayers

7.1 Introduction

Extensive efforts have been devoted to investigate the physical mechanisms of the exchange bias because of the fundamental interest and important technical applications [1]. Most of the research focused on the investigation of the exchange interaction between ferromagnetic (FM) and antiferromagnetic (AFM) bilayers with longitudinal anisotropy applied for storage industry. In the previous chapters, the strong exchange coupling between RE-TM bilayers with perpendicular anisotropy have be discussed in details. On the other hand, the planar exchange anisotropy was also found in the bilayers composed of ferromagnetic layer with in-plane anisotropy and ferrimagnetic rare-earth-transition-metal (RE-TM) alloys with perpendicular anisotropy [2]. Since RE-TM films are amorphous with strong exchange anisotropy coupled to FM, these bilayers can potentially replace the FM-AFM for applications [3-6]. Cain et al. proposed that the strong exchange coupling between RE-TM and FM resulted from the existence of a homogeneous and continuous interface in the bilayers [3-4]. However, the biasing mechanism was only described by indirect results because of difficulties in analyzing the orientation of magnetic moments in the films [6]. Over the last few years, X-ray magnetic circular dichroism (XMCD) technique has evolved into an important magnetometry tool [7]. It possesses high sensitivity to

element-specifically determine spin and orbital magnetic moments and their anisotropy in ferromagnets or ferrimagnets systems [8-10]. In this work, we deposited thin Co layers with various thicknesses on the TbFe to quantitatively derive the orientation of the moments at the interface from the XMCD measurements. By observing the variation of canting angles of Co and Fe with the Co thickness, we can concretely build up a scheme to clarify the source of exchange bias in the bilayers with perpendicular and longitudinal anisotropies. In addition, the TbFe/Co bilayers composed of the TbFe layers with different compositions were also examined in the experiments.

7.2 Experimental Procedures

The $Tb_xFe_{(100-x)}$ 300 Å / Co y Å were deposited by magnetron sputtering at the base pressure of 3×10^{-7} torr onto Si substrates, where x and y respectively varied from 14.0 to 33.6, and 5 to 150. The compositions of TbFe films were controlled by adjusting the sputtering current of Tb and Fe targets, and calibrated by Rutherford backscattering spectrometry. The TbFe/Co bilayers were sandwiched by SiN_x layers to prevent oxidation. An in-plane field of 150 Oe was applied during the deposition to induce the exchange-biasing field. A vibrating sample magnetometer (VSM) and Kerr-effect Tracer were used for measuring the magnetic properties. The Ku of single-layer TbFeCo was derived from the measurement of Hall Effect with an in-plane external field [11-12]. XMCD spectroscopy was utilized to derive the effective canting angles of Fe and Co in the bilayers through the total electron yield measurement. *L*-edge absorption spectra of Fe and Co were respectively obtained within the energy range of 695-740 eV and 770-810 eV. The energy resolution and degree of polarization at the Co, Fe edges are 0.2 eV and 60 %. All of the XMCD measurements were performed at room temperature without applied fields.

7.3 Results and Discussion

7.3.a Magnetic Properties of TbFe/Co Bilayers with Various Co Thickness

The Co anisotropy strongly depends on its thickness in the bilayers of $Tb_{21.3}Fe_{78.7}$ 300 Å / Co 5-150 Å. The single layer of $Tb_{21.3}Fe_{78.7}$ possessed the coercivity of 16.2 kOe in the out-of-plane direction and low magnetization of 15 emu/cm^3. The low magnetization was chosen to suppress the effect of dipole-dipole interaction on exchange bias. As 15 Å Co with in-plane anisotropy was deposited on 300 Å TbFe with the perpendicular anisotropy, not only the planar hysteresis loop was disappeared but the remanence magnetization was reduced as well, as shown in Fig. 7.1(a). In contrast, a square out-of-plane loop was obtained and its product of remanence magnetization and thickness (M_rt) was approximately equal to the M_rt sum of TbFe and Co. It implied that Co moments were aligned in the perpendicular direction and coherently rotated with the TbFe under the applied fields due to the strong exchange interaction between the bilayer. Similar to the effect of exchange coupling between soft and hard magnetic films, the effective coercivity of TbFe decreased from 16.2 kOe of single layer to 5.7 kOe in the bilayer. As the Co thickness increased to more than 25 Å, in-plane shifted loops were observed in the film plane. As shown in Fig. 7.1(b), the in-plane loops of 50 Å Co in the bilayer exhibited a biasing field of 145 Oe and an enhanced coercivity of 106 Oe. The oblique out-of-plane loop indicated that Co has a significant planar anisotropy in the bilayer. In addition, the direction of the exchange bias in the TbFe/Co bilayers was stably along the direction of the field during deposition, even after applying an

in-plane field of 20 kOe in an arbitrary direction at room temperature. However, the direction of the exchange anisotropy became controllable by heating the bilayers over 120°C, the Curie temperature of TbFe, for few seconds and cooling down under an in-plane field of 200 Oe because reorientation of Tb and Fe moments took place. Based on these results, we can infer that the direction of the exchange bias field was determined by the orientation of TbFe moments at the interface.

The in-plane coercivity (Hc) and biasing field (H_b) of Co also depended strongly on the Co thickness in the bilayer, as shown in Fig. 7.2. The Co in the bilayer possessed higher Hc than that in the single layer because of exchange interaction between TbFe and Co. With increasing thickness, the in-plane anisotropy of Co became dominant because surface anisotropy was weakened [13]. As the Co increased from 25 to 40 Å, the in-plane anisotropy of Co was enhanced, which forcing TbFe moments at the interface to align toward the in-plane orientation and lead to the increased in-plane Hc and H_b. With further increasing Co thickness, the in-plane anisotropy of Co was less changed; therefore, Hc and H_b were inversely proportional to Co thickness due to the characteristic of interfacial coupling of exchange bias, as observed in the in-plane FM/AFM bilayers. By deriving the slope of H_b versus the reciprocal of the M_rt of Co, we obtained the interfacial exchange energy of 0.12 ± 0.02 erg/cm^2 in the bilayers with Co thicker than 40 Å.

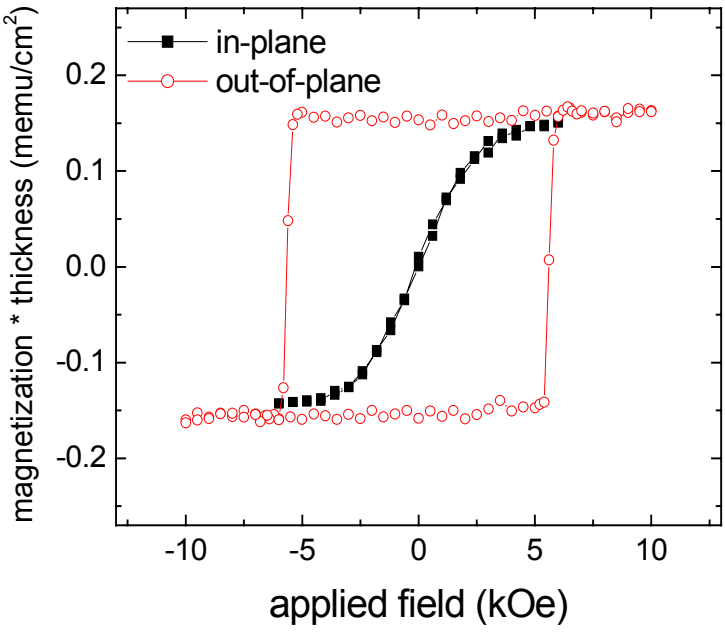

(a)

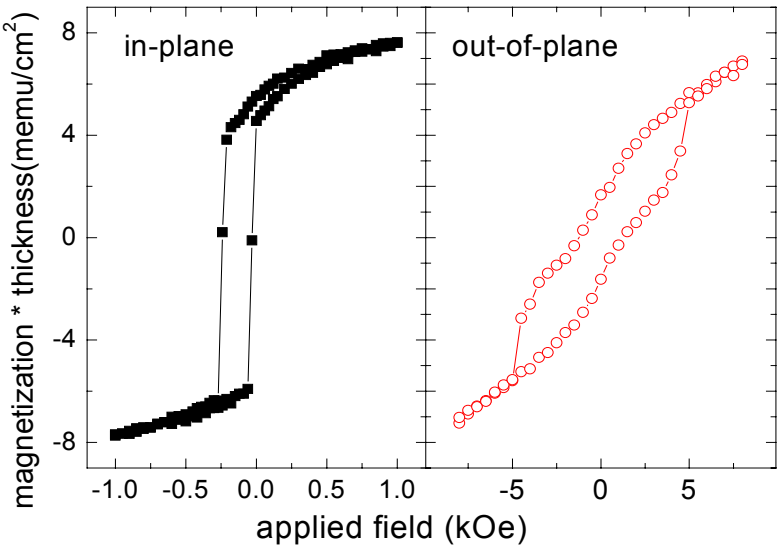

(b)

Fig. 7.1: In-plane and out-of-plane hysteresis loops of the bilayers with the Co of (a) 15 and (b) 50 Å.

.

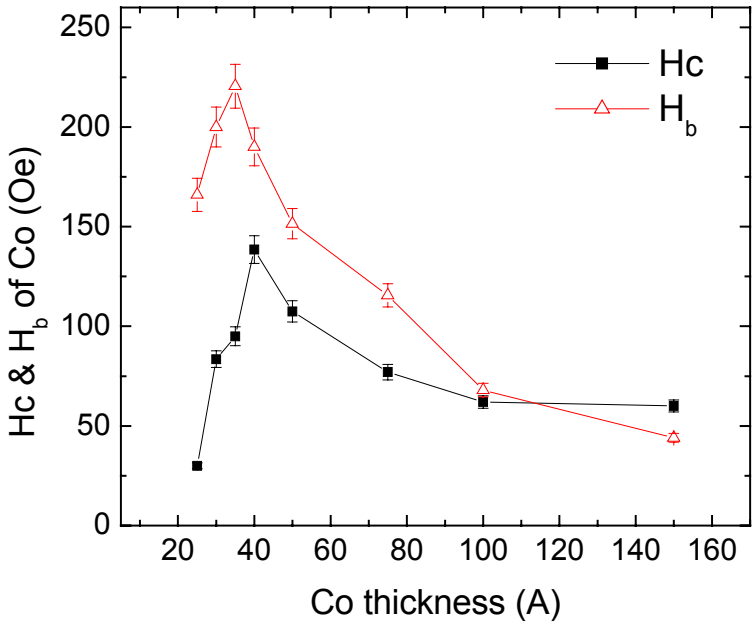

Fig. 7.2: Dependence of coercivity Hc and exchange bias H_b on Co thickness in the bilayers

7.3.b Co and Fe Orientations in TbFe/Co Bilayers with Various Co Thicknesses

XMCD spectroscopy was utilized to clarify the dependence of the Co- and Fe-moment orientation on Co thickness in the bilayers. Because of strong antiparallel exchange coupling between the TM and heavy RE moments [14], the orientation of Tb was considered to be aligned in the opposite direction of Fe moments. In the XMCD measurement, polarized X-ray was incident to the samples at an angle of 65 ° from the surface normal, as illustrated in Figs. 7.3(a) and 7.3(b). If

the direction of the in-plane component of incident X-ray is along the direction of the applied field during the deposition, we define it as the parallel (P-) incidence, indicated in Fig. 7.3(a). The opposite is the antiparallel (A-) incidence, shown in Fig. 7.3(b). Right and left circular polarized X-rays were sequentially illuminated to the bilayers to obtain *L*-edge absorption spectra of Fe and Co, related to the excitation of 2p core electrons to the unfilled 3d states. All of the XMCDs of Co and Fe in the experiments were derived by subtracting the spectrum of right circularly polarized X-ray from that of the left. Taking sampling depth (~8 nm) into the consideration, the XMCD signal of Co averaged over the entire the film, with the preponderance of the signal coming from the near-surface layers.

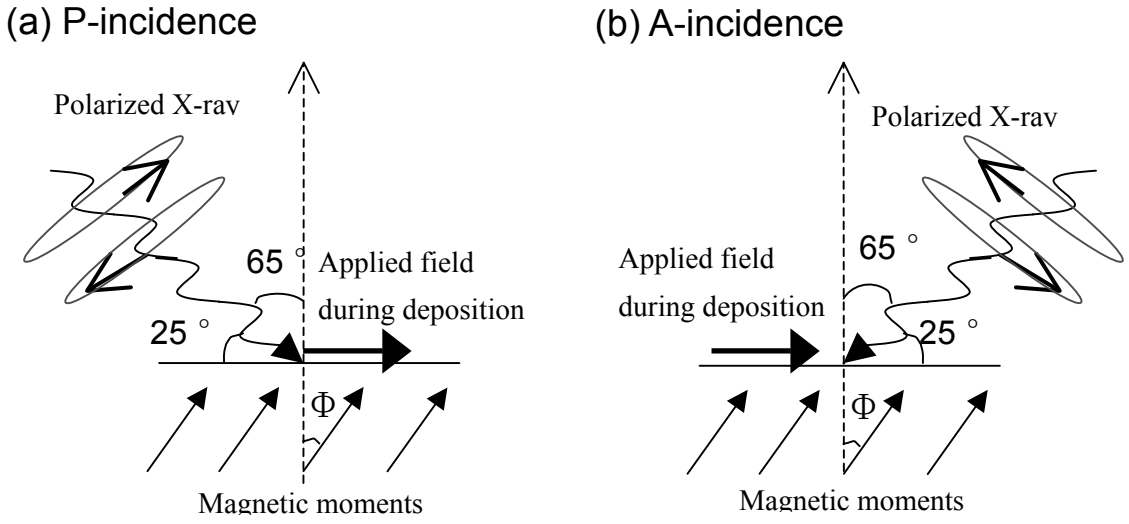

Fig. 7.3: Illustration of (a) P-incidence and (b) A-incidence in XMCD measurement.

On the other hand, the Fe signal came mainly from the interface region. As shown in Figs. 7.4(a) and 7.4(b), the normalized XMCDs of Co in P- and A-incidences are similar in the bilayer with 15 Å Co, but are almost reversed in the bilayer with 50 Å Co. In principle, the XMCD effect is quantitatively related to the amounts of magnetic moments and to the anisotropies of the spin density and orbital moments [7-8]. The dichroism effect in XMCD spectroscopy reaches the maximum if the photon spin and the magnetization directions are parallel or antiparallel, and becomes zero if their directions are perpendicular to each other. Therefore, we can consider the XMCD intensity I of Co as

$$I = I_0 \cos \Theta, \tag{7.1}$$

where I_0 is the maximum intensity related to the amount of spin and orbital moments and Θ is the angle between the magnetization orientation and the incident X-ray direction. If the Co moments were entirely perpendicular to the surface, the XMCD intensity of P- and A-incidences should be identical because the two incident X-rays had the same angle of 65° from perpendicular moments. Therefore, the similarity of the dichroisms of P- and A-incidences in Fig. 7.4(a) implies that the perpendicular anisotropy of 15 Å Co in the bilayer was induced by strong exchange coupling from TbFe. In contrast, the reversed dichroism signals observed in 50 Å Co indicated that the Co moments in the bilayer preferred the in-plane alignment.

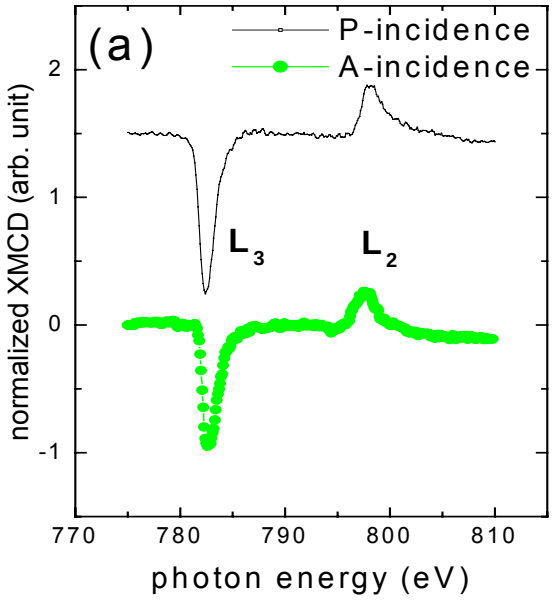

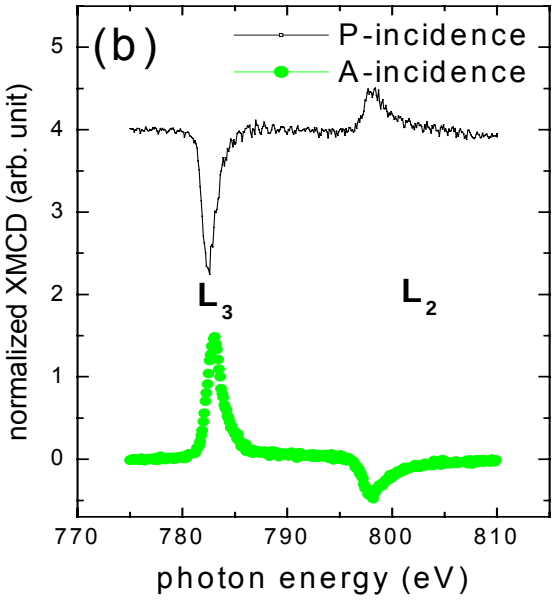

Fig. 7.4: Normalized XMCDs of P- and A-incidence in the TbFe/Co bilayer with the Co of (a) 15 Å and (b) 50 Å.

Furthermore, the orientation of Co moments near the surface and Fe moments near the interface of Co and TbFe in the bilayer can be quantitatively derived by XMCD measurements to concretely explore the origin of exchange bias in the TbFe/Co bilayers. As depicted in Fig. 7.3, if the orientation of the specific moment is aligned at an angle Φ from the surface normal, the dependence of XMCD intensity on the angle Φ can be given by

$$I_{L3,P} = I_0 \cos(180° - 65° - \Phi) = -I_0 \cos(\Phi + 65°) \tag{7.2}$$

and

$$I_{L3,A} = I_0 \cos(180° + 65° - \Phi) = -I_0 \cos(\Phi - 65°). \tag{7.3}$$

Here, $I_{L3,P}$ and $I_{L3,A}$ respectively expressed the XMCD intensity of the L_3-edgeof P- and A-incidences. Combining the Eqs. (7.2) and (7.3), the effective canting angle Φ of Co and Fe moments can be obtained by substituting the measured data of $I_{L3,P}$ and $I_{L3,A}$ into the following formula,

$$\tan\Phi = \cot 65° \times \frac{(I_{L3,A} - I_{L3,P})}{(I_{L3,A} - I_{L3,P})}. \tag{7.4}$$

Fig. 7.5 shows the variation of the Φ of Co and Fe with the Co thickness in the bilayers. Since the majority of the XMCD effect comes from the regions close to the surface, the derived Φ of Co and Fe in the bilayers particularly indicated the orientation of Co moments near the surface and

the Fe moments in the interface region. The orientation of near-interface Co can be reasonably assumed being parallel to near-interface Fe because of strong exchange interaction between Fe and Co moments. From the Fig. 7.5, the canting angles of Co and the near-interface Fe are quite similar, implying that the orientation variation of the Co magnetization across the film thickness is negligible. In the bilayer with 15 Å Co, both of Co and Fe moments preferred the out-of-plane alignment because of their small Φs of 15.4 ° and 13.1 ° from the surface normal. With increasing the thickness, the Co and near-interface Fe gradually lied in the plane. The spin orientations of Co and Fe at the interface are determined by the energy terms of spin-spin coupling, in-plane and perpendicular anisotropy. With decreasing thickness, the in-plane anisotropy of Co is reduced because surface anisotropy becomes significant in the thin films [11]. Therefore, perpendicular anisotropy of TbFe dominated the orientation of moments at the interface in the bilayer with 15 Å Co, which induced the out-of-plane Co moments through exchange coupling to TbFe. As the Co thickness increased, in-plane anisotropy of Co became dominant, which led to the in-plane alignment of interfacial Fe moments through the exchange coupling. Consequently, the existence of in-plane TbFe moments near the interface was responsible for the in-plane exchange bias in the TbFe/Co bilayers.

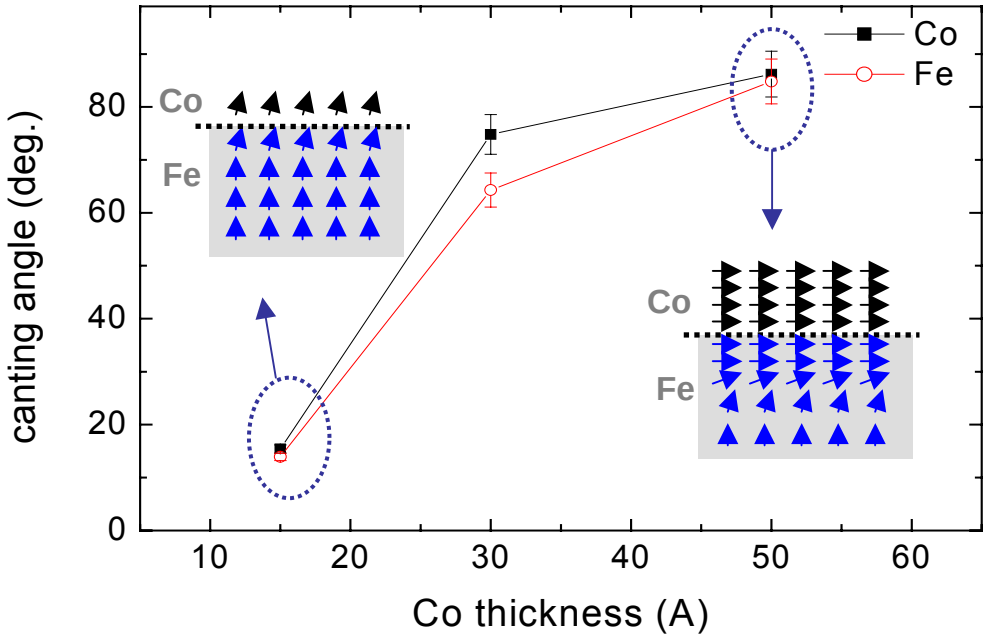

Fig. 7.5: Variation with Co thickness of canting angles of Co and interfacial Fe from the surface normal.

7.3.c Magnetic Behaviors of $Tb_xFe_{(100-x)}$/Co Bilayers

In the bilayers of $Tb_xFe_{(100-x)}$ 300 Å / Co 15 Å, the Co orientation depends strongly on the composition of TbFe, as shown in Fig. 7.6 (a). In the bilayers consisting of $Tb_{15.1}Fe_{84.9}$ film, the Co and interfacial Fe tilts respectively at the angles of 70.3 ° and 62.8 ° from the surface normal. With increasing the Tb content to 31.8, the canting angles of Co

and interfacial Fe approach to zero. In the out-of-plane-Ku measurement of TbFe, the Ku increases with the increase in Tb content from 15.1 to 31.8, as indicated in Fig. 7.6(b). The consistency between Figs. 7.6(a) and 7.6(b) implies that the enhanced out-of-plane TbFe anisotropy makes the Co spins prefer to align toward out-of-plane direction through strong exchange coupling between the two layers.

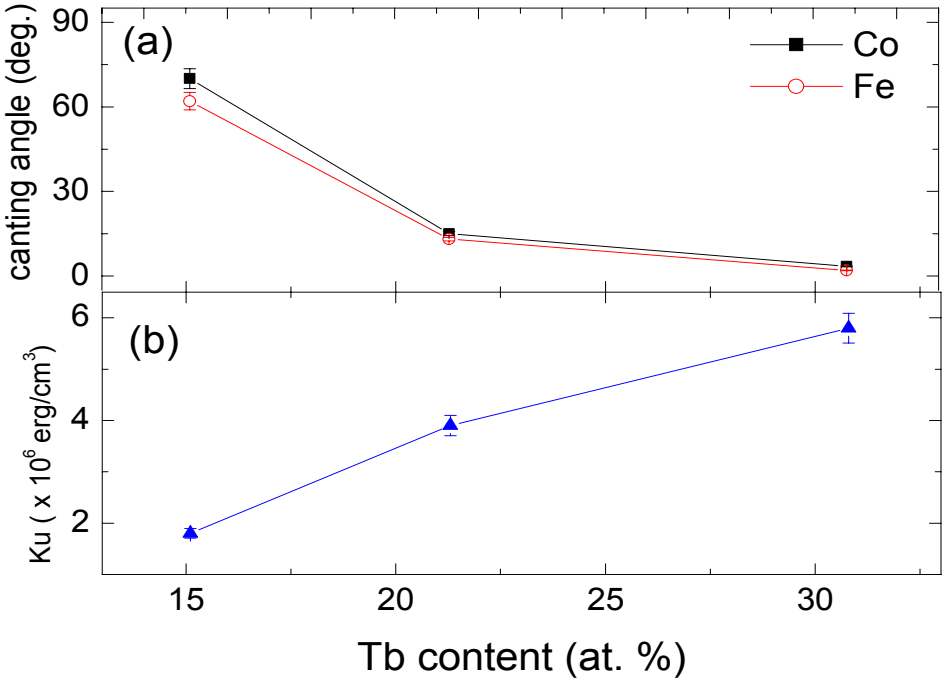

Fig. 7.6: (a)Canting-angle Dependence of Co and interfacial Fe spins on Tb content of TbFe in the bilayers of TbFe 300 Å /Co 15 Å; (b) Ku Variation of TbFe single layer with Tb content.

In addition, in-plane exchange bias of Co was explored in the $Tb_xFe_{(100-x)}$ 300 Å / Co 50 Å. As shown in Fig. 7.7, the exchange bias of

Co increases with increasing Tb content. However, as the Tb is more than 30.8, the biasing field rapidly decreases. According to the micromagnetic model proposed by Smith *et al.* [4], the magnitude of exchange bias is proportional to the in-plane anisotropy of in-plane RE-TM regions between in-plane ferromagnetic and out-of-plane ferrimagnetic layers. Although it is difficult to measure the in-plane anisotropy of the in-plane TbFe region, the in-plane Ku of TbFe in the experiments may vary with the Tb contents, leading to the variation of exchange fields.

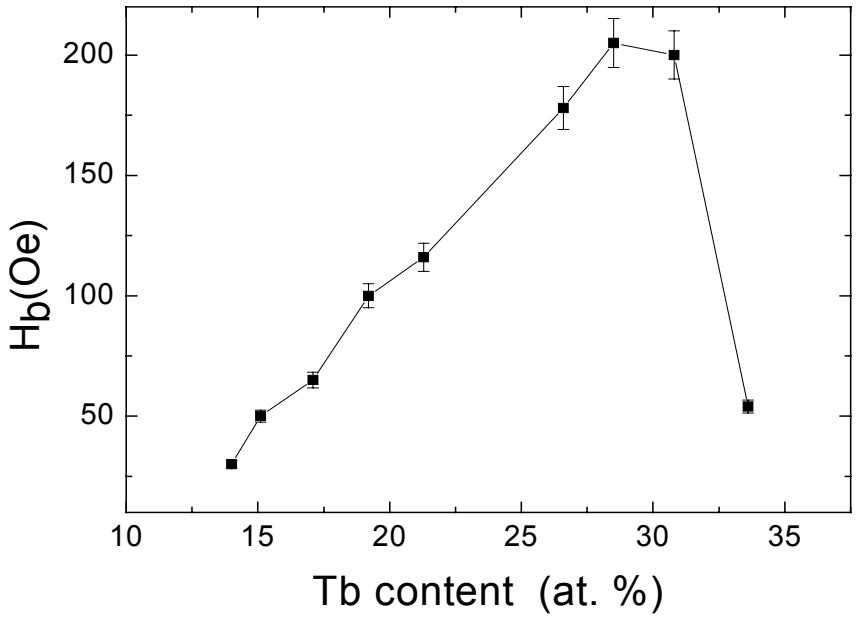

Fig. 7.7: Dependence of in-plane exchange bias of Co on Tb content of TbFe in the bilayers of TbFe 300 Å /Co 50 Å.

7.4 Conclusion

Magnetic properties of TbFe/Co bilayers are significantly affected by the anisotropy of TbFe and Co layers. By utilizing the technology of XMCD spectroscopy, we quantitatively determined the orientation of moments in the TbFe/Co exchange-biased bilayers. Through the mechanism of exchange coupling, the perpendicular anisotropy of 15 Å Co was induced by TbFe. With increasing the Co thickness, in-plane anisotropy of Co became dominant, which resulted in the preferred in-plane moments of Co and TbFe near the interface. The existence of in-plane TbFe moments near the interface led to the in-plane exchange bias fields. In addition, the Co spins tend toward the out-of-plane orientation as exchange-coupled by the TbFe with high perpendicular anisotropy.

Chapter 8

Giant Magnetoresistance Phenomenon in Ferrimagnetic/Cu/Ferrimagnetic-based Films

8.1 Introduction

Typical spin valves consist of ferromagnetic/spacer/ ferromagnetic/antiferromagnetic layers with the magnetization lying in the film plane. Differential spin scattering has been adopted for explaining the giant magnetoresistance (GMR) effect in spin valves [1]. Multilayers consisting of rare earth metals and transition metals show no GMR [2] while $(Co/Dy/Co/Cu/Co/Cu)_n$ multilayers show a positive GMR effect [3] (that is, smaller resistance in zero field than in the saturation field) at 4.2 K. The GMR ratio is defined as $(R_A\text{-}R_P)/R_P$, where R_P and R_A are the resistance of the multilayers or spin valves in which the net magnetizations of the magnetic layers are in the parallel and antiparallel states, respectively. Conventionally, the negative MR, generally observed in mutilayers or spin valves, represents that the MR is reduced with increasing fields and reaches its minimum at the saturation field. As introduced in the Section 2.4.d, the Dy and Co moments in the composite Co/Dy/Co layer aligned antiparallel because of antiferromagnetic

exchange, and the Dy determines the direction of net magnetization in the composite film. Therefore, the adjacent Co spins separated by spacer Cu are in the antiparallel alignments under a high field, leading to the positive GMR in the $(Co/Dy/Co/Cu/Co/Cu)_n$ multilayers. On the other hand, the trilayers made of $Co_{65}Fe_{35}/Ag/(Co_{65}Fe_{35})_{50}Gd_{50}$ also showed a large resistance in a high field [4] Authors have concluded that the conduction electrons were only scattered by Co or Fe moments. In this work, we fabricated a structure of spin valves composed of ferrimagnetic/spacer/ferrimagnetic layers with the magnetization perpendicular to the film planes. To understand the GMR effect of this perpendicular spin valve, the effects on GMR ratio of spacer thickness and of ferrimagnetic composition were investigated. In these ferrimagnetic spin valves, by changing the composition of ferrimagnets or by inserting a Co layer at the interface, the sign and the magnitude of GMR can be manipulated and enhanced. The mechanism of positive GMR in these ferrimagnetic spin valves will be discussed. In addition, indirect exchange coupling between Gd and Co at room temperature was observed and clarified. Furthermore, the GMR effect in TbCo/Co/Cu/Co/TbFeCo films is further investigated.

8.2 Experimental Procedures

Spin-valve-like films with the structure SiN_x/200 Å TbFeCo/ t Å Cu/100 Å GdFeCo (or TbFeCo)/SiN_x were prepared by dc magnetron sputtering onto Si wafers at room temperature. The spin valve was sandwiched by SiN_x protective layers to prevent TbFeCo and GdFeCo oxidation. Ferrimagnetic layers were cosputtered using a transition metal (TM: $Fe_{80}Co_{20}$ or pure Co) and a rare-earth target (RE: Tb or Gd). The composition of ferrimagnetic films was controlled by the relative sputtering power of TM and RE, and was calibrated by Rutherford backscattering spectrometry. After depositions, the samples were magnetized in the field of 14 kOe to saturate TbFeCo and GdFeCo. The hysteresis loops were measured using a vibrating sample magnetometer or perpendicular magneto-optical Kerr-loop tracer. Magnetoresistance was measured using a four-point probe with the applied field perpendicular to the film plane, which makes current direction perpendicular to the magnetization. Four points were aligned in a straight line. The MR ratio in the experiments is defined as $(R_A\text{-}R_P)/R_P$.

8.3 Results and Discussion

8.3.a Giant Magnetoresistance Effect in TbFeCo/Cu/GdFeCo Films

The hysteresis loop and MR curve of 200 Å $Tb_{20.5}(Fe_{80}Co_{20})_{79.5}$ (TM-rich)/17 Å Cu/100 Å $Gd_{22.4}(Fe_{80}Co_{20})_{77.6}$ (TM-rich) are shown in Fig. 8.1. The notation of TM-rich represents that the magnitude of the TM moments is larger than that of RE moments. The GdFeCo layer possessing low coercivity can be considered as the free layer in the spin-valve films. The compensation compositions of these ferrimagnets are about $Tb_{22.7}(Fe_{80}Co_{20})_{77.3}$ and $Gd_{23}(Fe_{80}Co_{20})_{77}$. The hysteresis loops [Fig. 1(a)] clearly demonstrate the characteristic of perpendicular magnetization with the coercivity of $Gd_{22.4}(Fe_{80}Co_{20})_{77.6}$ and $Tb_{20.5}(Fe_{80}Co_{20})_{79.5}$ of 110 Oe and 11.5 kOe, respectively. The distinguished difference in coercivity between ferrimagnets results in the antiparallel state of the net magnetization between ferrimagnetic layers can be achieved. The minor loop and the corresponding *R-H* curve are shown in Fig. (b) and (c), where an interlayer coupling of 270 Oe and the MR ratio of -1% are observed. In the Figs. 8.1(b) and 8.1(c), the state of parellel magnetizations in the two ferrimagnetic layers corresponds to a low-resistance state and high resistance was observed in the antiparallel

state, representing a negative MR effect in the spin-valve-like films consisting of TM-rich TbFeCo and GdFeCo layers. Since the measuring current is in the film plane, perpendicular to the magnetization, anisotropic magnetoresistance can be excluded. The four-point probes with a linear configuration for current and voltage probes exclude the probability of Hall effect contribution on resistance change. These results strongly suggest that the origin of the observed magnetoresistance is the GMR effect. However, the resistivity of amorphous ferrimagnets (ρ ~200 $\mu\Omega$-cm) is about 50 times larger than that of Cu, which leads to significant current shunting effect and to a small MR ratio.

Fig. 8.2 shows the dependence of absolute MR ratio and interlayer coupling on Cu thickness (all MR ratios in Fig. 8.2 are negative). The MR ratio decreased with increasing Cu thickness. In the spin valve, the magnitude of GMR is associated with the spin-dependent scattering of conducting electrons at the interface between the spacer and magnetic layers. In the case of thick Cu layer, most of conducting electrons flow in the Cu but do not cross the interface, resulting in a low GMR effect. In addition, Fig. 8.2 also indicates that the interlayer coupling in ferrimagnetic spin valves is significantly higher than that of ferromagnetic ones. The intelayer coupling also decreases with the increase in Cu thickness, which will be further discussed in the section 8.3.c.

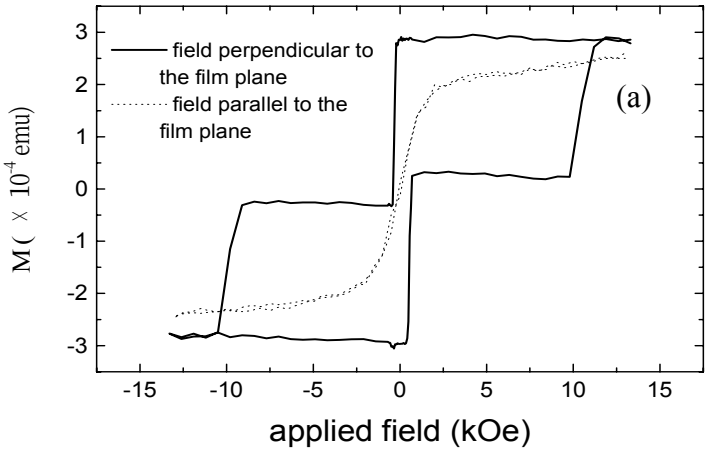
field perpendicular to the film plane
field parallel to the film plane
(a)
M(× 10-4 emu)
applied field (kOe)

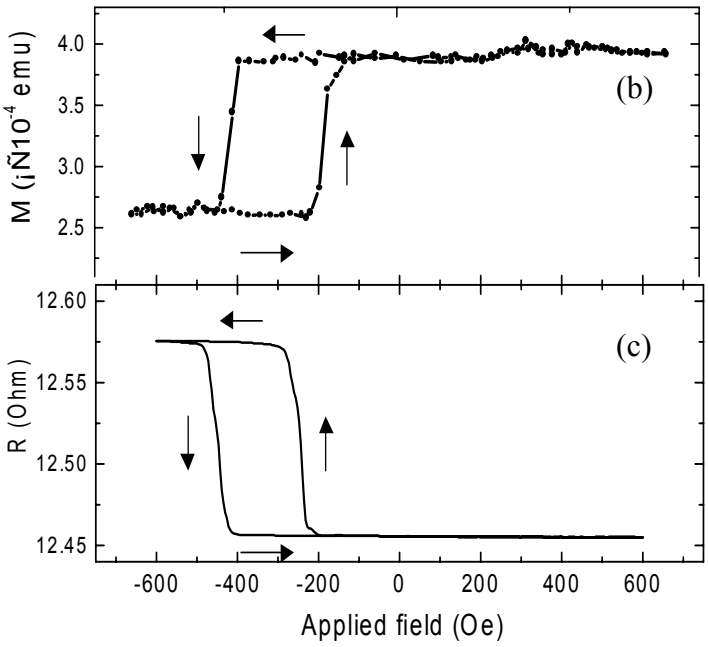
(b)
M (¡Ñ10-4 emu)
(c)
R (Ohm)
Applied field (Oe)

Fig. 8.1: (a) Hysteresis loop, (b) minor loop of (a), and (c) *R-H* curve of SiN/200 Å $Tb_{20.5}(Fe_{80}Co_{20})_{79.5}$ (TM-rich)/ 17 Å Cu/ 100 Å $Gd_{22.4}(Fe_{80}Co_{20})_{77.6}$ (TM-rich)/SiN. The arrows represent the sequence of the applied field.

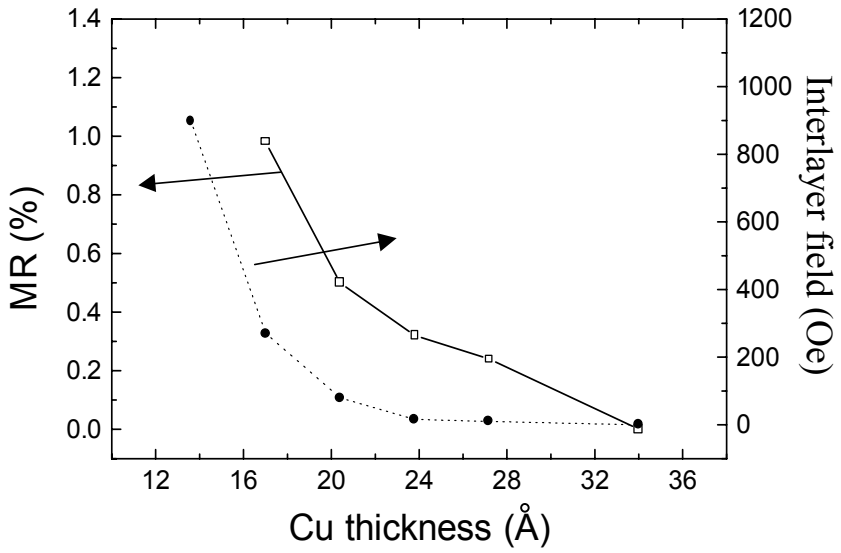

Fig. 8.2: Dependence of the absolute MR ratio and the interlayer coupling on the Cu thickness for SiN/200 Å $Tb_{20.5}(Fe_{80}Co_{20})_{79.5}$ (TM-rich)/t Å Cu/100 Å $Gd_{22.4}(Fe_{80}Co_{20})_{77.6}$ (TM-rich)/SiN. (All MR values are negative.)

8.3.b Positive GMR in TbFeCo/Cu/GdFeCo Films

In fact, spin valves consisting of both RE-rich TbFeCo and GdFeCo also showed negative GMR. On the other hand, for samples consisting of RE-rich TbFeCo [$Tb_{37.4.}(Fe_{80}Co_{20})_{62.6}$] and TM-rich GdFeCo [$Gd_{22.4}(Fe_{80}Co_{20})_{77.6}$] (or TM-rich TbFeCo and RE-rich GdFeCo), positive GMR values were observed, that is, the resistance is high at the positive saturation field, but is reduced when the magnetization becoms

anti-parallel, as shown in Fig. 8.3. For the samples consisting of TM-rich GdFeCo and RE-rich TbFeCo, when the net magnetizations are parallel in ferrimagnets, the sublattice magnetizations of transition metals are antiparallel. Since 4*f* electrons have little contribution to the differential spin scattering [2,4], the GMR effect in ferrimagnetic spin valves is mainly contributed from the 3*d* sublattice. When the magnetization of GdFeCo is switched, that is, the net magnetizations of GdFeCo and TbFeCo become antiparallel, the magnetizations of transition metals become parallel. Consequently, the antiparallel state of net magnetizations results in a small resistance, and a positive GMR effect.

A thin layer of Co was inserted between the RE-rich TbFeCo and Cu to manipulate the sign of GMR. In the Fig. 8.4, the positive GMR ratio increased with increasing Co thickness for the thickness less than 1 nm. When the thickness of Co reached 1.5 nm, the negative GMR appeared. As discussed in chapter 7, the thin Co on the TbFeCo film with high perpendicular anisotropy prefers out-of-plane orientation because of stong exchange interaction between two magnetic layers. Its magnetization is opposite to that of the Tb sublattice due to the antiferromagnetic exchange-coupling between transition metal and heavy rear-earth [8]. For Co thickness less than 1 nm, the composite layer $Tb_{27.6}(Fe_{80}Co_{20})_{72.4}$/Co is still RE-rich, so the net moment of the composite layer is opposite to the Co moment [Fig. 8.5(a)], but is aligned with the applied field. Consequently, for thin Co samples, the moments of two transition metals are opposite at saturation fields, resulting in a positive MR. Due to strong interfacial spin-dependent scattering at

Co/Cu, the positive MR increases with Co thickness. For the sample with 1.5 nm (or 2 nm) Co, the composite layer becomes TM-rich [Fig. 8.5(b)], leading to a parallel alignment of magnetizations of transition metals and to a negative MR. The reduced GMR with further increasing Co thickness more than 1.5 nm is mainly attributed to that the Co moments gradually tilt to in-plane orietation in the thick Co film exchange-coupled to a ferrimagnetic film with perpendicular anisotropy, as indicated in Fig. 7.5.

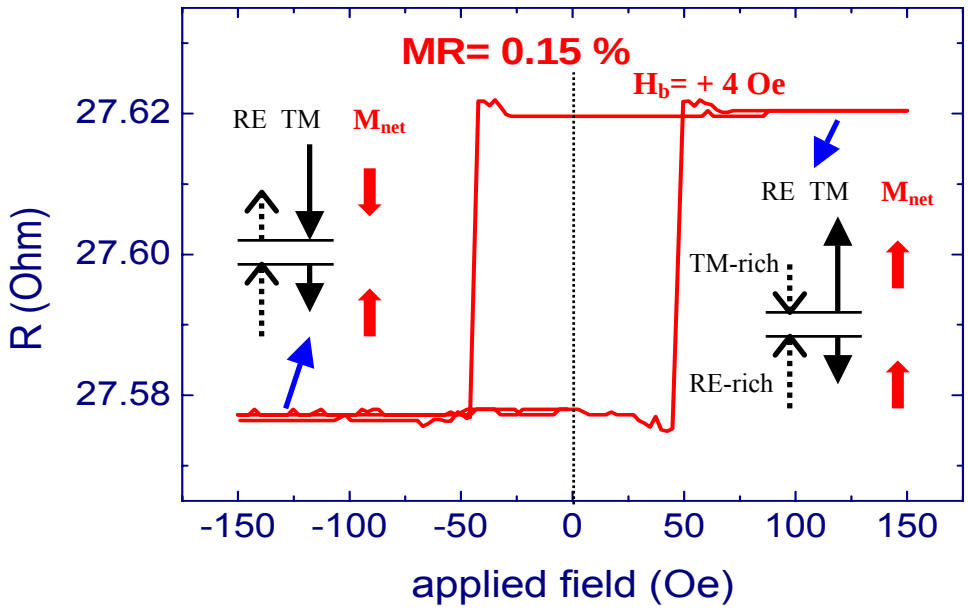

Fig. 8.3: R-H loop of 200 Å $Tb_{37.4}(Fe_{80}Co_{20})_{62.6}$ (RE-rich) /20 Å Cu/100 Å $Gd_{22.4}(Fe_{80}Co_{20})_{77.6}$ (TM-rich).

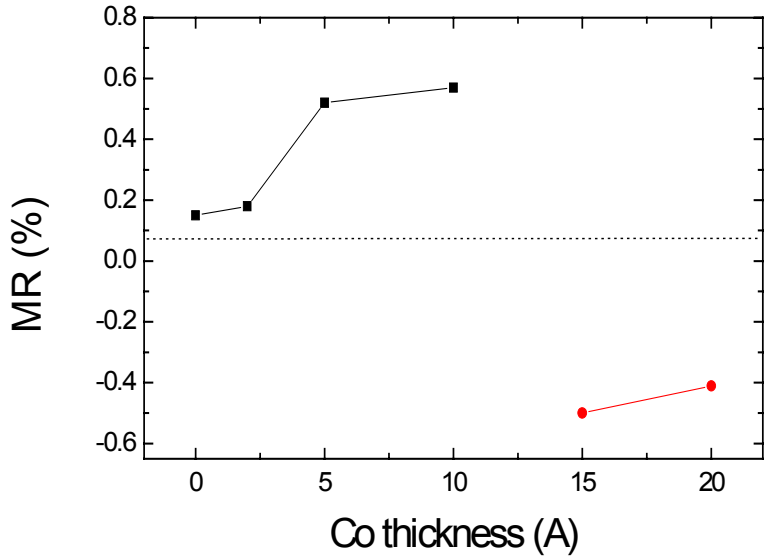

Fig. 8.4: Dependence of MR ratio on the Co thickness for 200 Å $Tb_{27.6}(Fe_{80}Co_{20})_{72.4}$ (RE-rich)/t Å Co/20 Å Cu/100 Å $Gd_{22.4}(Fe_{80}Co_{20})_{77.6}$ (TM-rich).

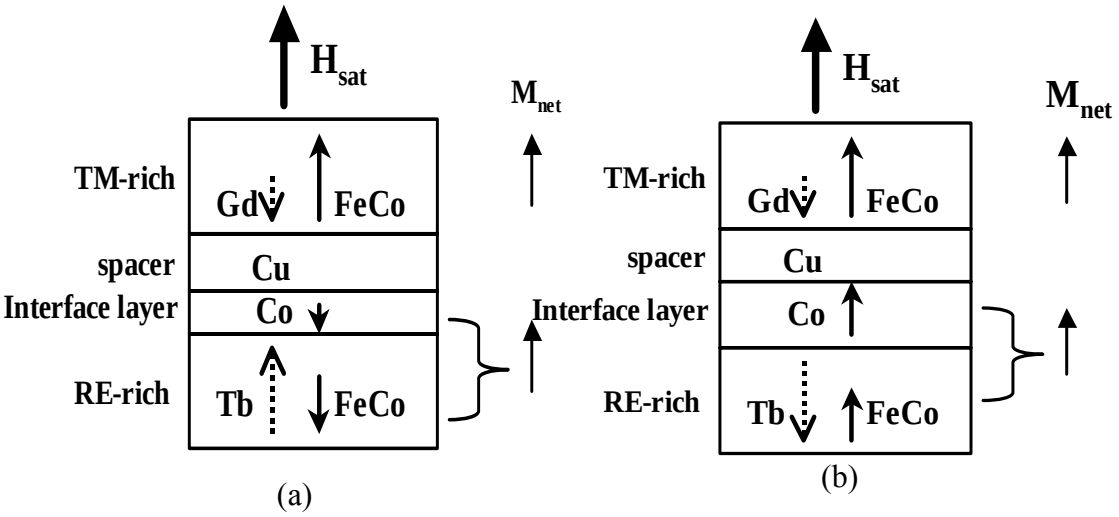

Fig. 8.5: Schematic diagrams for the direction of moments in TbFeCo (RE-rich)/t Å Co/Cu/GdFeCo (TM-rich). (a) $t \leq 1$ nm and (b) $t > 1$nm.

8.3.c Indirect Exchange Coupling in TbFeCo/Cu/GdFeCo Films

As indicated in Figs. 8.1(b) and 8.1(c), a negative biasing field was observed in the film of TM-rich TbFeCo / Cu / TM-rich GdFeCo. To clarify the static-coupling effect of TbFeCo on the shifting field of GdFeCo, a SiN_x layer of 1.3 nm, replacing the spacer of Cu, was inserted between 200 Å of $Tb_{20.5}(Fe_{80}Co_{20})_{79.5}$ and 100 Å of $Gd_{22.4}(Fe_{80}Co_{20})_{77.6}$. As shown in Fig. 8.6(a), a symmetry hysteresis loop of GdFeCo was obtained and the large shifting in Fig. 8.1(b) disappeared, implying that the magneto-static dipolar coupling between TbFeCo and GdFeCo is very weak because of low magnetization (TbFeCo 185 emu/cm^3; GdFeCo 84 emu/cm^3) of the ferrimagnetic films. Figs. 8.6(b) and 8.6(c) further indicates the minor and full loop in the film of TbFeCo/Cu/TbFeCo, where the two TbFeCo layers possess different coercivity. The non-shifting loop strongly evidences that the negative biasing field of GdFeCo in TbFeCo/Cu/GdFeCo is associated with an indirect antiparalllel exchange-coupling between Gd and Co (Fe) spins separated by Cu, which is consistent with the exchange interaction in the Co/Cu/Gd/Cu multilayers at low temperature [9]. The origin of this coupling is not clear but we speculate that it may result from that 5d delocolized spins of Gd ferromagnetically couple with 3d spins of Co (Fe) in the TbFeCo film by the electron transport through the Cu spacer [10-12]. Furthermore, antiferromagnetic exchange between 5d and 4f

spins in Gd [10-11] lead to an antiferromagnetic exchange coupling between 4f spins of Gd in GdFeCo and 3d spins of Co (Fe) in TbFeCo and, thus, negative exchange coupling in GdFeCo/Cu/TbFeCo. The indirct exchange coupling decreases monotonically with the Cu thickness, leading to the reduced biasing field of GdFeCo in Fig. 8.2. In addtion, the content of TbFeCo strongly affects the strength and direction of the indirect exchange coupling. As shown in the Figs. 8.2 and 8.3, the interlayer coupling significantly decreases when the content of Tb in TbFeCo increases from 20.5 to 37.4. In the films of TbFeCo/Co/Cu/GdFeCo, the sign and magnitide of the interlayer coupling also exhibit strong functions of Co thickness, indicated in Fig. 8.7. For Co thickness less than 1 nm, the composite $Tb_{27.6}(Fe_{80}Co_{20})_{72.4}$/Co is still RE-rich so that positive exchnage bias of the GdFeCo layer was observed. However, the exchange bias becomes negative since Co is more than 1.5 nm and $Tb_{27.6}(Fe_{80}Co_{20})_{72.4}$/Co changes to TM-rich. In addition, the indirect exchange coupling between Gd and Co spins was enhanced with increasing Co thickness.

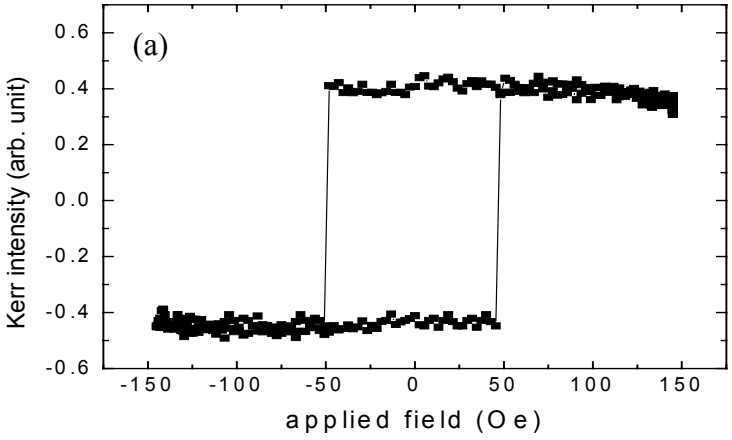
(a)
Kerr intensity (arb. unit)
0.6
0.4
0.2
0.0
-0.2
-0.4
-0.6
-150
-100
-50
0
50
100
150
applied field (Oe)

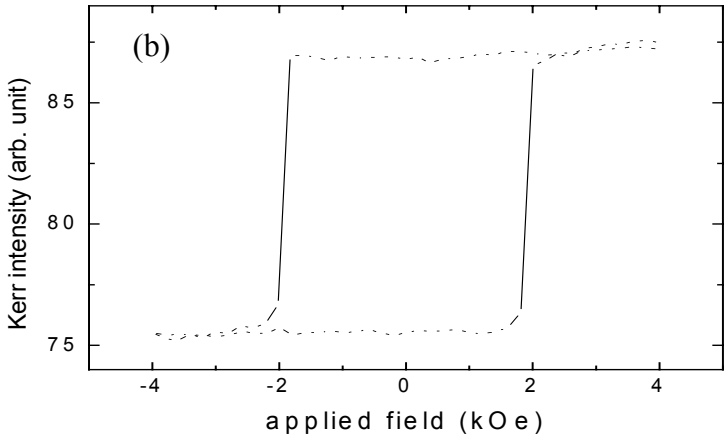
(b)
Kerr intensity (arb. unit)
85
80
75
-4
-2
0
2
4
applied field (kOe)

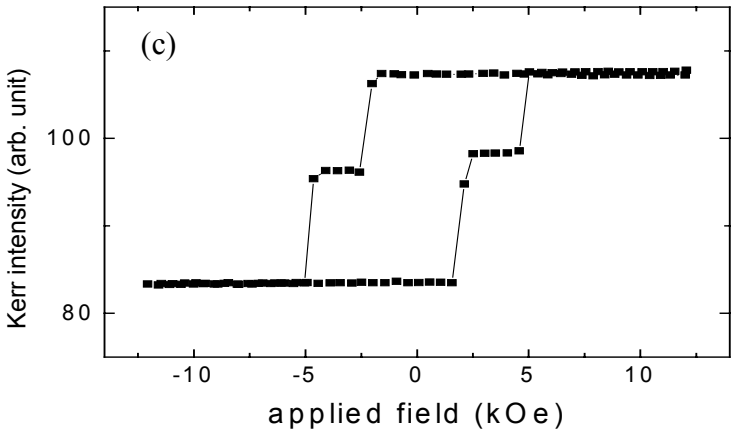
(c)
Kerr intensity (arb. unit)
100
80
-10
-5
0
5
10
applied field (kOe)

Fig. 8.6: (a) Minor loops of 200 Å TbFeCo (TM-rich) /15 Å SiNx/100 Å GdFeCo (TM-rich). (b) minor and (c) full loops of 200 Å TbFeCo (TM-rich) /15 Å Cu/100 Å TbFeCo (TM-rich).

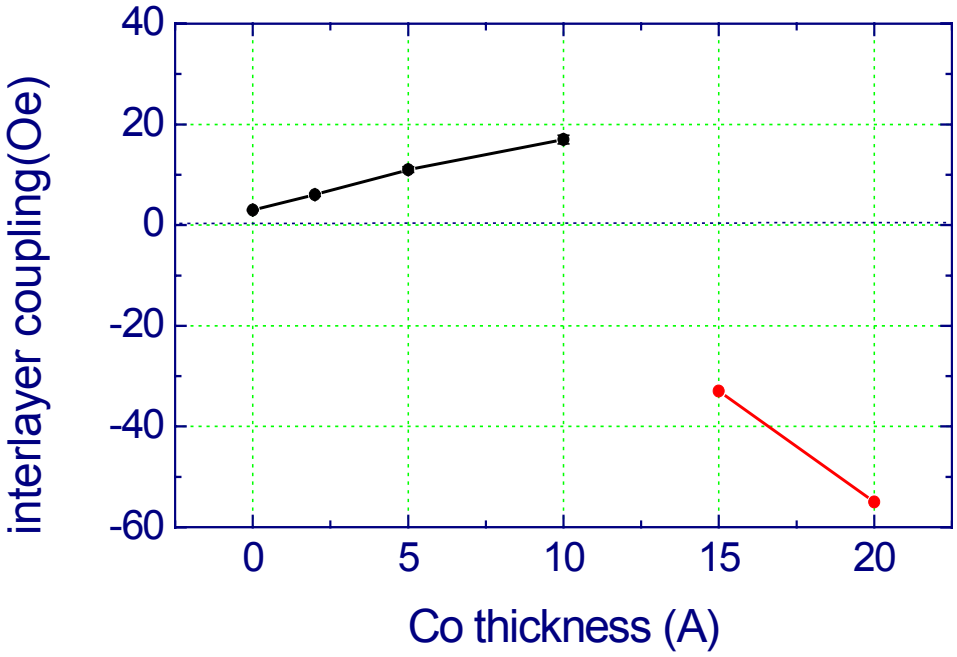

Fig. 8.7: Dependence of interlayer coupling on the Co thickness for 200 Å $Tb_{27.6}(Fe_{80}Co_{20})_{72.4}$ (RE-rich)/t Å Co/20 Å Cu/100 Å $Gd_{22.4}(Fe_{80}Co_{20})_{77.6}$ (TM-rich).

8.3.d MR in TbCo/Co/Cu/Co/TbFeCo Films

The MR more than 2.9 % was observed in the film composed of $Tb_{26.9}Co_{73.1}$10 nm/Co 1 nm/Cu 1.5 nm/Co 1 nm/ $Tb_{25.1.}(Fe_{80}Co_{20})_{74.9}$, as shown in Fig. 8.8(a). In the film, the coercivity of the composite TbCo/Co film is larger than that of the Co/TbFeCo, implying the MR loop in Fig. 8.8(a) is due to the magnetization switching of the

TbFeCo/Co. In addition, both of the TbCo/Co and Co/TbFeCo behaved like TM-rich, leading to a negative GMR. Figs. 8.8(b) and 8.8(c) further show the full hysteresis loop and R-H curve of the ferrimagnetic spin-valve-like film. From the two figures, it can be precisely clarified that the variation of the resistance in the film originates from GMR effect because the MR is associated with the resistance change between the parallel and antiparallel alignment of transition-metal spins in two composite ferrimagnetic layers. With increasing the Cu thickness to 2 nm, the MR in the film was enhanced to 4.29 %, shown in Fig. 8.9. As shown Figs. 8.8(a) and 8.9, the differences of R_A and R_P (ΔR) in two R-H loops are both about 0.51 ohms at the input current of 10 mA. Considering the geometries of measured samples and four-point probe, the sheet-resistance difference between R_A and R_P is about 2.04 ohm-cm. The MR enhancement in Fig. 8.9 is mainly due to the decreasing resistance in the film with thick Cu. Comparing with the ferromagnetic spin valve [13], the MR of 4.29 % is still low because intrinsic resistance of amorphous ferrimagnetic films is high. However, the ΔR in the ferrimagnetic spin-valve-like film is practically high enough to contribute a significant variation of output voltage. For comparison, we made a typical ferromagnetic spin valve composed of Ta 3.5 nm/ NiFe 4nm/ IrMn 8 nm/ Co 2.5 nm/ Cu 2.5 nm/ CoFe 4 nm/ Ta 3.5 nm. The sheet resistance R_P is about 20 ohm-cm, half or one-third of the R_P in ferrimagnetic spin valve. To achieve the MR of 10 %, the resistance change in the ferromagnetic spin valve needs to be more than 2.0 ohm-cm. The ferrimagnetic spin-valve-like films possess equivalent ΔR to

conventional ferromagnetic spin valves but even higher sheet resistance, which may be attractive for CPP applications to enhance the level of output signal [14-15].

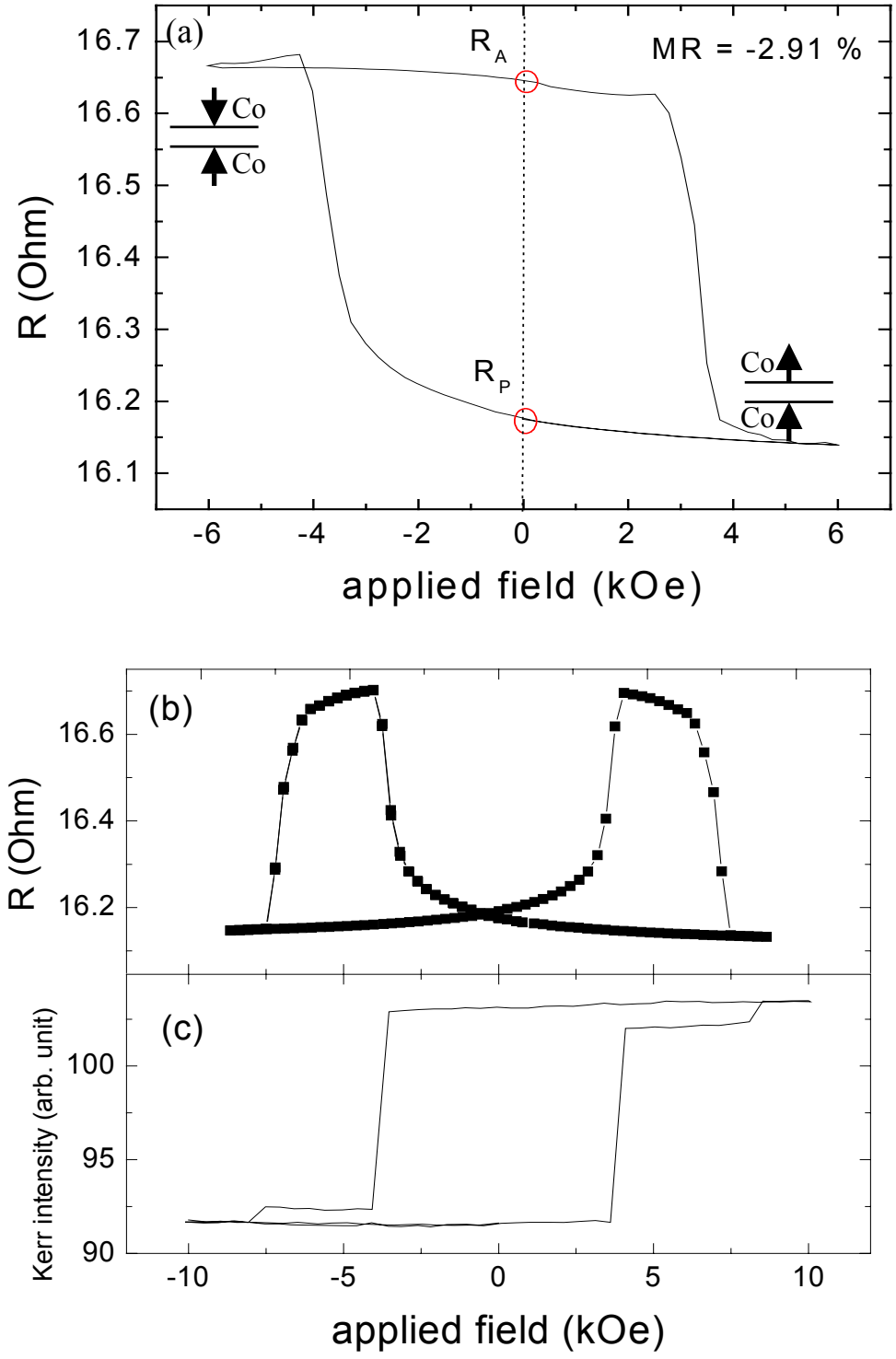

Fig. 8.8: (a) Minor, (b) full R-H loops, and (c) full Kerr-effect loop of $Tb_{26.9}Co_{73.1}$10 nm/Co 1 nm/Cu 1.5 nm/Co 1 nm/ $Tb_{25.1.}(Fe_{80}Co_{20})_{74.9}$.

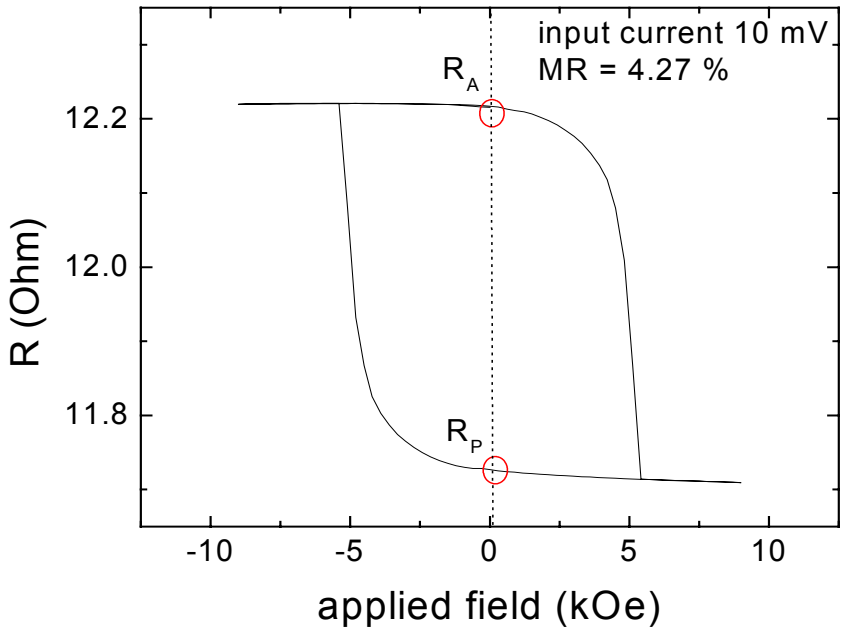

Fig. 8.9: Minor R-H loop of $Tb_{26.9}Co_{73.1}$10 nm/Co 1 nm/Cu 2 nm/Co 1 nm/ $Tb_{25.1.}(Fe_{80}Co_{20})_{74.9}$.

8.4 Conclusion

In conclusion, ferrimagnetic spin valves were fabricated with the magnetization perpendicular to the film planes. For samples consisting of both TM-rich (or both RE-rich) TbFeCo and GdFeCo, negative GMR values were obtained. For the samples consisting of RE-rich TbFeCo and TM-rich GdFeCo, a positive GMR effect was observed. Since the spin-dependent scattering potential for the rare earth was quite weak, the observed GMR effect was mainly contributed by the transition metals. Although the net magnetizations of TM-rich GdFeCo and RE-rich TbFeCo were in the same direction under a saturation field, the moments of transition metals in the two layers were antiparallel aligned, leading to a high resistance at a saturation field and thus a positive GMR. In addition, an indirect exchange coupling between the Gd and Co (Fe) separated by Cu spacer leads to the shifted hysteresis loop of GdFeCo in the TbFeCo/Cu/GdFeCo film. A thin layer of Co was inserted between RE-rich TbFeCo and Cu to manipulate and enhance the sign and the magnitude of GMR. Furthermore, a large GMR more than 4.2 % was observed in the film of TbCo/Co/Cu/Co/TbFeCo, which may be a potential candidate for CPP applications.

Chapter 9

Conclusions

This dissertation has presented the study of exchange-coupling behaviors in the TbFeCo bilayers with perpendicular anisotropy, and in the TbFe/Co bilayers respectively with perpendicular and longitudinal anisotropy. The applications of exchange coupling in these bilayers for hybrid recording and ferrimagnetic spin valve with perpendicular anisotropy have been further discussed. Several important results are summarized here.

In the investigation of exchange coupling in the bilayers both with perpendicular anisotropy, the exchange-bias films of ferrimagnetic/ ferrimagnetic, ferromagnetic/ ferromagnetic, and ferromagnetic/ antiferromagnetic bilayers were fabricated to investigate their interfacial exchange energy $\triangle\sigma$. We have demonstrated high interfacial exchange energy (>5 erg/cm^2) in TbFeCo bilayers. A highly-uncompensated-spin interface is proposed to explain the strong exchange bias in TbFeCo bilayer systems. IrMn/NiFe exhibited weaker exchange bias than SmCo/NiFe due to the AF-coupling between the adjacent Mn-Mn atoms, verifying the importance of an uncompensated-spin interface to exchange bias. In the bilayers with highly-uncompensated-spin interface, as TbFeCo films, the amount of uncompensated spins is a weak function of

interface roughness, leading to less dependence of $\triangle\sigma$ upon interfacial morphology. By adjusting the composition of TbFeCo films, we further demonstrated that the high Ku of the pinning layer significantly enhances the $\triangle\sigma$.

Based on the facts of strong exchange interaction in TbFeCo bilayers, RE-TM exchange-couple dual layer media with high magnetization and large coercivity were investigated for heat-assisted magnetic recording. Through the strong exchange coupling between TbFeCo layers with perpendicular anisotropy, the coercivity of the TbFeCo with high magnetization of 370 emu/cm^3 could be greatly enhanced from 0.95 to 6 kOe. In addition, the A-type ECDL films exhibit larger coercivity enhancement than the P-type because of the interfacial-wall formation. The coercivity enhancement in the A-type media is proportional to interfacial-wall energy and, thus, magnetic anisotropy. Therefore, the A-type ECDL media composed of TM-rich readout layer and RE-rich memory layer with high magnetic anisotropy are preferred for the hybrid recording because of the consideration of high coercivity enhancement. Furthermore, the interfacial-wall energy in ECDL films is less dependent on thickness of readout and memory layer. Thin readout layer possesses high effective coercivity because the coercivity enhancement is inversely proportional to its thickness. In the thermomagnetic-writing testing, we can reliably record the marks in the A-type media with TM-rich readout layer by using MO-disk tester. In magnetic-flux-detection testing, the TbFeCo disks fabricated at high vacuum exhibit low media-noise

examined by GMR sensor. Consequently, the A-type ECDL TbFeCo media with magnetization over 370emu/cm^3 and high stability are potentially applicable for heat-assisted magnetic recording.

In the investigation of exchange coupling in the bilayers respectively with perpendicular and longitudinal anisotropies, thin Co layers with various thicknesses were deposited on the TbFe layers. Magnetic properties of the TbFe/Co bilayers are significantly affected by the anisotropy of TbFe and Co layers. By utilizing the technology of XMCD spectroscopy, we quantitatively determined the orientation of moments in the TbFe/Co exchange-biased bilayers. Through the mechanism of exchange coupling, the perpendicular anisotropy of 15 Å Co was induced by TbFe. With increasing the Co thickness, in-plane anisotropy of Co became dominant, which resulted in the preferred in-plane moments of Co and TbFe near the interface. The existence of in-plane TbFe moments near the interface led to the in-plane exchange bias fields. In addition, the Co spins tend toward the out-of-plane orientation as exchange-coupled by the TbFe with high perpendicular anisotropy. The anisotropy of TbFe also significantly influences the planar exchange bias of thick Co in the TbFe/Co.

On the other hand, the TbFeCo/Cu/GdFeCo films were fabricated to explore the GMR effect in the ferrimagnetic spin-valve-like films. For samples consisting of both TM-rich (or both RE-rich) TbFeCo and GdFeCo, negative GMR values were obtained. For the samples

consisting of RE-rich TbFeCo and TM-rich GdFeCo, a positive GMR effect was observed. Since the spin-dependent scattering potential for the rare earth was quite weak, the observed GMR effect was mainly contributed by the transition metals. When the applied field switched the magnetization of GdFeCo, the moments of transition metals were parallel aligned, leading to a small resistance and thus positive GMR. In addition, an indirect exchange coupling interaction between the Gd and Co (Fe) separated by Cu spacer lead to the shifted hysteresis loop of GdFeCo in the TbFeCo/Cu/GdFeCo film. As mentioned in the above, through strong exchange coupling with ferrimagnetic RE-TM films, the thin Co prefer out-of-plane orientation. Therefore, a thin layer of Co was inserted between RE-rich TbFeCo and Cu to manipulate and enhance the sign and the magnitude of GMR. A large GMR more than 4.2 % was observed in the film of TbCo/Co/Cu/Co/Cu/TbFeCo, which may be a potential candidate for CPP applications.